MODELLING OF LONG WAVE PROPAGATION USING THE RADIAL BASIS FUNCTION COLLOCATION METHOD

by

Cenk Güngör

B.S., Civil Engineering, Yıldız Technical University, 2000

M.S., Civil Engineering, Boğaziçi University, 2005

Submitted to the Institute for Graduate Studies in
Science and Engineering in partial fulfillment of
the requirements for the degree of
Doctor of Philosophy

Graduate Program in Civil Engineering

Boğaziçi University

2015

ACKNOWLEDGEMENTS

I would like to express my sincere gratitude to Assoc. Prof. Osman S. Börekçi for accepting to supervise my thesis and also for teaching, orienting, and motivating me throughout my studies and for his fatherly attitude above all.

I would like to express my sincere appreciation to my co supervisor Prof. Ahmet Cevdet Yalçıner for his endless and invaluable support, academic and intellectual supervision.

I would like to thank the members of my thesis committee, Prof. Cem Avcı, Assoc. Prof. Yasin Fahjan, Assist. Prof. Sami And Kılıç and Assoc. Prof. Emre Otay, for their hearty support, great sympathy and contributions to my coastal engineering education with their invaluable knowledge and experiences.

I am grateful to Prof. Robert G. Dean, Prof. Vedat Yerlici and Prof. Akın Tezel for their both direct and indirect contributions to my academic and intellectual development. "Requiescat in pace, Prof. Robert G. Dean!"

My most willingly thanks are to my brethren Yavuz Tokmak, Ali Erdoğan, Fatin Dilmen, Özkan Tosun and Ömer Işık for their invaluable supports, endless patience and everlasting encouragement. Also, I am indebted to Tuba Sural Fehr and the members of the Boğaziçi University coastal group-Yiğit Altan, Mohammadsadegh Aslani, Cihan Bayındır, Emin Çiftçi, Hüseyin Demir, Soner Kural, Andrea Mueller, Arzu Samancı, Ufuk Şahin, Burak Timuçin, Gökalp Topçu and Ulvi Şensoy- and all my other graduate friends studied in the Civil Engineering Department.

Finally, I am grateful to my precious sister, Burcu Güngör, uncle Prof. Atilla Güngör and my family who were always by me at every stage of this study. I dedicate this thesis to them as this would not have been possible without their love and devotion.

ABSTRACT

MODELLING OF LONG WAVE PROPAGATION USING THE RADIAL BASIS FUNCTION COLLOCATION METHOD

In this thesis, the depth averaged equations of motion and continuity, satisfying certain additional conditions on the boundaries for long wave propagation will be presented. An efficient meshless numerical scheme, which is an easily adaptable convergent new technique, based on the Radial Basis Functions Collocation Method has been employed in the model. Long wave propagation model is developed using the nonlinear shallow water equations which is applicable at different water depths, including the run-up regions. In the model, flow resistance can optionally be introduced through the bottom shear stress and the dispersion effect is neglected. From coastal and ocean engineering aspects, water wave propagation to coastal zones directly effects coastal morphology. The obtained water velocity fluxes and elevations which are an important parameter for the force on the structures can easily be tested by interdisciplinary works. A numerical model case study is presented. The method has proved itself to be an efficient method in the sense of the programming effort and the computation times. Therefore the efficiency of the method in terms of programming effort can be attributed to the fact that collocation nodes are placed easily in the regular, irregular and adjustable computation domains. Besides, reduced computation time is also an important issue about the efficiency of the models. Applying different RBF and techniques were found to be a promising method for the long wave propagation and the run-up. Thus the philosophy of this study is to bring a more elaborate, advanced, living model in the future that can be updated and modified by the help of RBF. RBF has the advantages of meshless structure, convergent new technique which decreases computational time, easily formulated for hyperbolic, elliptic and parabolic problems.

ÖZET

UZUN DALGALARININ RADYAL BAZLI FONKSİYON KOLOKASYON METODU İLE MODELLENMESİ

Bu tezde uzun dalga yayılımı için sınırları üzerinde bazı ek koşulları sağlayan derinlik üzerinde ortalaması alınmış hareket ve süreklilik denklemlerinin birlikte çözümleri sunulmuştur. Verimli, kolay, ağsız sayısal, yakınsak yeni bir modelleme tekniği olan radyal bazlı fonksiyon kolakasyon yöntemi kullanılmıştır. Uzun dalga yayılım modeli lineer olmayan sığ su denklemlerini ki bunlar çoğu su derinliklerinde ve hatta tırmanma senaryolarında kullanılmıştır. Model akımına direnç olarak taban sürtünmesi isteğe bağlı eklenebilinir ve modelde yayılım etkisi ihmal edilmiştir. Kıyı ve okyanus mühendisliği açısından, kıyı bölgeleri için su dalga yayılımı doğrudan kıyı morfolojisini etkilemektedir. Yapılar üzerindeki etkisini hesaplamak için önemli bir parametre olan elde edilen su hız ve yükseklikleri kolayca ortak disiplinler arası çalışmalarda ve testlerde kullanılabilinir. Bir sayısal modelleme çalışması bu çalışmada sunulacaktır. Yöntem programla çabası ve hesaplama süreleri açısından kendinin etkili bir yöntem olduğunu kanıtlamıştır. Bu nedenle programlama çabası açışından yöntemin verimliliği kolay yerleştirilen düzenli düzensiz ve ayarlanabilinir kolokasyon noktalarına atfedilebilinir. Ayrıca RBF kullanarak hesaplama sürelerinin azaltılması modelin verimliliği acısından önemli bir konudur. Farklı RBF ve teknikleri uygulanması, uzun dalga yayılımı ve tırmanma problemleri için umut verici bir yöntem olabilir. Dolayısı ile bu çalışmanın felfesefesi; ağsız yapısı kolay adapte methodolojisi, hesaplama süresini azaltan yakınsak yeni bir teknik oluşu, hiperbolik, eliptik ve parabolic problemlerde kolay formüle edilişi, ve kolay ayarlanabilir veya düzensiz alanlarda hesaplamada zaman tasarufu sağlamasıdır.

TABLE OF CONTENTS

LIST OF FIGURES

LIST OF TABLES

LIST OF SYMBOLS

a, b	Time instant
A	Mixing (diffusion) coefficient
A_h	Horizontal Mixing coefficient
A_z	Vertical Mixing coefficient
B	Boundary operator
c	Shape parameter
$c_{1,2}$	Lagrangian coefficients
c_{n+1}	Corrector at n+1
c_w	Wave celerity
d	Total depth
D	Domain operator
f	Coriolis parameter
f^{-1}	Inverse of interpolant matrix
f^x	First derivative of f on the x direction
f^{xx}	Second derivative of f on the x direction
f^y	First derivative of f on the y direction
f^{yy}	Second derivative of f on the y direction
f_{ij}	Basis function, elements of interpolant matrix
F	System matrix
g	Gravitational acceleration
H	Elevation from datum plane
h	Depth
J	Jacobian
$J_{0,1}$	0^{th} and 1^{st} order Bessel function of first kind
k	Wave number
$k_{1,2,3,4}$	RK O(4) evaluations per time step
K	Switch
L	Channel length
L_0	Wave length

p	Pressure
$p()$	Univariate polynomial
p	Predictor at n+1
p_a	Atmospheric pressure
p_o	Hydrostatic pressure
p_{mod}	Modifier
R	Shapiro response function
r	Internodal distance
r_{av}	Average internodal distance
r_{min}	Minimum internodal distance
s	Vertical coordinate below the bottom
S_0^x	Bottom slope along direction x
S_0^y	Bottom slope along direction y
t	Time
T	Wave period
u	Horizontal velocity component
u_i^b	Unknown function
u_z	zero velocity gradient
$\bar{u}$	Depth averaged horizontal velocity component
U_0	Lagrangian velocity
v	Transverse velocity component
$\bar{v}$	Depth averaged transverse velocity component
w	Vertical velocity component
$w_{1,2}$	Sponge Layer damping coefficients
x	x-coordinate
y	y-coordinate
z	z-coordinate
α_j^b	Unknown coefficients at time b
$\alpha_{1,2}$	Sponge layer coefficient
β	Coefficients

χ	Transformed position
η	Free surface elevation with respect to the mean surface level
λ	Variable
∇_h^2	2D Laplace operator
ν	Order of modified Bessel function
ω	Wave frequency
Ω	Earth's angular velocity
Ω_B	Boundary
Ω_D	Domain
ϕ	Function
ϕ^{ext}	Artificial boundary
ρ	Density
σ	Variable
ρ_0	Density of water
τ_b^x	Bottom shear stress along x
τ_b^y	Bottom shear stress along y
τ_s^x	Surface shear stress along x
τ_s^y	Surface shear stress along y
Θ	Latitude
ζ, τ	Transformed coordinates

LIST OF ACRONYMS/ABBREVIATIONS

$1D$	One-dimensional
$2D$	Two-dimensional
$3D$	Three-dimensional
$ABMO(4)$	Adams-Bashforth predictor and Adams-Moulton corrector of 4^{th} order
BBC	Bottom Boundary Condition
BC	Boundary Condition
BEM	Boundary Element Method
$BIEM$	Boundary Integral Equation Method
BVP	Boundary Value Problem
CFL	Courant-Friedrichs-Lewy Condition
$COMCOT$	Cornell Multi-grid Coupled Tsunami Model
FEM	Finite Element Method
FDM	Finite Difference Method
FFT	Fast Fourier Transformation
$FUNWAVE$	Fully Nonlinear Boussinesq Wave Model
FVM	Finite Volume Method
$KFSBC$	Kinematic Free Surface Boundary Condition
GE	Governing Equation
IC	Initial Condition
IVP	Initial Value Problem
LHS	Left Hand Side
$LSWE$	Linear Shallow Water Wave Equation
LU	Lower upper
$MHO(4)$	Milne predictor and Hamming corrector of 4^{th} order
$MOST$	Method of Splitting Tsunami
MQ	Multiquadrics
MWL	Mean Water Level
$NAMIDANCE$	Tsunami Simulation/Visualization Code

NSE	Navier-Stokes Equations
PDE	Partial Differential Equation
RBF	Radial Basis Function
$RBFCM$	Radial Basis Function Collocation Method
RHS	Right Hand Side
$RK\,O(4)$	Runge-Kutta of 4^{th} order
RMS	Root Mean Square
$NSWE$	Nonlinear Shallow Water Wave Equations
SWE	Shallow Water Wave Equations
$TUNAMI - N2$	Tohoku University's Numerical Analysis Model for Investigation of Near-field Tsunami
$TUNAMI - NUS$	Tohoku University's Numerical Analysis Model for Investigation of Near-field Tsunami modified by National University of Singapore
UN	Ursell Number

1. INTRODUCTION

Intensive investigations and significant progresses have been made over the last century in order to accurately predict wave propagation in coastal zones. Due to the complexity of wave motion, accurate prediction still remains a challenge for coastal engineers and scientists. Wave properties, such as the wave heights and the steepness of wave fronts, significantly change as waves propagates towards shores and wave breaking starts to take place in the surf zone.

In order to describe accurately the propagation of waves, it is of necessity to use three-dimensional (3D) spaces. For most of the coastal engineering applications it is convenient to set up approximate two dimensional models that eliminate the vertical dependency. The main reason to establish two-dimensional (2D) models is that 3D models are complex and demand much more computer resources to obtain numerical solutions. In addition to this fact, 2D models are moderately good approximations to 3D models under certain conditions, i.e. small wave amplitude (the linear wave approximation), small water depth (the long wave approximation) and nonlinear models such as Boussinesq models. As a result, many investigations have been concentrated on deriving 2D wave equations and on developing the corresponding 2D numerical solutions. The existing models include the ray tracing and the mild slope model (Berkhoff, 1982) which are based on the linear wave approximation, and the nonlinear shallow water (NSWE) model (Airy, 1845; Lamb, 1945), the Boussinesq models (Boussinesq, 1872; Peregrine, 1967; Madsen *et al.*, 1991; Nwogu, 1993; Wei and Kirby, 1995), the Serre models, the Hamiltonian formulation models, and the Green-Naghdi models, which are based on the long wave approximation. All these models have been shown to be successful in determining wave properties accurately when applied within their ranges of validity. These models can describe, to varying degrees of accuracy in representing nonlinearity and dispersion, most phenomena exhibited by non-breaking waves in finite depths.

Airy's theory (1845) or the NSWE model is the earliest approximate model to describe the propagation of waves in the shallow water regions. The basic assumption for the model is that the dispersion effect is negligibly small; however, there is no restriction on the nonlinearity. Among the approximate long wave models, the set of governing equations for the NSWE model has the simplest form. However, the model works quite well for the condition that the ratio of the water depth to wave length is small, such as in the surf zone and swash zone where the water depth is extremely small or for simulating tides, tsunamis, and infra-gravity waves whose wave lengths are quite large. These flows display a 3D structure due to bottom friction and density stratification. Early numerical model, owing perhaps to limitations in computing capability, were mostly based on the Airy (1845) theory wherein the pressure distribution in the vertical is assumed to be hydrostatic. This approximation is known as the Boussinesq approximation and is also part of many modern models.

A wide variety of problems, such as atmospheric flows (Charney*et al.*, 1950), tidal flows (Hendershott, 1981), tidal mixing (Ridderinkhof, 1990), residual currents (Nihoul and Ronday, 1975), storm surges (Dube *et al.*, 1985), flows around structures (Stelling, 1983), dam break waves (Alcrudo and Garcia-Navarro, 1993), river (Ogink *et al.*, 1986) and coastal currents (Wind and Vreugdenhil, 1986), lake currents (Simons, 1980), tsunamis (Shokin and Chubarow, 1980), internal waves (Garvine, 1987) and planetary flows (Dowling and Ingersoll, 1989), can be modeled using the shallow water equations (SWEs).

In the near shore region, where the relative water depth is shallow, the wave amplitude may be large and the wave becomes nonlinear. The nonlinearity becomes increasingly dominant with decreasing water depth. Hence, numerical models based on the linear wave theory will not provide an accurate simulation of near shore wave phenomena.

With the availability of advanced computing facilities, numerical model has become an attractive means of studying wave propagation and transformation. The shift from physical modeling towards numerical modeling has resulted in rapid developments

of numerical methods for solving water wave equations. The greatest advantage of the numerical model over the physical model is its ability to determine the required information at a much shorter period with a comparatively larger degree of accuracy. Different from numerical modeling, physical modeling needs more cost, space and staff for the set up. The same numerical model may also be used repeatedly on different problems with only some minor modifications of boundary conditions, bathymetry and incident wave condition.

This study is mainly concerned with the development of a meshless numerical model to solve incompressible water wave motion based on the NSWE. Based on SWE wave models are applicable where the water depth is much less than the horizontal scale of motion. They are used to model tides, tsunamis and surges in coastal areas. Thus, the main aim of this thesis is to develop and validate a numerical model to accurately model NSWE flow in domains with fixed boundaries i.e. sponge layer treatment and domains with moving boundaries.

NSWE models are simultaneous nonlinear partial differential equation models representing conservation of mass and conservation of momentum. In some circumstances to perform a simulation and stability analysis, the NSWE can be linearized. Analytical solutions of the linearized shallow water (LSWE) wave models have been found only for a small number of domains of simple geometric shape. As coastal domains do not have simple geometric shapes, analytical solutions do not, in general, exist. For coastal domains, there is only limited experimental data in order to test numerical solutions and for domains of flow without exact solutions the equations must be approximately solved by numerical methods. Also, analytical solutions for domains of flow with simple geometric shapes are very useful for testing numerical solutions.

There exist analytical solutions of both LSWE (Lamb, 1945, Ippen, 1966, Lynch and Gray, 1978) and NSWE (Airy, 1845) for domains with fixed boundaries. Also, there exist analytical moving boundary solutions NSWE (Carrier and Greenspan, 1958). None of the moving boundary solutions contain friction.

Some analytical solutions of the one-dimensional (1D) NSWE for a basin with a horizontal bed and constant rectangular cross section will be used in this thesis; the basin is closed at one end and at the other end has an open sea boundary, at which there is sinusoidal forcing.

The developed meshless numerical model is coded in Fortran'90 and validated both against analytical solutions for flow in a basin of constant depth and in a basin of linearly varying depth. In this thesis a convergence study of the model is carried out for a rectangular basin of linearly varying depth using analytical solutions of the one dimensional linear shallow water wave equations.

The structure of this thesis is outlined below. Chapter 2 presents the literature review of thesis. Chapter 3 presents the mathematical background of the model flow. The governing equations of the 2D NSWE and its derivation are given in detail. Chapter 4 presents the numerical model of the flow is investigated. RBF interpolation and RBFCM are reviewed. Numerical formulation by RBF, boundary and initial conditions and time marching types are presented in details. The model's solution strategy and convergence also given in Chapter 4. In Chapter 5, fixed and moving boundary analytical solutions reviewed. Theoretical development of the long wave propagation and run-up model on a sloping beach for case studies 1 and 2 is given. Long wave propagation problems in 1D and 2D with sponge treatment are given in case studies 3 and 4. In Chapter 6 the conclusions of this thesis are presented with suggestions for further research.

2. LITERATURE REVIEW

The linear water wave theory is based on the assumptions that the wave amplitude be everywhere small compared with the water depth. Nevertheless this cannot be true around shoreline where water depth is close to zero, therefore linear theory is not a good approximation around shoreline. This is because the wave speed from linear theory approaches to zero when wave propagates from deep water to the shoreline and finally, the waves gets reflected from the bottom, run up the beach as long as its momentum is nonzero and run-up stopped at the point where its momentum is zero. There is no run-up and run-down process on the beach for linear theory which is not a physical reality. The reason for this nonphysical result is that nonlinear effects are neglected. When including nonlinear terms, the wave speed never reaches to zero at the real shoreline point thus observing wave running up and down on the beach, instead of stopping at the nonmoving shoreline. In nonlinear theory, the run-up is defined on the physical ground neglecting only the viscous effects by the wave elevation.

The physical picture for the longshore variations of run-up due to oblique incidence upon beaches is a 3D problem. The run-up of waves normally incident upon beaches is 2D, x and z. The governing equations for the (x,t) domain formulation for normal incidence is a special case and have one space, x and one time, t. Due to the difficulties of capturing the moving shoreline of this nonlinear problem, results to only few analytic studies have been reported since the 1950's. Analytical solutions to problems of nonlinear wave run-up on planar beaches exist only for the special case of 2D (x,t) waves disregarding dispersion and other effects.

Some planar beach problems of run-up have also been investigated. Carrier and Greenspan (1958) presents an elegant analytical solution, Carrier (1966) and Tuck and Hwang (1972) introduce a cunning transformation to map the NSWE into a linear form, Spievogel (1975) apply Carrier and Greenspan's theory. Many studies in the literature from a mathematical point of view, is the extension of the Carrier and Greenspan (1958) transformation used early in the theory of water waves.

In addition to these studies, Synolakis (1987) developed an approximate nonlinear theory for the run-up of solitary waves by introducing a matching condition at the junction of a sloping plane beach and exterior uniform ocean. Synolakis' conclusion which is made under linear wave assumption, is that the maximum run-up predicted by the nonlinear theory is identical with the maximum run-up predicted by the linear theory. The SWEs do not have solutions for prorogating wave of permanent form, even in water of uniform depth. A solitary wave continuously becomes more steepened forward as computation time goes on for the lack of dispersive effects to balance out the wave steepening according to this model. One and a half decade ago, Li and Raichlen (1999) have found a nonlinear correction to Synolakis's formula for which nonbreaking waves on beaches decreases as the beach slope steepens.

In three dimensions (2+1), Carrier and Noiseux (1983), based on LSWE theory, analyzed the reflection of a long wave obliquely incident on sloping plane beach. Later, Borcchini and Peregrine (1996) introduce a weakly nonlinear theory for calculating run-up at small angles of incidence. In 1998, Kanoğlu and Synolakis presented long wave evolution and run-up on piecewise linear 1D and 2D bathymetries with a numerical model of LSWEs.

In numerical studies, the difficulty is capturing moving shoreline on sloping beaches. This has been undertaken popularly by moving boundary from wet grid to dry grid or by extrapolation in time steps.

Numerical treatments of shoreline starts with Hibberd and Peregrine (1979) who studied the run-up of a sloping beach by using the finite difference method to compute numerical solutions of the SWE. Gaining information around the shoreline is mainly achieved by linear extrapolation which is not physical and introduces considerable errors.

Long-wave equations in the Lagrangian description which account for weakly nonlinear and dispersive processes for wave propagation not to avoid the moving shoreline difficulty is used by Pedersen and Gjevik (1983), Zelt (1986, 1991) and Zelt and

Raichlen (1990). This approach produces additional nonlinear terms in the basic governing equations which makes the solution more difficult.

Assuming potential theory and using the finite difference method (FDM), finite element method (FEM) or the boundary integral equation method (BIEM), the run-up problem was solved by Kim *et al.*, (1983), Grilli (1997) and Grilli *et al.*, (1997). In the Kim *et al.*, (1983) study, the whole free surface including the shoreline becomes a moving boundary. The BIEM solutions are 2D. Their achievement in resolving nonlinear effects is noteworthy.

Titov and Synolakis (1995) treated the shoreline by adding an artificial relation which is not physical. This term, zero velocity gradient (u_z=0) introduces some considerable error in the computation of run-up.

Tuba Ozkan-Haller and Kirby (1997) present, a Fourier-Chebyshev collocation method for the SWE in resolving a problem of periodic 3D shoreline run-up for normal incidence of ocean waves on periodically curved beach, yielding noteworthy results.

In experimental studies, Hall and Watts (1953) investigated the vertical rise of solitary waves on impermeable slopes. Synolakis (1987) updated Hall and Watts's (1953) maximum run-up data. Yeh *et al.*, (1989) introduce bore propagation near the shoreline on a uniform sloping beach. Zelt (1991) studied the run-up of nonbreaking and breaking solitary waves on plane beaches. Liu *et al.*, (1995) presented a series of large scale laboratory experiments on the interactions of solitary waves climbing up a circular island. Li and Raichlen (1999) applied advanced technologies to their laboratory measurements of wave evolution.

In summary, the literature seems to have focused on the NSWE for modeling 2D ocean waves on shelves and beaches (Liu *et al.*, 1995) while disregarding the geometry of the third dimension and the dispersive effects.

When the nonlinear effects are taken into consideration, the exact governing equations for determining a moving inviscid shoreline are introduced based on the local Lagrangian coordinates. A numerical scheme has been applied for the efficient evaluation of these governing equations by Zhang (1996). Zhang's scheme is shown to accurately approximate the analytic solution of the shallow water equations. The maximum run-up of solitary wave predicted in the Zhang's study (1996) by the SWE depends on the initial location of the solitary wave. The maximum run-up of solitary wave changes in value because of the fact that the wave becomes increasingly more steepened in the absence of dispersive effects in the long travel time. It is larger than that predicted by linear long wave theory. For this reason, the dispersive effects are important especially in 2D problems to keep nonlinear effects balanced at the equilibrium and tend to reduce the run-up. Thus, the main objective is to have the first principles of coastal physics well understood for this ideal case without the additional effects of dispersion and dissipation (including wave breaking, bottom friction, wind stress, Coriolis effects, etc., as energy sources and sinks). These additional effects need to be taken into account in further studies since these effects become significant at least around the moving shoreline where the water depth vanishes. Hence, linear run-up theory has validity, even though it cannot predict, equally accurately as nonlinear theory of the transient wave profiles near the moving shoreline and the time for reaching maximum run-up.

Throughout the history of long wave investigations or tsunami investigations, various approaches were used to determine the hydrodynamics by laboratory experiments, analytical calculations and numerical computations. Numerical modeling of propagation and run-up is widely studied by many researchers. There are different approaches in terms of the algorithms used in numerical models. The analysis are performed by numerical modeling by applying valid calculation theories. It is necessary and essential to validate and verify the numerical modeling tool before analyzing the wave motion. Some studies including numerical modeling approaches and validation and verification of numerical models are given in the following;

For the propagation of waves; many numerical models are used to make short-term and long-term predictions for academic and operational purposes. Among these, the most commonly used numerical models are the Cornell Multi-grid Coupled Tsunami Model (COMCOT) (Liu *et al.*, 1994; 1998), Tohoku University's Numerical Analysis Model for Investigation of Near-field Tsunami (TUNAMI-N2) (Imamura, 1995) and Method of Splitting Tsunami (MOST) (Titov and Synolakis, 1998). These three models solve NSWE using the FDM. There are also models developed at the using the FVM such as HyFlux2 that is used by the European Commission Joint Research Center for tsunami forecasting and warning all over the world (Franchello and Krausmann, 2008). COMCOT, TUNAMI-N2 and MOST have been validated at National Science Foundation workshop in Catalina Island in 1995 and 2004 by comparing their results with benchmark problems. These three codes were the only ones that can solve wave motions in 2D at that time (Synolakis and Bernard, 2006).

TUNAMI-N2 and Tsunami Simulation/Visualization Code (NAMIDANCE), which were originally authored for the Tsunami Inundation Modeling Exchange (TIME) program under the supervision of United Nations Educational, Scientific and Cultural Organization (Goto *et al.*, 1997; Shuto *et al.*, 1990; Imamura, 1989) in Disaster Control Research Center, Tohoku University in Sendai, Japan, was modified, improved and registered in United States of America granting copyright to Professors Imamura, Yalciner and Synolakis in 2000 (Yalçıner *et al.*, 2001; Yalciner *et al.*, 2002; Yalçıner *et al.*, 2003; Yalçıner *et al.*, 2004; Kurkin *et al.*, 2003; *Zahibo et al.*, 2003; Zaitsev *et al.*, 2002; Zaitsev *et al.*, 2008; Özer *et al.*, 2008, 2011; Yalçıner *et al.*, 2010, 2012).

The numerical modeling has been continuously improved, and now it is one of the most operative tools used for the prediction of hazards (Shuto, 1991). The computations are principally based on the long wave theory (Shuto, 1991). Shuto (1991) compared the numerical results of three long wave theories in deep water to discuss the dispersion effects on propagation: linear Boussinesq, Boussinesq and linear long wave.

Kirby (1996) investigated dispersive long waves in water of variable depth and Shi *et al.*, (2012) describe the theory and numerical implementation of a fully nonlinear

Boussinesq wave model called Fully Nonlinear Boussinesq Wave Model (FUNWAVE) which is a phase-resolving, time-stepping Boussinesq model for ocean surface wave propagation in the nearshore.

Imamura (1995) described a method of setting initial and boundary conditions of the linear long wave theory and asserted that long travel distance may yield dispersion of wave components, and therefore physical dispersion term should be included, i.e. the equations of higher order approximation should be used.

Sato (1996) reports a numerical simulation of long wave propagation for the 1993 Southwest Hokkaido earthquake tsunami. The model is based on the Boussinesq equation, which includes the effects of frequency dispersion. Energy dissipation due to breaking at the tsunami wave front is modeled. The validity of the model was tested with the existing laboratory data of dispersive wave trains breaking on a slope. The model was then applied to the simulation of the 1993 Southwest Hokkaido earthquake tsunami around the southern part of Okushiri Island. Comparison with the physical model demonstrates that it is the dispersion of the wave front which caused focusing of the wave energy at the narrow region on the lee side of the island, consequently increasing the tsunami height.

One of the most comprehensive studies about numerical modeling is Synolakis and Bernard (2006) which collect and summarize the approaches for long wave numerical calculations. They emphasize the improvements in simulations by numerical modeling after the devastating 2004 Sumatra tsunami.

Yalçıner and Synolakis give a brief review of generation, propagation and coastal amplification of tsunamis (in Sumer *et al.*, 2007).

Dao and Tkalich (2007) studied the sensitivity of the modified version of the numerical model TUNAMI-N2 considering astronomic tide, sea bottom friction, dispersion, Coriolis force, and spherical curvature by modeling the 2004 Sumatra event as the tsunami scenario. The code was modified and the resulting version is called

TUNAMI-N2-NUS which solve NSWE. The code uses the Boussinesq Equations when the dispersion effect is considered.

The validation and verification of tsunami numerical models are essential if the outputs of the models will be used by governmental policies in emergency evacuation planning. Synolakis *et al.*, (2008) discussed analytical, laboratory and field benchmark tests with which tsunami numerical models can be validated and verified. The benchmark tests are described in detail as well as their expected solutions. They also discuss the scientific and operational evaluation of the model and the necessity of continuous validation and verification processes in the case that new knowledge and data are acquired. It is emphasized that operational tsunami models have to be tested after each tsunami event with real time data for hind casting.

Besides numerical modeling, there are various studies regarding the analytical solutions of tsunami propagation and run-up most of which are tested and compared with the results of laboratory experiments. The analytical solutions of tsunamis are reviewed and some of the studies in literature are summarized in the following.

One of the earliest analytical solutions of tsunami motion is that of Thacker (1981) which introduced some exact solutions of the NSWE. The exact solutions correspond to time-dependent motions in parabolic basins and the shoreline is assumed to move freely. Thacker provided a solution for a flood wave if the parabolic basin is reduced to a planar one. These exact solutions provide a valuable comparison test for numerical models. It is also emphasized that since the numerical integration of NSWE with the required assumptions is not easy, it is more practical to use the analytical solutions.

Liu *et al.*, (1995) investigated run-up of solitary waves on a circular island. They studied the interactions of solitary waves climbing up a circular island and carried out a series of large-scale laboratory experiments with waves of different incident height-to-depth ratios and different crest lengths. They also developed a numerical model based on the 2D SWE including run-up calculations. Under certain conditions, they observed run-up and wave trapping on the back side of the island.

Kanoğlu and Synolakis (1998) investigated long wave run-up on piecewise linear topographies and developed a general solution method for determining the amplification factor of different ocean topographies consisting of linearly varying and constant-depth segments to study how spectral distributions evolve over bathymetry. They used their results to study the evolution of solitary waves.

Kanoğlu (2004) solved the initial value problem of the nonlinear evolution, shoreline motion and flow velocities of long waves climbing sloping beaches analytically for different initial wave forms. He proposed that any initial wave form can first be represented in the transformation space by the linearized form of the Carrier-Greeenspan transformation for the spatial variable, and then the nonlinear evolutions of these initial waveforms can be directly evaluated. After the necessary transformations, he introduced a simplified equation for the calculation of run-up/run-down motion of the shoreline. This approach is applied to Gaussian and leading-depression N-wave initial forms presented by Carrier *et al.*, (2003), and the results are compared. Kanoğlu (2004) concluded that his study is simpler than that of Carrier *et al.*, (2003) and produces identical results since his analysis does not need to solve singular elliptic integrals. He also suggested that, based on the convenience of NSWE for the quantitative and qualitative predictions, the method outlined in his study may be useful to assess the impact of long waves generated by seafloor displacements and to validate numerical codes.

The above mentioned method described in Kanoğlu (2004) is also applied to different N-wave initial forms, such as leading-depression isosceles N-wave and generalized N-wave initial forms. Tadepalli and Synolakis (1994) use a first-order theory for the N-wave forms and derive asymptotic results for the maximum run-up. They stated that a class of N-shaped waves was found in their study with very interesting behavior which is said to be a new phenomenon for tsunami run-up studies. Similar trends were observed by Tadepalli and Synolakis (1994) in their maximum run-up results.

3. THE MATHEMATICAL MODEL OF THE FLOW

3.1. Background

Starting from the mathematical description of the physical phenomena the mathematical statement of fundamental physical principles results in differential equations. In fluid flow calculations, differential equations express a certain conservation principle and each equation embodies a certain physical quantity as its depended variable, like velocity or mass fraction and implies a balance between the various factors that has an effect on the variable. One of the problems of physics and engineering is the propagation problem. Propagation problems are initial boundary value problems that have an unsteady state and the subsequent behavior of a system given the initial state that needs to be predicted. The governing equations for a well-posed propagation problem are parabolic or hyperbolic.

The Navier-Stokes equations (NSE) are derived from the general principle of mass and momentum conservation that is able to describe any type of fluid flow including water waves. Without a hydrostatic pressure assumption and with the inclusion of a proper turbulence model, it is possible for an NSE model to simulate difficult wave problems, e.g., wave-structure interactions, wave-current interactions, and breaking or nonbreaking waves. With almost no theoretical limitation, this type of model seems to be the best choice. However, the main barrier that prevents the wide application of such a model is the expensive computational effort. Thus it is restricted to the simulation of local wave phenomena near the location of interest. To solve this expensive computational effort, depth averaged models such as Wave spectral models, Mild-slope equation wave models, Quasi-three-dimensional hydrostatic pressure wave models, Boussinesq equation wave models or SWE wave models need to be established rather than deep varying ones according to their modeling capability and validity.

To model long waves, SWE model is more likely to be adopted. Compared with the Boussinesq model, the SWE model is simpler because the flow is assumed to be

uniform across the water depth and the wave-dispersive effect is neglected. The SWE model has a wide application range in modeling tsunami, tides, storm surges, and river flows. The main limitation of the SWE model is that it is suitable only for flows whose horizontal scale is much larger than vertical scale.

3.2. Governing Equations of the System

In the fluid flow research, the physical phenomena are represented by the conservation of mass and momentum. In the most general case the NSE are the governing differential equations. Representing the fluid flow, The SWE are derived from these equations under some assumptions and relevant theory. The assumptions considered in deriving the SWE can be summarized as follows.

First assumption, the fluid is well-mixed vertically with a hydrostatic pressure gradient. The vertical acceleration is dominated by gravity, so that the vertical pressure profile is hydrostatic. The pressure at the surface of the fluid is atmospheric. Secondly, the density of the fluid is constant and large salinity variations or temperature variations in the vertical direction would cause a variable density. Thirdly, water waves of long wave lengths are studied. Short wave phenomena where vertical acceleration is important cannot be modeled. Last assumption, the viscosity term is negligible. Kinnmark (1989), referring to Dronkers (1964), stated that the viscosity term is often physically negligible.

3.2.1. Three Dimensional Equations

To determine the calculation in water bodies, one need to solve the set of time averaged momentum and continuity equations derived from the Reynolds-averaged NSEs (Kowalik and Murty, 1993) in rectangular system of coordinates given by

$$\frac{Du}{Dt} - fv = -\frac{1}{\rho}\frac{\partial p}{\partial x} + A\nabla^2 u \tag{3.1}$$

$$\frac{Dv}{Dt} + fu = -\frac{1}{\rho}\frac{\partial p}{\partial y} + A\nabla^2 v \tag{3.2}$$

$$\frac{Dw}{Dt} = -\frac{1}{\rho}\frac{\partial p}{\partial z} - g + A\nabla^2 w \tag{3.3}$$

$$\frac{\partial \rho}{\partial t} + \frac{\partial}{\partial x}(\rho u) + \frac{\partial}{\partial y}(\rho v) + \frac{\partial}{\partial z}(\rho w) = 0 \tag{3.4}$$

where u, v and w are the mean velocity components in x-y- and z- directions, respectively, A is mixing (diffusion) coefficient, p is the pressure and ρ is the density. The operator D/Dt is the material derivative.

$$\frac{D}{Dt} = \frac{\partial}{\partial t} + u\frac{\partial}{\partial x} + v\frac{\partial}{\partial y} + w\frac{\partial}{\partial z} \tag{3.5}$$

In these equations, the Coriolis parameter,

$$f = 2\Omega \sin\Theta \tag{3.6}$$

is a function of the earth's angular velocity $\Omega = 7.29 * 10^{-5} s^{-1}$ and the latitude, Θ.

Considering the fact that the horizontal dimensions of the water body are usually much larger than its vertical dimensions, for oceanic flows, the mixing (diffusion) term is split into horizontal and vertical mixing terms as

$$\begin{aligned} A\nabla^2 u &= A_h \nabla_h^2 u + A_z \tfrac{\partial^2 u}{\partial z^2} \\ A\nabla^2 v &= A_h \nabla_h^2 v + A_z \tfrac{\partial^2 v}{\partial z^2} \end{aligned} \tag{3.7}$$

where the parameters A_h and A_z are the horizontal and vertical mixing coefficients,

respectively, and the 2D Laplace operator defined as,

$$\nabla_h^2 = \frac{\partial^2}{\partial x^2} + \frac{\partial^2}{\partial y^2} \tag{3.8}$$

Therefore from Equation 3.1 to Equation 3.3 can be rewritten as

$$\frac{\partial u}{\partial t} + u\frac{\partial u}{\partial x} + v\frac{\partial u}{\partial y} + w\frac{\partial u}{\partial z} - fv = -\frac{1}{\rho}\frac{\partial p}{\partial x} + A_z\frac{\partial^2 u}{\partial z^2} + A_h\nabla_h^2 u \tag{3.9}$$

$$\frac{\partial v}{\partial t} + u\frac{\partial v}{\partial x} + v\frac{\partial v}{\partial y} + w\frac{\partial v}{\partial z} + fu = -\frac{1}{\rho}\frac{\partial p}{\partial y} + A_z\frac{\partial^2 v}{\partial z^2} + A_h\nabla_h^2 v \tag{3.10}$$

$$\frac{\partial w}{\partial t} + u\frac{\partial w}{\partial x} + v\frac{\partial w}{\partial y} + w\frac{\partial w}{\partial z} = -\frac{1}{\rho}\frac{\partial p}{\partial z} - g + A_z\frac{\partial^2 w}{\partial z^2} + A_h\nabla_h^2 w \tag{3.11}$$

The hydrostatic approximation is only related to the vertical component of the equation of the motion, Equation 3.3 or Equation 3.11. If the flow is considered to be predominantly horizontal and the vertical acceleration is small compared to the gravitational acceleration, such as in coastal and estuarine-flows, the equation of vertical motion can be reduced to the hydrostatic law (Proudman, 1953) and becomes

$$-\frac{1}{\rho}\frac{\partial p}{\partial z} - g = 0 \tag{3.12}$$

Equation 3.12 indicates that the pressure variation in the vertical direction is hydrostatic. When we assume that the pressure at the surface is only atmospheric, the solution to Equation 3.12 simply is

$$p - p_a = \rho g\,(\eta - z) \tag{3.13}$$

where p_a is the atmospheric pressure.

Although the vertical acceleration was assumed to be negligible and the vertical equation has been reduced to the equation of hydrostatic, the vertical velocity still can be calculated from Equation 3.4, the equation of continuity. Substitution of these results into Equation 3.9 and Equation 3.10, the system of equations with hydrostatic approximation yields

$$\frac{Du}{Dt} - fv = -\frac{1}{\rho}\left(\frac{\partial p_a}{\partial x}\right) - g\frac{\partial \eta}{\partial x} + \frac{1}{\rho}\left(\frac{\partial}{\partial z}A_z\frac{\partial u}{\partial z} + A_h\nabla^2 u\right) \tag{3.14}$$

$$\frac{Dv}{Dt} + fu = -\frac{1}{\rho}\left(\frac{\partial p_a}{\partial y}\right) - g\frac{\partial \eta}{\partial y} + \frac{1}{\rho}\left(\frac{\partial}{\partial z}A_z\frac{\partial u}{\partial z} + A_h\nabla^2 u\right) \tag{3.15}$$

The SWE are composed of the depth integrated horizontal components of the momentum equation and the continuity equation. Both the sea surface

$$z = \eta(x, y, t) \tag{3.16}$$

and the sea bottom

$$z = -h(x, y, t) \tag{3.17}$$

may in general be functions of x, y and t as seen in Figure 3.1. At both the sea surface and at the bottom, kinematic boundary conditions must be satisfied. Differentiating these expressions in time one can obtain the boundary conditions. The Kinematic free surface boundary condition (KFSBC) which states a fluid particle remains on the free surface, meaning, the free surface is a sharp boundary between the two fluids with no flow through it, has been used as a boundary condition and gives,

$$w\left(\eta\right) = \frac{d\eta}{dt} = \frac{\partial \eta}{\partial t} + \frac{\partial \eta}{\partial x}\frac{\partial x}{\partial t} + \frac{\partial \eta}{\partial y}\frac{\partial y}{\partial t} = \frac{\partial \eta}{\partial t} + u\frac{\partial \eta}{\partial x} + v\frac{\partial \eta}{\partial y} \tag{3.18}$$

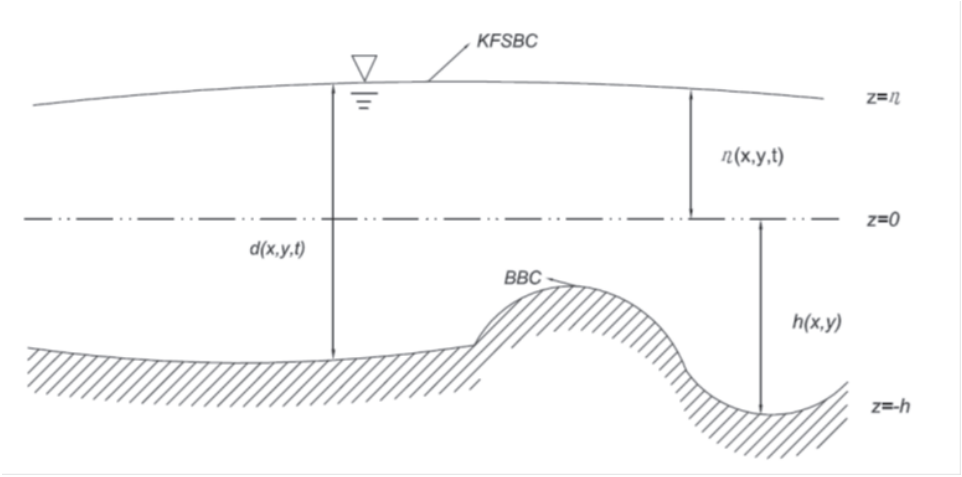

Figure 3.1. Cross Section of a Water Body.

Thus, the forces acting on the fluid at the free surface are in equilibrium known as the momentum conservation or the dynamic condition at the free surface. At the bottom the kinematic bottom boundary condition (BBC) which requires that the flow be parallel to the bottom becomes,

$$w\left(\eta\right)=\frac{d\eta}{dt}=\frac{\partial\eta}{\partial t}+\frac{\partial\eta}{\partial x}\frac{\partial x}{\partial t}+\frac{\partial\eta}{\partial y}\frac{\partial y}{\partial t}=\frac{\partial\eta}{\partial t}+u\frac{\partial\eta}{\partial x}+v\frac{\partial\eta}{\partial y} \tag{3.19}$$

The depth averaged form of the continuity equation is obtained by integrating three dimensional continuity Equation 3.4 over depth using the Leibnitz Rule (Appendix A) for changing the order of differentiation and integration in the second and third integrals and direct evaluation of the first and last integrals yields

$$\int_{-h}^{\eta}\frac{\partial\rho}{\partial t}dz=\frac{\partial}{\partial t}\int_{-h}^{\eta}\rho dz \tag{3.20}$$

$$\int_{-h}^{\eta}\frac{\partial(\rho u)}{\partial x}dz=\frac{\partial}{\partial x}\int_{-h}^{\eta}\rho u dz-\rho u\frac{\partial\eta}{\partial x}\bigg|_{z=\eta}-\rho\,u\frac{\partial h}{\partial x}\bigg|_{z=-h} \tag{3.21}$$

$$\int_{-h}^{\eta} \frac{\partial(\rho v)}{\partial y} dz = \frac{\partial}{\partial y} \int_{-h}^{\eta} \rho v dz - v\rho \frac{\partial \eta}{\partial y}\bigg|_{z=\eta} - \rho v \frac{\partial h}{\partial y}\bigg|_{z=-h} \tag{3.22}$$

$$\int_{-h}^{\eta} \frac{\partial(\rho w)}{\partial z} dz = \rho \left(w|_{\eta} - w|_{-h} \right) \tag{3.23}$$

Using the boundary conditions given in Equation 3.18 and Equation 3.19, the depth average continuity equation becomes

$$\begin{aligned} &\int_{-h}^{\eta} \left(\tfrac{\partial \rho}{\partial t} + \tfrac{\partial(\rho u)}{\partial x} + \tfrac{\partial(\rho v)}{\partial y} + \tfrac{\partial(\rho w)}{\partial z} \right) dz = \tfrac{\partial}{\partial t} \int_{-h}^{\eta} \rho dz + \tfrac{\partial}{\partial x} \int_{-h}^{\eta} \rho u dz + \tfrac{\partial}{\partial y} \int_{-h}^{\eta} \rho v dz \\ &+ \underbrace{\rho \left[w - \frac{\partial \eta}{\partial t} - u\frac{\partial \eta}{\partial x} - v\frac{\partial \eta}{\partial y} \right]_{z=\eta}}_{=0(KFSBC)} \underbrace{- \rho \left[w + \frac{\partial h}{\partial t} + u\frac{\partial h}{\partial x} + v\frac{\partial h}{\partial y} \right]_{z=-h}}_{=0(BBC)} = 0 \end{aligned} \tag{3.24}$$

or

$$\frac{\partial}{\partial t} \int_{-h}^{\eta} \rho dz + \frac{\partial}{\partial x} \int_{-h}^{\eta} \rho u dz + \frac{\partial}{\partial y} \int_{-h}^{\eta} \rho v dz = 0 \tag{3.25}$$

For an incompressible fluid, the density is constant over the depth, knowing that we talk about a vertically well-mixed fluid phenomenon, and if we define depth averaged quantities in the following manner,

$$\bar{u} = \frac{1}{d} \int_{-h}^{\eta} u dz \qquad \bar{v} = \frac{1}{d} \int_{-h}^{\eta} v dz \tag{3.26}$$

where $d = h + \eta$ than Equation 3.25 integrates to

$$\frac{\partial}{\partial t}(h + \eta) + \frac{\partial}{\partial x} \left[\bar{u}(h + \eta) \right] + \frac{\partial}{\partial y} \left[\bar{v}(h + \eta) \right] = 0 \tag{3.27}$$

where $\bar{u}$ and $\bar{v}$ are the depth averaged values of u and v respectively.

Equation 3.27 can be written by dropping the overbars and the final form of the continuity equation in water bodies is obtained

$$\frac{\partial d}{\partial t} + \frac{\partial \left(ud\right)}{\partial x} + \frac{\partial \left(vd\right)}{\partial y} = 0 \tag{3.28}$$

The vertically averaged forms of momentum equations are obtained by a series of virtually identical steps. For the sake of brevity the specific arguments will be applied only to Equation 3.14 with the integrated form of Equation 3.15 deduced by analogy. Starting with the left hand side (LHS) of the x-component of the momentum equation, with a constant ρ is

$$LHS = \int_{-h}^{\eta} \frac{\partial u}{\partial t} dz + \int_{-h}^{\eta} u \frac{\partial u}{\partial x} dz + \int_{-h}^{\eta} v \frac{\partial u}{\partial y} dz + \int_{-h}^{\eta} w \frac{\partial u}{\partial z} dz - \int_{-h}^{\eta} fv dz \tag{3.29}$$

and application of Leibnitz' rule to the local acceleration we have

$$\int_{-h}^{\eta} \frac{\partial u}{\partial t} dz = \frac{\partial}{\partial t} \int_{-h}^{\eta} u dz - u|_{\eta} \frac{\partial \eta}{\partial t} - u|_{-h} \frac{\partial h}{\partial t} \tag{3.30}$$

Noting that

$$u\frac{\partial u}{\partial x} = \frac{\partial u^2}{\partial x} - u\frac{\partial u}{\partial x}, \quad v\frac{\partial u}{\partial y} = \frac{\partial (uv)}{\partial y} - u\frac{\partial v}{\partial y} \quad \text{and} \quad w\frac{\partial u}{\partial z} = \frac{\partial (uw)}{\partial z} - u\frac{\partial w}{\partial z} \tag{3.31}$$

Application of Leibnitz' rule to the first two convective acceleration terms in Equation 3.14 are transformed as,

$$\int_{-h}^{\eta} u \frac{\partial u}{\partial x} dz = \frac{\partial}{\partial x} \int_{-h}^{\eta} u^2 dz - \int_{-h}^{\eta} u \frac{\partial u}{\partial x} dz - u^2\Big|_{\eta} \frac{\partial \eta}{\partial x} - u^2\Big|_{-h} \frac{\partial h}{\partial x} \tag{3.32}$$

$$\int_{-h}^{\eta} v \frac{\partial u}{\partial y} dz = \frac{\partial}{\partial y} \int_{-h}^{\eta} uv dz - \int_{-h}^{\eta} u \frac{\partial v}{\partial y} dz - (uv)|_{\eta} \frac{\partial \eta}{\partial y} - (uv)|_{-h} \frac{\partial h}{\partial y} \tag{3.33}$$

and the direct integration for the last convective acceleration term is

$$\int_{-h}^{\eta} w\frac{\partial u}{\partial z}dz = -\int_{-h}^{\eta} u\frac{\partial w}{\partial z}dz + (uw)|_{\eta} - (uw)|_{-h} \tag{3.34}$$

The combination of the convective horizontal terms from Equation 3.32 to Equation 3.34 is

$$\begin{gathered} \frac{\partial}{\partial t}\int_{-h}^{\eta} u dz + \frac{\partial}{\partial x}\int_{-h}^{\eta} u^2 dz + \frac{\partial}{\partial y}\int_{-h}^{\eta} uv dz \\ -u|_{\eta}\underbrace{\left(-w + \frac{\partial \eta}{\partial t} + u\frac{\partial \eta}{\partial x} + v\frac{\partial \eta}{\partial y}\right)}_{=0(KFSBC)} - u|_{-h}\underbrace{\left(-w + \frac{\partial h}{\partial t} + u\frac{\partial h}{\partial x} + v\frac{\partial h}{\partial y}\right)}_{=0(BBC)} \\ -\int_{-h}^{\eta} u\underbrace{\left(\frac{\partial u}{\partial x} + \frac{\partial v}{\partial y} + \frac{\partial w}{\partial z}\right)}_{=0(continuity)} dz \end{gathered} \tag{3.35}$$

The term in this equation multiplied with $u(\eta)$ is zero by the KFSBC, Equation 3.18 and the term multiplied with $u(-h)$ is zero by the BBC, Equation 3.19. The last term in Equation 3.35 is zero since the term in the brackets is the continuity Equation 3.4. The LHS of Equation 3.14 may now be written as

$$LHS = \frac{\partial}{\partial t}\int_{-h}^{\eta} u dz + \frac{\partial}{\partial x}\int_{-h}^{\eta} u^2 dz + \frac{\partial}{\partial y}\int_{-h}^{\eta} uv dz - \int_{-h}^{\eta} fv dz \tag{3.36}$$

where the additional depth averaged quantity is defined in the following manner,

$$\bar{u}\bar{v} = \frac{1}{d}\int_{-h}^{\eta} uv dz \tag{3.37}$$

Then, LHS of the equation is

$$LHS = d\left(\frac{\partial \bar{u}}{\partial t} + \bar{u}\frac{\partial \bar{u}}{\partial x} + \bar{v}\frac{\partial \bar{u}}{\partial y} - f\bar{v}\right) \tag{3.38}$$

The integration of the right hand side (RHS) of the x-component of the momentum is

as follows

$$RHS = \int_{-h}^{\eta} \frac{1}{\rho}\frac{\partial p_a}{dx}dz - \int_{-h}^{\eta} g\frac{\partial \eta}{dx}dz + \int_{-h}^{\eta} \frac{\partial}{dz}A_z\frac{\partial u}{\partial z}\partial z + \int_{-h}^{\eta} A_h\nabla^2 u dz \tag{3.39}$$

The depth average of the pressure term is

$$\int_{-h}^{\eta} \frac{1}{\rho}\frac{\partial p_a}{\partial x}dz = \frac{1}{\rho}\frac{\partial p_a}{\partial x}(h+\eta) \tag{3.40}$$

$$\int_{-h}^{\eta} g\frac{\partial \eta}{\partial x}dz = g\frac{\partial \eta}{\partial x}(h+\eta) \tag{3.41}$$

The depth average of the mixing term in the vertical is

$$\rho\int_{-h}^{\eta} \frac{\partial}{\partial z}\left(A_z\frac{\partial u}{\partial z}\right)dz = \tau_x^s - \tau_x^b \tag{3.42}$$

$$\rho\int_{-h}^{\eta} \frac{\partial}{\partial z}\left(A_z\frac{\partial v}{\partial z}\right)dz = \tau_y^s - \tau_y^b \tag{3.43}$$

where τ_x^b, τ_y^b is the bottom shear stresses, τ_x^s, τ_y^s is the wind induced surface shear stress in the x-direction and y- direction respectively. The components of the stress are defined as,

$$\rho A_z\frac{\partial u}{\partial z} = \tau_x \quad \text{and} \quad \rho A_z\frac{\partial v}{\partial z} = \tau_y \tag{3.44}$$

The depth average of the mixing term in the horizontal is

$$\int_{-h}^{\eta} A_h\nabla^2 u dz = dA_h\nabla^2\bar{u} \tag{3.45}$$

and then Equation 3.39 turns to,

$$RHS = d\left(\frac{1}{\rho}\frac{\partial p_a}{\partial x} + g\frac{\partial \eta}{\partial x} + \frac{\left(\tau_x^s - \tau_x^b\right)}{d\rho} + A_h\nabla^2\bar{u}\right) \tag{3.46}$$

Writing the full equation and dropping the overbars,

$$\frac{\partial u}{\partial t} + u\frac{\partial u}{\partial x} + v\frac{\partial u}{\partial y} - fv = -\frac{1}{\rho}\frac{\partial p_a}{\partial x} - g\frac{\partial \eta}{\partial x} + \frac{\left(\tau_x^s - \tau_x^b\right)}{\rho d} + A_h\nabla^2 u \tag{3.47}$$

Also, with similar applications the integration of the y-momentum Equation 3.15 can be written as,

$$\frac{\partial v}{\partial t} + u\frac{\partial v}{\partial x} + v\frac{\partial v}{\partial y} - fu = -\frac{1}{\rho}\frac{\partial p_a}{\partial y} - g\frac{\partial \eta}{\partial y} + \frac{\left(\tau_y^s - \tau_y^b\right)}{\rho d} + A_h\nabla^2 v \tag{3.48}$$

At scales less than 10 km the mixing in the horizontal, A_h, is usually negligible in comparison to the mixing in the vertical and at distances larger than 1km the Coriolis term begins to dominate over nonlinear terms which can be disregarded (Kowalik and Murty, 1993). The pressure term in the depth averaged form of the momentum equations in x-direction and y-direction in Equation 3.47 and Equation 3.48 is $\partial p_a/\partial x$ and $\partial p_a/\partial y$. However the atmospheric changes are not as large as those in oceans and open seas, therefore the pressure terms are neglected in the present study.

Hence the momentum and equations with Coriolis term and continuity equation in the present study can be summarized without shear stresses on the surface and bottom in non-conservation form as follows,

$$\frac{\partial u}{\partial t} + u\frac{\partial u}{\partial x} + v\frac{\partial u}{\partial y} - fv = -g\frac{\partial \eta}{\partial x} \tag{3.49}$$

$$\frac{\partial v}{\partial t} + u\frac{\partial v}{\partial x} + v\frac{\partial v}{\partial y} + f\,u = -g\frac{\partial \eta}{\partial y} \tag{3.50}$$

and

$$\frac{\partial d}{\partial t} + \frac{\partial\,(ud)}{\partial x} + \frac{\partial\,(vd)}{\partial y} = 0 \tag{3.51}$$

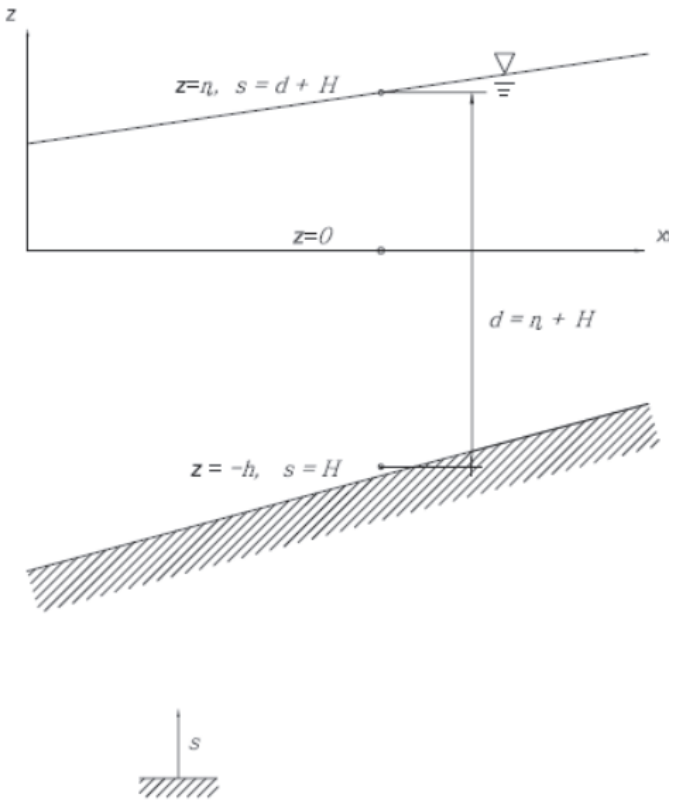

Figure 3.2. A Typical Vertical Cross Section and Definition of Parameters.

With the vertical coordinates located below the bottom, as shown in Figure 3.2, one can rewrite the equations in terms of the variation of the total flow depth, d and with the slopes defined below,

$$\frac{\partial \eta}{\partial x} = \frac{\partial d}{\partial x} + \frac{\partial H}{\partial x} \;\; and \;\; \frac{\partial \eta}{\partial y} = \frac{\partial d}{\partial y} + \frac{\partial H}{\partial y} \tag{3.52}$$

Defining $z = \eta \rightarrow s = d + H$, $S_0^x = -\frac{\partial H}{\partial x}$ and $S_0^y = -\frac{\partial H}{\partial y}$ where is bottom slope in the

x and y directions, respectively. H is the elevation from the datum plane to the bed,

$$\frac{\partial \eta}{\partial x} = \frac{\partial d}{\partial x} - S_0^x \ \ and \ \ \frac{\partial \eta}{\partial y} = \frac{\partial d}{\partial y} - S_0^y \tag{3.53}$$

and Equation 3.52 yields,

$$\frac{\partial u}{\partial t} + u\frac{\partial u}{\partial x} + v\frac{\partial u}{\partial y} = -g\frac{\partial d}{\partial x} + gS_0^x \tag{3.54}$$

$$\frac{\partial v}{\partial t} + u\frac{\partial u}{\partial x} + v\frac{\partial u}{\partial y} = -g\frac{\partial d}{\partial y} + gS_0^y \tag{3.55}$$

$$\frac{\partial \eta}{\partial t} + \frac{\partial (ud)}{\partial x} + \frac{\partial (vd)}{\partial y} = 0 \tag{3.56}$$

These first two momentum Equation 3.54 and Equation 3.55, with the continuity Equation 3.56 will be used for the long wave propagation with RBFs in the following sections.

4. THE NUMERICAL MODEL OF THE FLOW

4.1. Background

A wide list of numerical techniques can be chosen to attempt to solve the reduced set of differential equations through a process of mathematical modeling. It is not easy to obtain the exact solutions, so numerical methods must be resorted to. There are a lot of numerical techniques in the literature. The most common methods are the FDM, FEM, and Finite Volume Method (FVM); which can be classified as mesh-based domain discretization techniques. Another popular scheme is the Boundary Element Method (BEM), which provides numerical solutions to boundary integral equations. BEM differs from traditional methods in the sense that only the boundary needs to be discretized and BEM is an integral method thus, the dimension of the problem is reduced.

These conventional methods are derived from assumptions of local interpolation schemes, which require a mesh to support the localized approximations. Even though, significant advances have been made in the area of mesh generation over the last few decades, it still remains a complex and time consuming process, particularly for complex high-dimensional geometries and evolving boundaries. In general it can be said that meshing is an issue that over-complicates the art of numerical modeling.

Being different from mesh-based methods, a class of new methods, known as meshless methods, has been developed, which are also referred to in the literature as meshfree, element-free, gridless, cloud methods. In mesh-free methods, physical domain is discretized into a scattered set of points and uses shape functions to interpolate the field variables at a global level, there is no dependency on a mesh generation program and computed results are generally smooth therefore, it requires no post-processing.

Meshless methods can be grouped into two according to their discretization scheme as Galerkin-based Meshless Method and Collocation based Meshless Method.

The first meshless method which is developed in the late 1970's is the Smooth Particle Hydrodynamics method. Nayroles *et al.*, (1992) developed the Diffuse Element Method for structural analysis which is later improved to Element-Free Galerkin method by Belytschko *et al.*, (1994). After that, many meshless methods were proposed, such as the Reproducing Kernel Particle Method, the Natural Element Method, the free-mesh method, the finite spheres method, the local Petrov-Galerkin method and the h-p cloud method, all of which are representatives of Galerkin-Based Meshless Method which has a high accuracy and good stability. They need numerical integration to form the discretized system equations. The main drawback is that the integrals in the weak form must be evaluated properly.

Collocation based Meshless Methods use the strong form of the governing equations to avoid numerical integration in deriving the discretized system equations. Finite Point Method, Point Collocation Formulation, Dual Reciprocity Method, Least-Square Collocation Meshless Method, and RBFCM all belong to this group. These methods are very efficient due to their implementation and independence of problem dimension. A comparative analysis of these methods can be found in Viana *et al.*, (2007) and Nguyen *et al.*, (2008). RBFCM is the method used in this thesis.

4.2. RBF Interpolation and Collocation Method

To majority of scientific and engineering community, RBF which uses the one-dimensional distance variable irrespective of dimensionality has become a quite brand-new concept. The RBF method was first used by Hardy (1971) for the interpolation of geographical scattered data, and later used by Kansa (1990a; 1990b) for the numerical solution of partial differential equations (PDEs). Since the pioneering works of Franke (1982) who presented a review of several types of RBFs for scattered data interpolation, and works of Johnson (1985) and Kansa (1990a; 1990b), the research into the RBF theory and its applications have grown. In the following studies the effectiveness of the technique was demonstrated by Goldberg and Chen (1997) and investigations on applications to Initial value problems (IVP) have been carried out by Hon *et al.*, (1997).

RBF has been successfully applied to a number of areas such as convection-diffusion problems (Boztosun, *et al.*, 2002), nonlinear problems (Hon, 1997; Hon and Mao, 1998; Shu *et al.*, 2004; Sarra, 2004; Williams and Jensen, 2000), heat conduction problems (Lui and Lu, 2005), and free boundary problems (Soroushian and Farjoodi, 2006) and heat transfer problems (Zerroukat *et al.*, 2000 and Chantasiriwan, 2007).

To demonstrate the RBF theory clearly, the function u is first approximated with global RBF f_{ij}, as;

$$u_i^b = f_{ij}\alpha_j^b \tag{4.1}$$

$$u_i^b(x,t) = \sum_{j=1}^{N} f(r_{ij})\,\alpha_j^b = \sum_{j=1}^{N} f(\|x_i - x_j\|)\,\alpha_j^b \tag{4.2}$$

where i denotes the node on the domain,b s the time step, N refers to number of nodes defined on the domain, $\|\,.\,\|$ denotes the common choice of Euclidean norm, the nodes $x_j, = 1, 2, ..., N$ are the centers of the RBF interpolant and can be chosen arbitrarily in the domain of interest, hence creating a truly meshfree method. "r" is the distances between the nodes on the domain in 3D denoted with the Pythagorean relations and defined in Equation 4.3 and α_j^b's are the unknown coefficients to be calculated at the time instant, b. The only geometric property that is used in an RBF approximation is the pairwise distances between points that are easy to compute in any number of space dimensions

$$r_{ij} = \sqrt{(x_i - x_j)^2 + (y_i - y_j)^2 + (z_i - z_j)^2} \tag{4.3}$$

Let's call the elements of $f(\|x_i - x_j\|, c_j)$ which are the elements of matrix F as shown

in Equation 4.4 and the free parameter, c_j is defined as the shape parameter.

$$F = \begin{bmatrix} f_{11} & f_{12} & . & f_{1N} \\ f_{21} & . & . & . \\ . & . & . & . \\ f_{N1} & . & . & f_{NN} \end{bmatrix} \tag{4.4}$$

Then Equation 4.1 may be organized as,

$$\begin{bmatrix} \\ F \\ \\ \end{bmatrix} \begin{bmatrix} \alpha_1 \\ . \\ \alpha_N \end{bmatrix}^b = \begin{bmatrix} u_1 \\ . \\ u_N \end{bmatrix}^b \tag{4.5}$$

The method works with points scattered throughout the domain of interest, and the RBF interpolant is a linear combination of RBFs. Given scalar function values $u_i = u(x_i, c)$ the expansion coefficients α_j^b are obtained by solving a system of linear equation as given in Equation 4.5 where the interpolation matrix satisfies $f(\|x_i - x_j\|, c_j)$. At each time step, b, the coefficient matrix remains constant, which means while α_j^b changes the u values change. The mathematical reasoning, derivations and applications to different fields can be found in Buhmann (2003), Wendland (2004) and Fasshauer (2007).

This kind of meshless method in the field of function approximation instead of derivative approximation is due to the pioneering effort of Kansa (1990a; 1990b), who solved PDEs by collocation employing RBF. This method is known as the unsymmetric RBFCM where the unknown function is expanded in terms of RBFs. RBFCM possesses the following advantages; First of all, it is a truly mesh-free method, and is independent of spatial dimension in the sense that the convergence order is of $O\left(h^{d+1}\right)$; where h is the density of the collocation points and d is the spatial dimension (Kansa and Hon, 2000). Secondly, Shu *et al.*, (2004) stated that, as the spatial dimension, D, of the problem increases the convergence order also increases, and hence, much fewer scattered collocation points will be needed to maintain the same accuracy as compared

with conventional FDM, FEM and FVM. This shows the applicability of the RBFs for solving high-dimension problems. Thirdly, Sarra, (2004) stated that the choice of basis function is another flexible feature of RBF methods. RBFs can be globally supported, infinitely differentiable, and contain a free parameter, c, called the shape parameter. Among the interpolation methods for scattered data sets, RBFs outperforms best regarding its accuracy, stability, efficiency, memory requirement, simplicity and straightforwardness of the implementation (Larsson and Fornberg, 2003). The performance of RBF for solving different problems depend on not only the number of nodes but also by the RBF's types which are given in Section 4.2.1. In addition to the advantages of meshless RBFCM, method may have negative drawbacks. As the number of centers or nodes on the domain grows, the method needs to solve a relatively large algebraic system. Moreover, Heryudono and Driscoll (2007) stated that full dense, nonsymmetric and ill-conditioned interpolation matrix causes instability that makes spectral convergence difficult to achieve. This behavior is manifested as a classic accuracy and stability trade-off. Several strategies have been successful to some extent in reducing the ill-conditioning problem when using RBF methods in PDE problems as stated in Fasshauer (1996), Kansa and Hon (2000) and Sarra (2004). The strategies include one or a combination of these;

- Variable MQ shape parameters based upon the local radius of curvature of the function being solved,
- A truncated MQ basis function having a finite, rather than a full band-width,
- Preconditioning the interpolation matrix by using matrix preconditioners,
- Replacement of global solvers by block partitioning, LU decomposition schemes,
- Augmented approximation by adding a polynomial term to approximation function,
- Domain decomposition technique,
- Adaptive meshless method,
- Symmetric collocation method assures a non-singular system of equations.

4.2.1. Types of RBF

There are infinite numbers of possible RBFs and the most common RBFs can be categorized into three main groups according to their differentiability and supported features (Larsson and Fornberg, 2003 and Börekçi, 2005). Some of the functions include free-parameter and some of them are parameter-free. The choice of suitable RBFs can vary in terms of the problem types. In the first group, piecewise smooth functions and parameter-free RBFs, in the second group, infinitely smooth functions with a free parameter RBFs, and in the third group, compactly supported piecewise polynomials with free parameter for adjusting the support so called, Wendland functions, are shown in Table 4.1, Table 4.2 and Table 4.3, respectively. Furthermore, Iske (2003) established tables for Fourier transforms and convergence rates of some radial basis functions.

Table 4.1. Piecewise Smooth RBFs.

Piecewise Smooth RBFs	$f(r)$
Piecewise Polynomials	$r^{\beta} \beta > 0, \beta \in 2N+1$
Powerspline	$-r^{\beta} \beta > 0, \beta \in 2N+1$
βth Order Spline (Thin Plate Spline, $\beta = 2$)	$r^{\beta} \ln r \beta > 0, \beta \in 2N$

Table 4.2. Infinitely Smooth RBFs.

Infinitely Smooth RBFs	$f(r)$
Multiquadrics (MQs)	$\sqrt[\beta]{r^2+c^2} \beta > 0, \beta \in 2N+1$
Inverse Multiquadrics	$^{-}\sqrt[\beta]{r^2+c^2} \beta > 0, \beta \in 2N+1$
Inverse Quadratics	$1/\sqrt[\beta]{r^2+c^2} \beta > 0, \beta \in 2N+1$
Exponential Spline	$\exp(-cr)$
Gaussian Spline	$\exp(-c^2 r^2)$
Matern Spline	$\exp(-cr) K_{\nu}(cr)$

In Table 4.1 and Table 4.2 N refers to natural numbers $0, 1, 2, ..., N$ and ν is the modified Bessel function of order ν .

Table 4.3. Wendland's Positive Definite Functions With Compact Support.

Dimension	$f(r)$	Smoothness
$d = 1$	$f_{1,0} = (1-r)_+$	C^0
	$f_{1,1} = (1-r)^3 + (3r+1)$	C^2
	$f_{1,2} = (1-r)^5 + (8r^2+5r+1)$	C^4
$d \leq 3$	$f_{3,0} = (1-r)_+^2$	C^0
	$f_{3,1} = (1-r)^4 + (4r+1)$	C^2
	$f_{3,2} = (1-r)^6 + (35r^2+18r+3)$	C^4
	$f_{3,3} = (1-r)^8 + (32r^3+25r^2+8r)$	C^6
$d \leq 5$	$f_{5,0} = (1-r)_+^3$	C^0
	$f_{5,1} = (1-r)^5 + (5r+1)$	C^2
	$f_{5,2} = (1-r)^7 + (16r^2+7r+1)$	C^4

In Table 4.3 $()_+$ operator is used to express $f(r)$ as an univariate polynomial $p(r)$ or 0 depending on the values of r and defined as

$$f(r) = \begin{cases} p(r), & if\, 0 \leq r < 1 \\ 0, & if\, r \geq 1 \end{cases} \tag{4.6}$$

PDE applications with smooth solutions, the infinitely smooth RBFs are preferable, mainly because they lead to higher accuracy. The infinitely smooth RBFs exhibit exponential or spectral convergence as a function of center spacing and as the nodes get denser, while the piecewise smooth types give algebraic convergence (Heryudono and Driscoll, 2007). In addition, it is shown that the MQ method is more accurate as grid spacing and time step decrease, a random arrangement of nodes does not affect the accuracy of the method significantly. In this study the MQRBF method is used as an acceptable alternative numerical method for solving SWEs.

4.2.2. RBF-MQ's Shape Parameter

For RBF-MQ, different approaches for the selection of the shape parameters exist. A number of studies have been conducted to determine the optimum value of the shape parameter, c, yet there is still no conclusive answer. Hardy (1971) proposed selecting the parameter based on average of smallest internodal distances, r_{av}, in Equation 4.7

$$c = 0.815 r_{av} \tag{4.7}$$

Tarwater (1985) showed that by increasing c , the root mean square (RMS) error, Equation 4.9 dropped to a minimum and then sharply increased afterwards. Moody and Darken (1989) suggested a simple varied shape parameter. Carlson and Foley (1991) found that the shape parameter is problem dependent and the optimum shape parameter depends on the behavior of the function to be approximated. Madych (1992) demonstrated that significant improvement can be achieved in the accuracy of the RBF interpolant by increasing the c value. Franke and Schaback (1998) proposed a method based on the smallest circle spanning all the data points. Wang and Liu (2002) studied the effect of shape parameters on the numerical accuracy of MQ. Cheng *et al.*, (2003) showed that for very large c values RMS error is of exponential convergence but there's a trade-off (or uncertainty principle, Schaback, 1995) between the accuracy gained in interpolation by increasing the c parameter and the stability lost due to the large matrix condition number created. Hon *et al.*, (1997), and Wu and Hon (2003) proposed choosing c as

$$c = 4 r_{\min} \tag{4.8}$$

where $r_{\min}$ is the minimum intermodal distance in the domain. Also, they obtained satisfactory results for c, between $5r_{av}$ and $8r_{av}$.

The RMS error which evaluates the average error that is distributed to all part of the so-called numerical solution at a certain time is

$$RMS = \sqrt{\frac{1}{N}\sum_{i=1}^{N}\left(\frac{u^i_{numerical} - u^i_{analytical}}{u^i_{analytical}}\right)} \tag{4.9}$$

where N denotes the total number of nodes. Kansa and Hon (2000) state that regular node distribution on the domain and shape parameter can affect the RMS in numerical solution of PDE's.

4.3. Numerical Formulation by RBFCM

The unsteady, two dimensional governing Equation 3.49-Equation 3.51 of the present study are,

$$\frac{\partial u}{\partial t} + u\frac{\partial u}{\partial x} + v\frac{\partial u}{\partial y} = -g\frac{\partial \eta}{\partial x} \tag{4.10}$$

$$\frac{\partial v}{\partial t} + u\frac{\partial v}{\partial x} + v\frac{\partial v}{\partial y} = -g\frac{\partial \eta}{\partial y} \tag{4.11}$$

$$\frac{\partial \eta}{\partial t} + \frac{\partial}{\partial x}\left[(h+\eta)u\right] + \frac{\partial}{\partial y}\left[(h+\eta)v\right] = 0 \tag{4.12}$$

or defining $\partial h/\partial x = S_x$ and $\partial h/\partial y = S_y$ Equation 4.12 and rearranging, Equation 4.12 yields,

$$\frac{\partial \eta}{\partial t} = -u\left(S_x + \frac{\partial \eta}{\partial x}\right) - (h+\eta)\frac{\partial u}{\partial x} - v\left(S_y + \frac{\partial \eta}{\partial y}\right) - (h+\eta)\frac{\partial v}{\partial y} \tag{4.13}$$

where S_x and S_x are the slopes in the x and y directions, respectively. For constant depth their values are zero.

For an IVP associated with the unknown function u,

$$\begin{aligned} Du &= \varphi, \quad on\, \Omega_D \\ Bu &= \psi, \quad on\, \Omega_B \end{aligned} \tag{4.14}$$

where L and B are differential operators, and Ω_D and Ω_B are the problem domain and boundary, a solution to the IVP may be formed with the use of Equation 4.1 which transforms to

$$\begin{aligned} Du &= (Df_{ij})\,\alpha_j = \varphi_i \\ Bu &= (Bf_{ij})\,\alpha_j = \xi_i \end{aligned} \tag{4.15}$$

A system can be formed in the form in matrix notation as

$$\left[\begin{array}{c} Df \\ Bf \end{array} \right] \{\alpha\} = \left\{ \begin{array}{c} \varphi \\ \xi \end{array} \right\} \; or \; [F]\,\{\alpha\} = \{S^*\} \tag{4.16}$$

The F matrix will be formed from the BVP formulation, placement of the nodes, and selection of the RBF and the shape parameter, c. $\{S^*\}$ will be formed from the initial conditions, boundary conditions and the governing equations. Estimation of the unknown values for the problem becomes as simple as determining the unknown $\{\alpha\}$ and applying the RBFCM.

$$u_i = f_{ij}\alpha_j^u \; or \; \alpha_i^u = f_{ij}^{-1}u_j \tag{4.17}$$

$$v_i = f_{ij}\alpha_j^v \; or \; \alpha_i^v = f_{ij}^{-1}v_j \tag{4.18}$$

$$\eta_i = f_{ij}\alpha_j^\eta \; or \; \alpha_i^\eta = f_{ij}^{-1}\eta_j \tag{4.19}$$

where u_i, v_i and η_i denote the x-direction and y-direction velocities and water surface elevation at a collocation point, respectively. f is the interpolation matrix and f^{-1} is the inverse of the interpolation matrix, with its ijth component defined by the relationship given in Table 4.4. depending on RBFMQ, and their derivatives are given as,

Table 4.4. MQRBF and its First and Second Order Derivatives.

	MQRBF
f	$\sqrt{r^2+c^2}$
f^x	$\frac{(x_i-x_j)}{f}$
f^y	$\frac{(y_i-y_j)}{f}$
f^{xx}	$\frac{c^2+(y_i+y_j)^2}{f^3}$
f^{yy}	$\frac{c^2+(x_i+x_j)^2}{f^3}$

$$u_i^x = \left(\frac{\partial u}{\partial x}\right)_i = \frac{\partial f_{ij}}{\partial x}\alpha_j^u = f_{ij}^x\alpha_j^u \ \ and \ \ u_i^y = \left(\frac{\partial u}{\partial y}\right)_i = \frac{\partial f_{ij}}{\partial y}\alpha_j^u = f_{ij}^y\alpha_j^u \tag{4.20}$$

$$v_i^x = \left(\frac{\partial v}{\partial x}\right)_i = \frac{\partial f_{ij}}{\partial x}\alpha_j^v = f_{ij}^x\alpha_j^v \ \ and \ \ v_i^y = \left(\frac{\partial v}{\partial y}\right)_i = \frac{\partial f_{ij}}{\partial y}\alpha_j^v = f_{ij}^y\alpha_j^v \tag{4.21}$$

$$\eta_i^x = \left(\frac{\partial \eta}{\partial x}\right)_i = \frac{\partial f_{ij}}{\partial x}\alpha_j^\eta = f_{ij}^x\alpha_j^\eta \ \ and \ \ \eta_i^y = \left(\frac{\partial \eta}{\partial y}\right)_i = \frac{\partial f_{ij}}{\partial y}\alpha_j^\eta = f_{ij}^y\alpha_j^\eta \tag{4.22}$$

$$u_i^{xx} = \left(\frac{\partial^2 u}{\partial x^2}\right)_i = \frac{\partial^2 f_{ij}}{\partial x^2}\alpha_j^u = f_{ij}^{xx}\alpha_j^u \, and \ v_i^{yy} = \left(\frac{\partial^2 v}{\partial y^2}\right)_i = \frac{\partial^2 f_{ij}}{\partial y^2}\alpha_j^v = f_{ij}^{yy}\alpha_j^v \tag{4.23}$$

The x-direction momentum Equation 4.10, the y-direction momentum Equation 4.11

and the continuity Equation 4.12 become,

$$\frac{\partial u_i}{\partial t} = -\left(D^u_{ij} f^x_{jk} f^{-1}_{kl} u_l + D^v_{ij} f^y_{jk} f^{-1}_{kl} u_l + g f^x_{ij} f^{-1}_{jk} \eta_k\right) \tag{4.24}$$

$$\frac{\partial v_i}{\partial t} = -\left(D^u_{ij} f^x_{jk} f^{-1}_{kl} v_l + D^v_{ij} f^y_{jk} f^{-1}_{kl} v_l + g f^y_{ij} f^{-1}_{jk} \eta_k\right) \tag{4.25}$$

$$\frac{\partial \eta_i}{\partial t} = -\left(S_x u_i + D^u_{ij} f^x_{jk} f^{-1}_{kl} \eta_l + D^{h+\eta}_{ij} f^x_{jk} f^{-1}_{kl} u_l\right) \tag{4.26}$$

$$-\left(S_y v_i + D^v_{ij} f^y_{jk} f^{-1}_{kl} \eta_l + D^{h+\eta}_{ij} f^y_{jk} f^{-1}_{kl} v_l\right) \tag{4.27}$$

where $\mathrm{D}^{(\cdot)}_{ij}$ is the matrix containing $(\cdot)$ on its main diagonal and zero elsewhere.

In the RBFCM procedure for solving PDE's, the solution is constructed from GEs, BCs and/or the ICs. The data centers are placed inside the domain and on the boundaries. The locations for the RBF centers are more flexible and it is also possible to place them outside the domain. Next section gives a brief summary of BCs and ICs.

4.4. Boundary Conditions and Initial Conditions

Most realistic ocean models numerically solve the primitive equations, which consist of the momentum and continuity equations with hydrostatic and Boussinesq approximations, equations for conservation of heat and salinity, and an equation of state with appropriate boundary conditions. The efficient evaluation of accurate radiation boundary conditions for time domain simulations of wave propagation on unbounded spatial domains needs to be considered. This issue has long been a primary stumbling block for the reliable solution of this important class of problems.

In recent years, a number of new approaches have been introduced which have radically changed the situation. These include methods for the fast evaluation of the exact nonlocal operators which is the composition of a spatial and temporal operator

in special geometries, novel sponge layers with reflectionless interfaces, and improved techniques for applying sequences of approximate conditions to higher order. These methods involve a variety of techniques (Colonius, 2004) including characteristic-based decomposition (Giles, 1990; Poinsot and Lele, 1992; Tam and Dong, 1996), flow dissipation (Israeli and Orszag, 1981; Freund 1997), grid-stretching/slow-down operators (Colonius *et al.*, 1993; Karni 1996), supergrid modeling (Colonius and Ran, 2002), and perfectly matched layers (Hu *et al.*, 2008; Hu, 2008). These new developments can provide an essentially complete solution of the numerical radiation condition problems.

In the present study, the boundary conditions are expressions of the same physical principals in the set of governing equations such as no slip boundary condition and kinematic and dynamic boundary conditions which are briefly explained and used in Section 3.2.1. The case studies are subjected to kinematic free surface boundary condition on the surface, i.e. on the $z = \eta(x, y, t)$. No flux on the side boundaries, wall condition, is applied.

A cold start or a warm start is selected due to the nature of the case studies. Given the initial conditions for a cold start

$$u^0 = u(x, y, 0),\ v^0 = v(x, y, 0) \ \text{ and } \ \eta^0 = \eta(x, y, 0) \tag{4.28}$$

Initial conditions of the wave elevations and velocities are obtained from previous studies. Periodic incident wave boundary condition or analytic solutions of wave elevations are used to drive the waves.

Defining artificial boundaries is a necessity in any non-global ocean or any propagation model. One must prescribe boundary conditions for such artificial interfaces in order to close the system of equations and to yield a well-posed problem which ensures the uniqueness of the solution and its stability with regard to initial datum at the interface. However the choice of global or local open boundary conditions (OBCs) is a difficult problem, which has been the subject of numerous studies ranging from

purely mathematical approaches to specific modeling applications. The main goal of the OBC's is to evacuate the outgoing information reaching the boundary. On the other hand, numerical studies can use complex and realistic models, but their results seem generally dependent on the test cases. They may not give any information on its accuracy or relevance with regard to the true solution. In the literature, radiation methods, Flather condition, absorbing conditions, characteristic waves amplitude methods, and relaxation methods are generally used as OBC types in wave simulations. Extensive reviews of various nonreflecting OBC were made by Givoli (1991) and Tsynkov (1998).

A very popular class of OBCs is radiation methods which are based on the Sommerfeld condition (Sommerfeld, 1949) which fully justified in the context of wave equations. The Sommerfeld radiation boundary condition may be given as

$$\frac{\partial \phi}{\partial t} + c\frac{\partial \phi}{\partial x} = 0 \tag{4.29}$$

The condition specifies the transport of the quantity ϕ through the open boundary Γ with the velocity c and n is the out normal vector. The Sommerfeld condition is appropriate for wave propagation problems with constant phase velocity, and corresponds to setting the incoming characteristic to zero. Orlanski (1976) proposed a numerical implementation of this Sommerfeld condition for more complex hyperbolic flows such as the collapse of a mixed region in a stratified fluid and the spatially growing Kelvin-Helmholtz instability in an unbounded shear flow. Engquist and Majda (1977) proposed a high order 2D open boundary condition when the main propagation direction is in the x-direction.

$$\frac{\partial^2 \phi}{\partial t^2} + \frac{\partial^2 \phi}{\partial t \partial x} - \frac{c^2}{2}\frac{\partial^2 \phi}{\partial y^2} = 0 \tag{4.30}$$

One way of preventing outgoing waves from reflecting from the artificial numerical boundaries is to introduce an absorbing layer rather than look for more efficient nonreflecting boundary conditions. Absorbing boundary conditions which are generally global in time and space are exact relations satisfied by the outgoing quantities

at the open boundary. Mathematical foundation and its practical efficiency in several domains of applications make this approach used in the literature. However, it is not feasible in practice since there is no artificial boundary.

A widely-used class of OBCs is relaxation methods whose goal is to relax the model solution ϕ towards the external layer ϕ^{ext} on the artificial boundary. Thus, the efficient way of preventing outgoing waves from reflecting from the artificial numerical boundaries is to introduce a relaxation method rather than searching for more efficient non-reflecting boundary conditions. This approach consists in extending the computational domain Ω by defining an additional domain Ω_s (the sponge layer), which interface with Ω is Γ. Thus, unlike viscous damping on the boundaries, Relaxation methods are often performed jointly with a sponge layer approach. One simple approach to treat the external boundaries is to use the sponge terms (Israeli and Orszag 1981; Bodony 2006). The increase of the computational cost introduced by the additional layer and its solution in the sponge layer are the drawbacks of this method. With this method the NSWE are artificially modified as following Wei and Kirby (1999) and Chawla and Kirby (2000):

$$\frac{\partial u}{\partial t} + u\frac{\partial u}{\partial x} + v\frac{\partial u}{\partial y} = -g\frac{\partial \eta}{\partial x} \underbrace{-w_1(x)u - w_2(x)u_{xx}}_{inside\,the\,sponge\,layer\,in\,the\,x-direction} \tag{4.31}$$

$$\frac{\partial v}{\partial t} + u\frac{\partial v}{\partial x} + v\frac{\partial v}{\partial y} = -g\frac{\partial \eta}{\partial y} \underbrace{-w_1(y)v - w_2(y)v_{yy}}_{inside\,the\,sponge\,layer\,in\,the\,y-direction} \tag{4.32}$$

where

$$-w_1(x) = \left\{ \begin{array}{ll} 0 & x < x_s \\ \alpha_1 \omega f(x) & x \geq x_s \end{array} \right\} where \; f(x) = \frac{\exp\left(\frac{x-x_s}{x_l-x_s}\right)^n}{\exp(1)-1}$$
$$-w_2(y) = \left\{ \begin{array}{ll} 0 & y < y_s \\ \alpha_2 \upsilon f(y) & y \geq y_s \end{array} \right\} \qquad f(y) = \frac{\exp\left(\frac{y-y_s}{y_l-y_s}\right)^n}{\exp(1)-1}, \tag{4.33}$$

and

$$K_1 = Kw_1 \qquad K_2 = Kw_2$$
$$K = \begin{cases} 0 & x, y < x_s, y_s \\ 1 & x, y \geq x_s, y_s \end{cases} \tag{4.34}$$

Thus, in the absorbing layer, waves which decay in all directions of propagation and which match the internal solution. The discretized momentum equations for the sponge layer are

$$-\frac{\partial u_i}{\partial t} = D^u_{ij} f^x_{jk} f^{-1}_{kl} u_l + D^v_{ij} f^y_{jk} f^{-1}_{kl} u_l + g f^x_{ij} f^{-1}_{jk} \eta_k + D^{K_1}_{ij} u_j + D^{K_2}_{ij} f^{xx}_{jk} f^{-1}_{kl} u_l \tag{4.35}$$

$$-\frac{\partial v_i}{\partial t} = D^u_{ij} f^x_{jk} f^{-1}_{kl} v_l + D^v_{ij} f^y_{jk} f^{-1}_{kl} v_l + g f^y_{ij} f^{-1}_{jk} \eta_k + D^{K_1}_{ij} v_j + D^{K_2}_{ij} f^{yy}_{jk} f^{-1}_{kl} v_l \tag{4.36}$$

In this thesis for the OBC, radiation and relaxation methods are used. This kind of combined OBC was first used by Ohyama and Nadaoka (1991) in the literature. In addition to this, in this study, it was found that filtering was necessary in order to avoid temporal instabilities.

Low pass filters may be utilized in to rid the signal of high frequency waves. The Shapiro filter (Shapiro 1970, 1975) is a high order horizontal low pass filter that efficiently remove small scale grid noise without affecting the physical structures of a field. It can be applied at the end of the time step on both velocity and tracer fields. In the literature many researchers use Shapiro filter namely some, Lewis and Adams (1983), Kowalik and Murty (1993), Özkan-Haller and Kirby (1997). Shapiro (1971) defines a response function, R, that is the ratio of the original wave, f, to the filtered wave, f^*. For the ideal low pass filter that would be one for long waves and zero for short waves. The response function is at point i as such;

$$R_i = \frac{f^*_i}{f_i} = a_0 + 2a_1 \cos\theta + 2a_2 \cos 2\theta + ... + 2a_N \cos N\theta = 1 - \sin^{2N}\left(\frac{\theta}{2}\right) \tag{4.37}$$

where a_N is the amplitude of the wave component with wave number of k=2π/L in the fourier expansion. θ = k$\triangle x$ where $\triangle x$ is the collocation node interval. Starting from N=1 to 4 and using Equation 4.37 one can obtain the 3-5-7-9-... point filters and their stencils in Table 4.5 at the ith filtered wave below,

Table 4.5. Stencils of the Response Function for f_i^N for the Various Values of N.

N-1		f_i	$f_{i\pm1}$	$f_{i\pm2}$	$f_{i\pm3}$	$f_{i\pm4}$	$f_{i\pm5}$	$f_{i\pm6}$	$f_{i\pm7}$	$f_{i\pm8}$	$f_{i\pm9}$	$f_{i\pm10}$
0	$1/2^2$	(2	1)									
1	$1/2^4$	(10	4	-1)								
2	$1/2^6$	(44	15	-6	1)							
3	$1/2^8$	(186	56	-28	8	-1)						
4	$1/2^{10}$	(772	210	-120	45	-10	1)					
5	$1/2^{12}$	(3172	792	-495	220	-66	12	-1)				
6	$1/2^{14}$	(12952	3003	-2002	1001	-364	91	-14	1			
7	$1/2^{16}$	(52666	11440	-8008	4368	-1820	560	-120	16	-1)		
8	$1/2^{18}$	(213524	43758	-31824	18564	-8568	3060	-816	153	-18	1)	
9	$1/2^{20}$	(863820	167960	-125970	77520	-38760	15504	-4845	1140	-190	20	-1)

4.5. Time marching

The unsteady nature of the problem is accounted for by using an appropriate time integration scheme. There are a number of self-starting (single step) schemes namely; Euler method, modified Euler method, Heun method, Runge-Kutta methods, Taylor polynomial method. Also, there are commonly used multi-step methods such as Adams-Basforth method, Adams-Moulton method, Adams-Basforth-Moulton method. Since the predictor-corrector type of equations uses past information they do not have the ability to start initial value problems. Single step schemes are used at the beginning until the necessary information for predictor-corrector schemes is obtained.

As a time integration method, three fourth order, O(4), methods are investigated in this thesis. First one is a self starting Runge-Kutta method, RK O(4). Milne predictor and Hamming corrector, MH O(4) and Adams-Basforth predictor and Adams-Moulton corrector ABM O(4) are the second and third time integration methods that use a RK O(4) starter. Time marching three different schemes has been employed and comprised in the selected case studies in Chapter 5. ABM O(4) was selected and used among the others because they are known to work well for smooth problems. The discretized Equation 4.38, Equation 4.39, and Equation 4.40 will be used in the time

marching according to selected time integration type.

$$u_i^{(n+1)} = u_i^{(n)} - \delta t\Big(D_{ij}^u f_{jk}^x f_{kl}^{-1} u_l + D_{ij}^v f_{jk}^y f_{kl}^{-1} u_l + g f_{ij}^x f_{jk}^{-1} \eta_k\Big)^{(n)} \tag{4.38}$$

$$v_i^{(n+1)} = v_i^{(n)} - \delta t\Big(D_{ij}^u f_{jk}^x f_{kl}^{-1} v_l + D_{ij}^v f_{jk}^y f_{kl}^{-1} v_l + g f_{ij}^y f_{jk}^{-1} \eta_k\Big)^{(n)} \tag{4.39}$$

$$\eta_i^{(n+1)} = \eta_i^{(n)} - \delta t \begin{pmatrix} \alpha u_i + D_{ij}^u f_{jk}^x f_{kl}^{-1} \eta_l + D_{ij}^{h+\eta} f_{jk}^x f_{kl}^{-1} u_l \\ +\beta v_i + D_{ij}^v f_{jk}^y f_{kl}^{-1} \eta_l + D_{ij}^{h+\eta} f_{jk}^y f_{kl}^{-1} v_l \end{pmatrix}^{(n)} \tag{4.40}$$

The superscript n denotes the previous time step when all the values are known, n+1 denotes for the new time step.

4.5.1. Runge-Kutta O(4)

RKO(4) is a self starting method so that the initial input will be sufficient to proceed in time. It involves 4 evaluations per time step and local truncation error is fourth order as stated in Burden and Faires (1993). Also, since the expected results are smooth, adaptive step size control is not considered. To established an approximate solution to the initial-value problem can be stated as in Chapra and Canale (1988),

$$\phi' = f(t, \phi) \quad a \leq t \leq b \quad \phi(a) = \phi_0 \tag{4.41}$$

where ϕ is the unknown function of time t and ϕ' is the rate at which ϕ changes between the time a and b. The function f and the data a and the data ϕ_0 are given. The RKO(4) method poses the following for ϕ_{n+1} at some time step n+1 using value of at ϕ_n the step n.

$$\phi_{n+1} = \phi_n + \frac{\Delta t}{6}(k_1 + 2k_2 + 2k_3 + k_4) \tag{4.42}$$

where k_1,k_2, k_3 and k_4 can be seen in Equation 4.43 in terms of the time step, Δt.

$$\begin{aligned} k_1 &= f(t_n, \phi_n) \\ k_2 &= f(t_{n+\frac{1}{2}}, \phi_n + \tfrac{1}{2}k_1\Delta t) \\ k_3 &= f(t_{n+\frac{1}{2}}, \phi_n + \tfrac{1}{2}k_2\Delta t) \\ k_4 &= f(t_{n+1}, \phi_n + k_3\Delta t) \\ \phi_{n+1} &= \phi_n + \tfrac{\Delta t}{6}(k_1 + 2k_2 + 2k_3 + k_4) \end{aligned} \tag{4.43}$$

Algorithm for the RK O(4) time integration is as follows:

(i) Initialize u, v and η at the start of the time interval l, compute with appropriate boundary conditions, for discretized governing Equation 4.44 are used inside the domain,

$$\begin{aligned} k_1^u &= dt\left(-u^o u_x^o - v^o u_y^o - g\eta_x^o\right) \\ k_1^v &= dt\left(-u^o v_x^o - v^o v_y^o - g\eta_y^o\right) \\ k_1^\eta &= dt\left\{-\left[\left(h+\eta^o\right)u^o\right]_x - \left[\left(h+\eta^o\right)v^o\right]_y\right\} \end{aligned} \tag{4.44}$$

and inside the sponge layer Equation 4.45 are used.

$$\begin{aligned} k_1^u &= dt\left(-u^o u_x^o - v^o u_y^o - g\eta_x^o - w_1(x)\,u^o - w_2(x)\,u_{xx}^o\right) \\ k_1^v &= dt\left(-u^o v_x^o - v^o v_y^o - g\eta_y^o - w_1(y)\,v^o - w_2(y)\,v_{yy}^o\right) \\ k_1^\eta &= dt\left\{-\left[\left(h+\eta^o\right)u^o\right]_x - \left[\left(h+\eta^o\right)v^o\right]_y\right\} \end{aligned} \tag{4.45}$$

(ii) Increase the time step with 0.5 time increment and update the values as in Equation 4.46

$$\begin{aligned} u^n &\leftarrow u^o + \tfrac{1}{2}k_1^u \\ v^n &\leftarrow v^o + \tfrac{1}{2}k_1^v \\ \eta^n &\leftarrow \eta^o + \tfrac{1}{2}k_1^\eta \end{aligned} \tag{4.46}$$

Then, compute k_2^u, k_2^v and k_2^η in side the domain with appropriate boundary conditions as in Equation 4.46

$$\begin{aligned} k_2^u &= dt\left(-u^n u_x^n - v^n u_y^n - g\eta_x^n\right) \\ k_2^v &= dt\left(-u^n v_x^n - v^n v_y^n - g\eta_y^n\right) \\ k_2^\eta &= dt\left\{-\left[\left(h+\eta^n\right)u^n\right]_x - \left[\left(h+\eta^n\right)v^n\right]_y\right\} \end{aligned} \tag{4.47}$$

and inside the sponge layer as in Equation 4.48

$$\begin{aligned} k_2^u &= dt\left(-u^n u_x^n - v^n u_y^n - g\eta_x^n - w_1(x)\,u^n - w_2(x)\,u_{xx}^n\right) \\ k_2^v &= dt\left(-u^n v_x^n - v^n v_y^n - g\eta_y^n - w_1(y)\,v^n - w_2(y)\,v_{yy}^n\right) \\ k_2^\eta &= dt\left\{-\left[\left(h+\eta^n\right)u^n\right]_x - \left[\left(h+\eta^n\right)v^n\right]_y\right\} \end{aligned} \tag{4.48}$$

(iii) Update u^n, v^n, η^n respectively as stated in Equation 4.49

$$\begin{aligned} u^n &\leftarrow u^o + \tfrac{1}{2}k_2^u \\ v^n &\leftarrow v^o + \tfrac{1}{2}k_2^v \\ \eta^n &\leftarrow \eta^o + \tfrac{1}{2}k_2^\eta \end{aligned} \tag{4.49}$$

Compute k_3^u, k_3^v and k_3^η in side the domain with appropriate boundary conditions in Equation 4.50

$$\begin{aligned} k_3^u &= dt\left(-u^n u_x^n - v^n u_y^n - g\eta_x^n\right) \\ k_3^v &= dt\left(-u^n v_x^n - v^n v_y^n - g\eta_y^n\right) \\ k_3^\eta &= dt\left\{-\left[\left(h+\eta^n\right)u^n\right]_x - \left[\left(h+\eta^n\right)v^n\right]_y\right\} \end{aligned} \tag{4.50}$$

and inside the sponge layer as stated in Equation 4.51.

$$\begin{aligned} k_3^u &= dt\left(-u^n u_x^n - v^n u_y^n - g\eta_x^n - w_1(x)\,u^n - w_2(x)\,u_{xx}^n\right) \\ k_3^v &= dt\left(-u^n v_x^n - v^n v_y^n - g\eta_y^n - w_1(y)\,v^n - w_2(y)\,v_{yy}^n\right) \\ k_3^\eta &= dt\left\{-\left[(h+\eta^n)\,u^n\right]_x - \left[(h+\eta^n)\,v^n\right]_y\right\} \end{aligned} \tag{4.51}$$

Update, once more, the values u^n, ν^n, η^n as stated in Equation 4.52.

$$\begin{aligned} u^n &\leftarrow u^o + \tfrac{1}{2}k_3^u \\ v^n &\leftarrow v^o + \tfrac{1}{2}k_3^v \\ \eta^n &\leftarrow \eta^o + \tfrac{1}{2}k_3^\eta \end{aligned} \tag{4.52}$$

(iv) Increase the time step with 0.5 time increment, compute k_4^u, k_4^v and k_4^η inside the domain with appropriate boundary conditions as in Equation 4.53.

$$\begin{aligned} k_4^u &= dt\left(-u^n u_x^n - v^n u_y^n - g\eta_x^n\right) \\ k_4^v &= dt\left(-u^n v_x^n - v^n v_y^n - g\eta_y^n\right) \\ k_4^\eta &= dt\left\{-\left[(h+\eta^n)\,u^n\right]_x - \left[(h+\eta^n)\,v^n\right]_y\right\} \end{aligned} \tag{4.53}$$

and inside the sponge layer Equation 4.54 is used.

$$\begin{aligned} k_4^u &= dt\left(-u^n u_x^n - v^n u_y^n - g\eta_x^n - w_1(x)\,u^n - w_2(x)\,u_{xx}^n\right) \\ k_4^v &= dt\left(-u^n v_x^n - v^n v_y^n - g\eta_y^n - w_1(y)\,v^n - w_2(y)\,v_{yy}^n\right) \\ k_4^\eta &= dt\left\{-\left[(h+\eta^n)\,u^n\right]_x - \left[(h+\eta^n)\,v^n\right]_y\right\} \end{aligned} \tag{4.54}$$

Update, the old values u^n, ν^n, η^n with the new values $u^{n+1}, \nu^{n+1}, \eta^{n+1}$, respectively as stated in Equation 4.55.

$$\begin{aligned} u^n + 1 &\leftarrow u^o + \tfrac{1}{6}\left[k_1^u + 2(k_2^u + k_3^u) + k_4^u\right] \\ v^n + 1 &\leftarrow v^o + \tfrac{1}{6}\left[k_1^v + 2(k_2^v + k_3^v) + k_4^v\right] \\ \eta^n + 1 &\leftarrow \eta^o + \tfrac{1}{6}\left[k_1^\eta + 2(k_2^\eta + k_3^\eta) + k_4^\eta\right] \end{aligned} \tag{4.55}$$

4.5.2. Milne predictor and Hamming corrector of O(4) with a Runge-Kutta O(4) starter

Applying the self starting integrator such as the Runge-Kutta O(4), one can obtain the first 3 time steps to use in the Milne Hamming time marching schemes.

General procedure to approximate the solution of the initial value problem $\phi' = f(t, \phi)$ with $\phi(a) = \phi_0$ between $a \leq t \leq b$ using the Milne predictor with the Hamming corrector method from time step n to n+1 is as follows:
The classical predictor step is that of Milne (1953) given below in Equation 4.56.

$$p_{n+1} = \phi_{n-3} + \frac{4h}{3}\left(2f_{n-2} - f_{n-1} + 2f_n\right) \tag{4.56}$$

Given a stable predictor-corrector method, the only remaining problem is speed. It has become common practice to avoid the corrector iteration by taking the predicted value, inserting it in the right hand side of the corrector and accepting this value of the corrector as the new one. Hamming (1959) adds sophistication to this idea by modifying the predicted value by the estimated error in the predicted value at the previous step. The modifier step is

$$p_{\,\mathrm{mod}} = p_{n+1} + \frac{112}{121}\left(c_n - p_n\right), f_{n+1} = f(t_{n+1}, p_{\,\mathrm{mod}}) \tag{4.57}$$

Hamming (1959) developed a stable corrector to use with Equation 4.56 instead of Milne's (1953) corrector. The corrector step is

$$c_{n+1} = \frac{-\phi_{n-2} + 9\phi_n}{8} + \frac{3h}{8}\left(-f_{n-1} + 2f_n + f_{n+1}\right) \tag{4.58}$$

Thus at the n+1 time step, the unknown can be estimated as

$$\phi_{n+1} = c_{n+1} + \frac{9}{121}\left(p_{n+1} - c_{n+1}\right) \tag{4.59}$$

The discretized equations for predicted values of unknowns u,v velocities and η are

$$\begin{aligned}
(u_p)_i^{n+1} &= u_i^{n-3} + \tfrac{4\delta t}{3}\left(2fu_i{}^n - fu_i{}^{n-1} + 2fu_i{}^{n-2}\right) \\
(v_p)_i^{n+1} &= v_i^{n-3} + \tfrac{4\delta t}{3}\left(2fv_i{}^n - fv_i{}^{n-1} + fv_i{}^{n-2}\right) \\
(\eta_p)_i^{n+1} &= \eta_i^{n-3} + \tfrac{4\delta t}{3}\left(2f\eta_i^n - f\eta^{n-1} + 2f\eta_i{}^{n-2}\right)
\end{aligned} \tag{4.60}$$

where f is an operator

$$\begin{aligned}
fu_i^n &= f_{ik}u_k^n, \quad fu_i^{n-1} = f_{ik}u_k^{n-1}, \quad fu_i^{n-2} = f_{ik}u_k^{n-2} \\
fv_i^n &= f_{ik}v_k^n, \quad fv_i^{n-1} = f_{ik}v_k^{n-1}, \quad fv_i^{n-2} = f_{ik}v_k^{n-2} \\
f\eta_i^n &= f_{ik}\eta_k^n, \quad f\eta_i^{n-1} = f_{ik}\eta_k^{n-1}, \quad f\eta_i^{n-2} = f_{ik}\eta_k^{n-2}
\end{aligned} \tag{4.61}$$

The predicted values in Equation 4.60 are now modified using the estimated truncation error e from the previous time step. The modified unknowns, u,v velocities and η, are

$$\begin{aligned}
(u_{pm})_i^{n+1} &= (u_p)_i^{n+1} + \tfrac{9}{112}e_u^n \\
(v_{pm})_i^{n+1} &= (v_p)_i^{n+1} + \tfrac{9}{112}e_v^n \\
(\eta_{pm})_i^{n+1} &= (\eta_p)_i^{n+1} + \tfrac{9}{112}e_\eta^n
\end{aligned} \tag{4.62}$$

For n+1=4 the truncation error is taken as zero since no previous value has been determined yet. For the Hamming corrector step we have

$$\begin{aligned}
(u_c)_i^{n+1} &= \tfrac{1}{8}\left\{9u_i^n - u_i^{n-2} + 3\delta t\left[(fu^*)_i^{n+1} + 2fu_i^n - fu_i^{n-1}\right]\right\} \\
(v_c)_i^{n+1} &= \tfrac{1}{8}\left\{9v_i^n - v_i^{n-2} + 3\delta t\left[(fv^*)_i^{n+1} + 2fv_i^n - fv_i^{n-1}\right]\right\} \\
(\eta_c)_i^{n+1} &= \tfrac{1}{8}\left\{9\eta_i^n - \eta_i^{n-2} + 3\delta t\left[(f\eta^*)_i^{n+1} + 2f\eta_i^n - f\eta_i^{n-1}\right]\right\}
\end{aligned} \tag{4.63}$$

where

$$\begin{aligned}
(fu^*)_i^{n+1} &= fu_i\left[t^{n+1}, (u_{pm})_i^{n+1}\right] = fu_{ik}(u_{pm})_k^{n+1} \\
(fv^*)_i^{n+1} &= fv_i\left[t^{n+1}, (v_{pm})_i^{n+1}\right] = fv_{ik}(v_{pm})_k^{n+1} \\
(f\eta^*)_i^{n+1} &= f\eta_i\left[t^{n+1}, (\eta_{pm})_i^{n+1}\right] = f\eta_{ik}(\eta_{pm})_k^{n+1}
\end{aligned} \tag{4.64}$$

The truncation error may now be determined from Equation 4.65.

$$\begin{aligned}(e_u)_i^n &= \tfrac{9}{121}\left[(u_c)_i^{n+1} - (u_p)_i^{n+1}\right] \\ (e_v)_i^n &= \tfrac{9}{121}\left[(v_c)_i^{n+1} - (v_p)_i^{n+1}\right] \\ (e_\eta)_i^n &= \tfrac{9}{121}\left[(\eta_c)_i^{n+1} - (\eta_p)_i^{n+1}\right]\end{aligned} \tag{4.65}$$

The corrected values are modified and assigned as the values of u v and η for time step n+1 as seen in Equation 4.66.

$$\begin{aligned}u_i^{n+1} &= (u_c)_i^{n+1} - (e_u)_i^{n+1} \\ v_i^{n+1} &= (v_c)_i^{n+1} - (e_v)_i^{n+1} \\ \eta_i^{n+1} &= (\eta_c)_i^{n+1} - (e_\eta)_i^{n+1}\end{aligned} \tag{4.66}$$

4.5.3. Adams - Bashforth - Moulton Method of O(4) with a Runge-Kutta O(4) starter

Applying the self starting integrator such as the Runge-Kutta O(4), one can obtain the first 3 time steps to use in the Adams - Bashforth - Moulton time marching schemes.

General procedure to approximate the solution of the initial value problem $\phi' = f(t, \phi)$ with $\phi(a) = \phi_0$ between $a \leq t \leq b$ the Adams-Bashforth predictor and the Adams-Moulton corrector method from time step n to n+1 is as follows;

By using four-step Adams-Bashforth and Adams-Moulton methods together, the predictor formula is

$$p_{n+1} = \phi_n + \frac{h}{24}\left(-9f_{n-3} + 37f_{n-2} - 59f_{n-1} + 55f_n\right), f_{n+1} = f(t_{n+1}, p_{n+1}) \tag{4.67}$$

and the corrector formula is stated in Equation 4.68.

$$\phi_{n+1} = \phi_n + \frac{h}{24}(f_{n-2} - 5f_{n-1} + 19f_n + 9f_{n+1}) \tag{4.68}$$

In general for the k^{th}order,

$$k^{th}order \begin{cases} predictor: & p_{n+1} = \phi_n + \delta t \sum_{j=0}^{h-1} \frac{1}{c_k}\beta_j f_{n-j} + O\left(h^{m+1}\right) \\ corrector: & \phi_{n+1} = \phi_n + \delta t \sum_{j=0}^{h-1} \frac{1}{c_m}\beta_j f_{n+1-j} + O\left(\delta t^{m+1}\right) \end{cases} \tag{4.69}$$

Both formulas can be derived from the Taylor series expansions, for the predictor, the expansion is performed around n_i and for the corrector at n_{i+1}. Derivations in detail, stability and error analysis on the mentioned methods can be found in Chapra and Canale (1988). The predictor and corrector formulas are given in Table 4.6 and Table 4.7.

Table 4.6. Adams-Bashforth Predictors.

k	c_k	β_0	β_1	β_2	β_3	β_4	β_5	ε_t
1	1	1						$\frac{1}{2}(\delta t)^2 f'(\xi)$
2	2	3	-1					$\frac{5}{12}(\delta t)^3 f''(\xi)$
3	12	23	-16	5				$\frac{9}{24}(\delta t)^4 f'''(\xi)$
4	24	55	-59	37	-9			$\frac{251}{720}(\delta t)^5 f^{(4)}(\xi)$
5	720	1901	-2774	2616	-1274	251		$\frac{475}{1440}(\delta t)^6 f^{(5)}(\xi)$
6	1440	4277	-7923	9982	-7298	2877	-475	$\frac{19078}{60480}(\delta t)^7 f^{(6)}(\xi)$

Table 4.7. Adams-Moulton Correctors.

k	c_m	β_0	β_1	β_2	β_3	β_4	β_5	ε_t
2	2	1	1					$-\frac{1}{12}(\delta t)^3 f''(\xi)$
3	12	5	8	-1				$-\frac{1}{24}(\delta t)^4 f'''(\xi)$
4	24	9	19	-5	1			$-\frac{19}{720}(\delta t)^5 f^{(4)}(\xi)$
5	720	251	646	-264	106	-19		$-\frac{27}{1440}(\delta t)^6 f^{(5)}(\xi)$
6	1440	475	1427	-798	482	-173	27	$-\frac{863}{60480}(\delta t)^7 f^{(6)}(\xi)$

The predicted discretized values of unknowns; u, v velocities and η, are stated in Equation 4.70.

$$\begin{aligned}
(u_p)_i^{n+1} &= u_i^{n-3} + \tfrac{\delta t}{24}\left(55{fu_i}^n - 59{fu_i}^{n-1} + 35{fu_i}^{n-2} - 9{fu_i}^{n-3}\right) \\
(v_p)_i^{n+1} &= v_i^{n-3} + \tfrac{\delta t}{24}\left(55{fv_i}^n - 59{fv_i}^{n-1} + 35{fv_i}^{n-2} - 9{fv_i}^{n-3}\right) \\
(\eta_p)_i^{n+1} &= \eta_i^{n-3} + \tfrac{\delta t}{24}\left(55{f\eta_i}^n - 59{f\eta_i}^{n-1} + 35{f\eta_i}^{n-2} - 9{f\eta_i}^{n-3}\right)
\end{aligned} \tag{4.70}$$

where

$$\begin{aligned}
fu_i^n = f_{ik}u_k^n, fu_i^{n-1} = f_{ik}u_k^{n-1}, fu_i^{n-2} = f_{ik}u_k^{n-2}, fu_i^{n-3} = f_{ik}u_k^{n-3} \\
fv_i^n = f_{ik}v_k^n, fv_i^{n-1} = f_{ik}v_k^{n-1}, fv_i^{n-2} = f_{ik}v_k^{n-2}, fv_i^{n-3} = f_{ik}v_k^{n-3} \\
f\eta_i^n = f_{ik}\eta_k^n, f\eta_i^{n-1} = f_{ik}\eta_k^{n-1}, f\eta_i^{n-2} = f_{ik}\eta_k^{n-2}, fv_i^{n-3} = f_{ik}v_k^{n-3}
\end{aligned} \tag{4.71}$$

Discretized values in corrector step of the unknowns; u, v velocities and η, are in Equation 4.72.

$$\begin{aligned}
(u_c)_i^{n+1} &= u_i^n + \tfrac{\delta t}{24}\left(9\left(fu^*\right)_i^{n+1} + 19fu_i^n - 5fu_i^{n-1} + fu_i^{n-2}\right) \\
(v_c)_i^{n+1} &= v_i^n + \tfrac{\delta t}{24}\left(9\left(fv^*\right)_i^{n+1} + 19fv_i^n - 5fv_i^{n-1} + fv_i^{n-2}\right) \\
(\eta_c)_i^{n+1} &= u_i^n + \tfrac{\delta t}{24}\left(9\left(f\eta^*\right)_i^{n+1} + 19f\eta_i^n - 5f\eta_i^{n-1} + f\eta_i^{n-2}\right)
\end{aligned} \tag{4.72}$$

where

$$\begin{aligned}
\left(fu^*\right)_i^{n+1} &= fu_i\left[t^{n+1}, (u_{pm})_i^{n+1}\right] = fu_{ik}(u_{pm})_k^{n+1} \\
\left(fv^*\right)_i^{n+1} &= fv_i\left[t^{n+1}, (v_{pm})_i^{n+1}\right] = fv_{ik}(v_{pm})_k^{n+1} \\
\left(f\eta^*\right)_i^{n+1} &= f\eta_i\left[t^{n+1}, (\eta_{pm})_i^{n+1}\right] = f\eta_{ik}(\eta_{pm})_k^{n+1}
\end{aligned} \tag{4.73}$$

4.5.4. Solution Strategy and Convergence

In the present study, in order to solve unknown u, v velocities and free surface displacement, η, an iterative solution strategy is needed because of the non-linearity in the momentum equations. The algorithm starts with an initial guess of u and v. The discretized momentum Equation 4.38 and Equation 4.39 are solved to find u and v in

all nodes of domain. Using the new quantities, η computed by the continuity Equation 4.40, successively, the same algorithm applied to discretized equations. Updating the iteratively improved quantities, solution process computed until the convergence criteria satisfied.

The convergence of the process constructed with the difference of the new and pre-iterated surface elevation, η, values. Max error for surface elevation, η, is set to 1e-8. The pseudo code is given below. In the test runs, the model has taken minimum one and maximum five iterations to converge. Max. iteration is set to 10 iterations for the iteration loop. If the collocation nodes are selected too large or too small, this may cause oscillatory or divergent iterative solutions. However, the system cannot suffer from ill-conditioning if the node number is not higher than to some extent for this study the limit is between minimum 16 and maximum 256 nodes per wave length. Solution strategy as a pseudo code is:

- Wave parameters are set (wave amplitude, wave period ,dispersion relationship find the k value),
- Model parameters are set (time increment, max. iteration, max. error),
- Collocation nodes are set,
- Sponge parameters are set,
- RBFMQ shape parameter is set,
- Operators are set,
- Time Iteration method is set (for example,. RKO(4)),
- Time loop starts till the number of time step,
- k_1^u, k_1^η calculated to find u^n, v^n,
- $T = t + 0.5dt$ derivatives are computed,
- k_2^u, k_2^η are calculated to find u^n, v^n compute derivatives,
- k_3^u, k_3^η are calculated to find u^n, v^n,
- $T = t + 0.5dt$ derivatives are computed,
- k_4^u, k_4^η are calculated to find u^n, v^n and derivatives are computed,;
  - (i) Iteration loop starts,
  - (ii) Number of iteration $<$ max. number of iteration,

(iii) Error $\eta <$ max. error η,

(iv) Shapiro filter is called,

(v) Interchange of new values with the old values is set,

(vi) Iteration loop ends.

- Time loop ends.

5. APPLICATIONS AND DISCUSSION OF THE RESULTS

5.1. Background

Some analytical solutions of the shallow water wave equations exist both for domains with fixed boundaries and domains with moving boundaries. Some of these solutions are for linearized forms of the shallow water wave equations while others are for the NSWEs. The used linearized equations ignore the advective terms, the Coriolis terms, the viscosity terms and the wind stress terms. They assume that the oscillations of the water surface, η , are small compared to the total depth, $h + \eta$, and hence that the nonlinear continuity and momentum terms are replaced with the linear continuity and momentum terms.

5.1.1. Fixed Boundary Analytical Solutions

Some examples of fixed boundary analytical solutions are as follows. Lamb (1945) solved linearized forms of the shallow water wave equations to model tidal flow in channels of different shapes for frictionless flow. Ippen (1966) solved linearized forms of the shallow water wave equations to model tidal flow in channels of different shapes both for frictionless flow and linear friction. Lynch and Gray (1978) developed analytical solutions of the linearized shallow water wave equations. Their equations included linear friction and a wind stress term for constant depth, linearly varying depth and quadratically varying depths. The authors stated that their analytical solutions should prove useful for comparison with numerical models. The advantage of these analytical solutions over previous analytical solutions is that most previous analytical solutions were for frictionless flow and where their solutions were for frictional flow as well. Prandle and Rahman (1980) modelled tidal oscillations with linear friction in channels of varying depth and cross-section.

Some authors have considered tidal oscillations in estuaries when the water elevation, η, is not small compared with the mean water depth. Tidal oscillations in one dimensional estuaries were investigated by Airy in 1845 (discussed in Lamb (1945) and Rahman (1995)) using the method of perturbations. Kreiss (1957) included linear friction in analyzing nonlinear oscillations in a tidal channel of finite length. Proudman (1957) included quadratic friction in analyzing nonlinear oscillations due to tide and surge in a channel of finite length. Knight (1973) extended Proudman's work. His solution is obtained for an idealized estuary in which the channel is horizontal, of constant rectangular section, closed at one end and open at the other to tidal influence. The motion is considered to be one-dimensional, and the solution includes the effects of both the convective acceleration and friction terms. Gallagher and Munk (1971), Kabbaj and Provost (1980), and DiLorenzo (1988) all found second order solutions for quadratic frictional tidal flow in channels of finite length using perturbation methods. Friedrichs and Madsen (1992) produced a table showing the ratio of local acceleration to friction and of advection to friction in twelve estuaries.

In 1845 Airy investigated tidal flow in a channel of constant mean water depth, h, defined for $0 \leq x \leq \infty$, for when η, the water level, is not small compared with h. The equations of motion to be solved are based on Equation 4.10 and Equation 4.11, and the equation of continuity to be solved is based on Equation 4.12 with flow assumed only in the x-direction. The coriolis force, viscous forces, bottom friction and wind stress forces where omitted, but the nonlinear terms in the momentum and continuity equations were retained. The resulting nonlinear shallow water equations are,

$$\frac{\partial u}{\partial t} + u\frac{\partial u}{\partial x} + g\frac{\partial \eta}{\partial x} = 0 \tag{5.1}$$

and

$$\frac{\partial \eta}{\partial t} + \frac{\partial}{\partial x}\left[u\left(h+\eta\right)\right] = 0 \tag{5.2}$$

The channel is bounded by the open sea at $x = 0$ of constant depth and semi-infinite length, where the water elevation which is progressive is given by

$$\eta\,(0,t) = a_1 \cos \omega t \tag{5.3}$$

To solve this problem Airy used the method of successive approximations. The solutions for η and u have terms involving, ω, the angular frequency of the tidal oscillation plus terms involving twice the frequency, 2ω, the latter terms representing over tides, or tides of the second order. Airy's analysis did not extend to tides of higher order, i.e. to those whose frequencies are three, four or more times than of that of the forced frequency.

As a first approximation to the NSWE we have the linear equations.

$$\frac{\partial u}{\partial t} + g\frac{\partial \eta}{\partial x} = 0 \tag{5.4}$$

$$\frac{\partial \eta}{\partial t} + h\frac{\partial u}{\partial x} = 0 \tag{5.5}$$

The solutions of Equation 5.4 and 5.5 which are consistent with Equation 5.3 are

$$\eta = a_1 \cos \omega \left(t - \frac{x}{c}\right) \tag{5.6}$$

$$u = \frac{g a_1}{c} \cos \omega \left(t - \frac{x}{c}\right) \tag{5.7}$$

where c, the wave speed, is given by

$$c = \sqrt{gh} \tag{5.8}$$

As a second approximation these values of η and u in Equation 5.6 and Equation 5.7 are substituted in the nonlinear terms of Equation 5.1 and Equation 5.2 to obtain time derivatives of u and η.

$$\frac{\partial u}{\partial t} = -g\frac{\partial \eta}{\partial x} - \frac{\omega g a_1^2}{2ch}\sin 2\omega\left(t - \frac{x}{c}\right) \tag{5.9}$$

$$\frac{\partial \eta}{\partial t} = -h\frac{\partial u}{\partial x} - \frac{\omega g a_1^2}{h}\sin 2\omega\left(t - \frac{x}{c}\right) \tag{5.10}$$

Eliminating u from Equation 5.9 and Equation 5.10 one obtains

$$\frac{\partial^2 \eta}{\partial t^2} = gh\frac{\partial^2 \eta}{\partial x^2} - \kappa\cos 2\omega\left(t - \frac{x}{c}\right) \tag{5.11}$$

where

$$\kappa = \frac{a_1^2 g\omega^2}{c^2} + \frac{2a_1^2\omega^2}{h} \tag{5.12}$$

Equation 5.11 with Equation 5.12 can be solved by assuming that

$$\eta = a_1\cos\omega\left(t - \frac{x}{c}\right) + Ex\cos 2\omega\left(t - \frac{x}{c}\right) + Fxsin2\omega\left(t - \frac{x}{c}\right) \tag{5.13}$$

where E and F are constants. The constants E and F can be found by substituting Equation 5.13 in Equation 5.11 and equating coefficients of $\cos\omega\,(t - x/c)$ and $\sin\omega\,(t - x/c)$, giving

$$\eta = a_1\cos\omega\left(t - \frac{x}{c}\right) - \left(\frac{3a_1^2 g\omega}{4c^3}\right)x\sin 2\omega\left(t - \frac{x}{c}\right) \tag{5.14}$$

Eliminating η from Equation 5.9 and Equation 5.10 one obtains,

$$\frac{\partial^2 u}{\partial t^2} = gh\frac{\partial^2 u}{\partial x^2} - \left(\frac{3a_1^2 g\omega^2}{ch}\right)\cos 2\omega\left(t - \frac{x}{c}\right) \tag{5.15}$$

If one assumes that

$$\begin{aligned} u = &\tfrac{a_1 g}{c}\cos\omega\left(t-\tfrac{x}{c}\right) + P\cos 2\omega\left(t-\tfrac{x}{c}\right) + Qsin2\omega\left(t-\tfrac{x}{c}\right) \\ &+Rx\cos 2\omega\left(t-\tfrac{x}{c}\right) + Sxsin2\omega\left(t-\tfrac{x}{c}\right) \end{aligned} \tag{5.16}$$

where P, Q, R and S are constants. Upon substituting Equation 5.16 in Equation 5.15 one obtains

$$R = 0 \tag{5.17}$$

$$S = -\frac{3a_1^2\omega}{4h^2} \tag{5.18}$$

Substituting Equation 5.17 and Equation 5.18 in Equation 5.16 gives

$$\begin{aligned} u = &\tfrac{a_1 g}{c}\cos\omega\left(t-\tfrac{x}{c}\right) + P\cos 2\omega\left(t-\tfrac{x}{c}\right) + Qsin2\omega\left(t-\tfrac{x}{c}\right) \\ &-\tfrac{3a_1^2\omega}{4h^2}xsin2\omega\left(t-\tfrac{x}{c}\right) \end{aligned} \tag{5.19}$$

Substituting Equation 5.14 and Equation 5.19 in Equation 5.9 gives

$$P = -\frac{a_1^2 g}{8hc} \tag{5.20}$$

$$Q = 0 \tag{5.21}$$

Substituting Equation 5.20 and Equation 5.21 in Equation 5.19 gives

$$u = \frac{a_1 g}{c}\cos\omega\left(t-\frac{x}{c}\right) - \frac{a_1^2 g}{8hc}\cos 2\omega\left(t-\frac{x}{c}\right) - \frac{3a_1^2\omega}{4h^2}x\sin 2\omega\left(t-\frac{x}{c}\right) \tag{5.22}$$

From Equation 5.14 it can be seen that the approximate solution will be valid provided that the amplitude of the over tide term (i.e. the second order term) is small compared to the amplitude of the linear term, i.e. $a_1\omega x/ch$ is small.

5.1.2. Moving Boundary Analytical Solutions

Some examples of moving boundary analytical solutions are as follows. Carrier and Greenspan (1958) obtained moving boundary analytical solutions of the nonlinear shallow water equations for a water wave climbing a linearly sloping beach. Carrier and Greenspan's derivation is discussed in detail in Zhang (1996) and Johnson (1997). The procedure is discussed in detail here to show the complications involved in deriving the analytical solutions. The analytical solution will be used to validate the numerical model developed.

The equations of motion to be solved are based on Equation 4.10, Equation 4.11 and the continuity Equation 4.12, with flow assumed only in the x-direction and without any Coriolis effect, pressure driven forces, wind and bottom shear stresses. The resulting equations are

$$\frac{\partial u}{\partial t} + u\frac{\partial u}{\partial x} + \frac{\partial \eta}{\partial x} = 0 \tag{5.23}$$

and

$$\frac{\partial \eta}{\partial t} + \frac{\partial}{\partial x}\left[u\left(h+\eta\right)\right] = 0 \tag{5.24}$$

where $h = -\alpha x$, and applying a rescaling,

$$x' = x, \quad t' = \sqrt{\alpha}t, \; \eta' = \tfrac{\eta}{\alpha}, \; u' = \tfrac{u}{\alpha}, \tag{5.25}$$

The equations are then rewritten in terms of u', η', x' and t' which are successively transformed forms of u, η, x and t. Next two new variables, σ and λ, are introduced. These are defined in terms of the dimensionless variables (with primes dropped)

$$\sigma = 4\sqrt{\eta - x} \tag{5.26}$$

and

$$\lambda = 2\,(u + t) \tag{5.27}$$

Then Equation 5.23 and Equation 5.24 transform to the equations

$$\frac{\partial \sigma}{\partial t} + u\frac{\partial \sigma}{\partial x} + \left(\frac{\sigma}{4}\right)\frac{\partial \lambda}{\partial x} = 0 \tag{5.28}$$

$$\frac{\partial \lambda}{\partial t} + u\frac{\partial \lambda}{\partial x} + \left(\frac{\sigma}{4}\right)\frac{\partial \sigma}{\partial x} = 0 \tag{5.29}$$

Transforming the equations so that the independent and dependent variables are interchanged is achieved by applying the hodograph transformation which is defined as,

$$\frac{\partial x}{\partial \lambda} = -\frac{\partial \sigma_t}{J},\ \frac{\partial x}{\partial \sigma} = \frac{\lambda_t}{J},\ \frac{\partial t}{\partial \sigma} = -\frac{\lambda_x}{J}\,,\ \frac{\partial t}{\partial \lambda} = \frac{\sigma_x}{J} \tag{5.30}$$

where the Jacobian is

$$J = \frac{\partial\,(\sigma, \lambda)}{\partial\,(x, t)} = \begin{vmatrix} \sigma_x & \sigma_t \\ \lambda_x & \lambda_t \end{vmatrix} = \sigma_x\lambda_t - \sigma_t\lambda_x \tag{5.31}$$

The transformation yields.

$$\frac{\partial x}{\partial \lambda} - u\frac{\partial t}{\partial \lambda} + \left(\frac{\sigma}{4}\right)\frac{\partial t}{\partial \sigma} = 0 \tag{5.32}$$

$$\frac{\partial x}{\partial \sigma} - u\frac{\partial t}{\partial \sigma} + \left(\frac{\sigma}{4}\right)\frac{\partial t}{\partial \lambda} = 0 \tag{5.33}$$

Substituting $t = \lambda/2 - u$ from Equation 5.27 into these equations gives

$$\left(x + \frac{u^2}{2}\right)_\lambda - \frac{\sigma}{4}u_\sigma - \frac{u}{2} = 0 \tag{5.34}$$

$$\left(x+\frac{u^2}{2}+\frac{\sigma^2}{16}\right)_\sigma-\left(\frac{\sigma u}{4}\right)_\lambda=0 \tag{5.35}$$

where the subscripts indicate differentiation with respect to the subscripted variable.

It follows from Equation 5.35 that there is a variable $\phi(\sigma,\lambda)$, such that

$$x+\frac{u^2}{2}+\frac{\sigma^2}{16}=\frac{\phi_\lambda}{4} \tag{5.36}$$

and

$$\frac{\sigma u}{4}=\frac{\phi_\sigma}{4} \tag{5.37}$$

Substituting Equation 5.36 and Equation 5.37 into Equation 5.34 gives a linear equation

$$(\sigma\phi_\sigma)_\sigma-\sigma\phi_{\lambda\lambda}=0 \tag{5.38}$$

Thus, the original nonlinear equations have been reduced to a linear equation. The instantaneous shoreline is at σ=0. Far away from the shoreline nonlinear effects are small and σ=0 as stated in Synolakis (1987).

Carrier and Greenspan (1958) obtained a number of solutions of Equation 5.38. The choice of a function $\phi(\sigma,\lambda)$ which satisfies Equation 5.38 defines η, u, x, and t in terms of parametric coordinates σ and λ. In particular, if the Jacobian $\partial(x,t)/\partial(\sigma,\lambda)$ never vanishes in $\sigma>0$, the implicitly defined solutions η and u will be single-valued and such solution represents nonbreaking waves. Thus, a particular simple solution of Equation 5.38 can be given by

$$\phi=AJ_0(\omega\sigma)\cos(\omega\lambda-\psi) \tag{5.39}$$

where $A\leq 1$ is a constant for a valid mapping, J_0 is the usual notation for 0^{th} order Bessel function of the first kind and ψ is the phase lag. No loss in generality ensures

when the phase lag, ψ, is taken to be zero or ω is put equal to unity. A wave of unit frequency in the dimensionless time variable travels shoreward and this wave is reflected and travels out to sea of an unit frequency. This solution is

$$\phi = AJ_0(\sigma)\cos\lambda \tag{5.40}$$

Using Equation 5.26, Equation 5.27, Equation 5.36, Equation 5.37 and Equation 5.40, exact solutions for $\eta(x,t)$ and $u(x,t)$ can easily be found in terms of σ and λ as

$$\eta = \frac{\phi_\lambda}{4} - \frac{u^2}{2} = -\frac{A}{4}J_0(\sigma)\sin\lambda - \frac{A^2J_1^2(\sigma)}{2\sigma^2}\cos^2\lambda \tag{5.41}$$

where J_1 is the usual notation for 1^{st} order Bessel function of the first kind.

$$u = \frac{\phi_\sigma}{\sigma} = -\frac{AJ_1(\sigma)\cos\lambda}{\sigma} \tag{5.42}$$

$$x = -\frac{\sigma^2}{16} + \frac{\sigma_\lambda}{4} - \frac{u^2}{2} = -\frac{\sigma^2}{16} - \frac{A}{4}J_0(\sigma)\sin\lambda - \frac{A^2J_1^2(\sigma)}{2\sigma^2}\cos^2\lambda \tag{5.43}$$

$$t = \frac{\lambda}{2} - u = \frac{\lambda}{2} + \frac{AJ_1(\sigma)\cos\lambda}{\sigma} \tag{5.44}$$

The resulting wave running up the sloping beach is periodic for $0 < A \leq 1$. To find the resultant wave at any time t, a value of σ is substituted in Equation 5.44 to find λ numerically by iteration. Then the values of σ and λ are substituted in Equations 5.41, Equation 5.42, and Equation 5.43 to find η, u and x. Using another value of σ, new value of λ is found and so on. Then the process is repeated for other values of t.

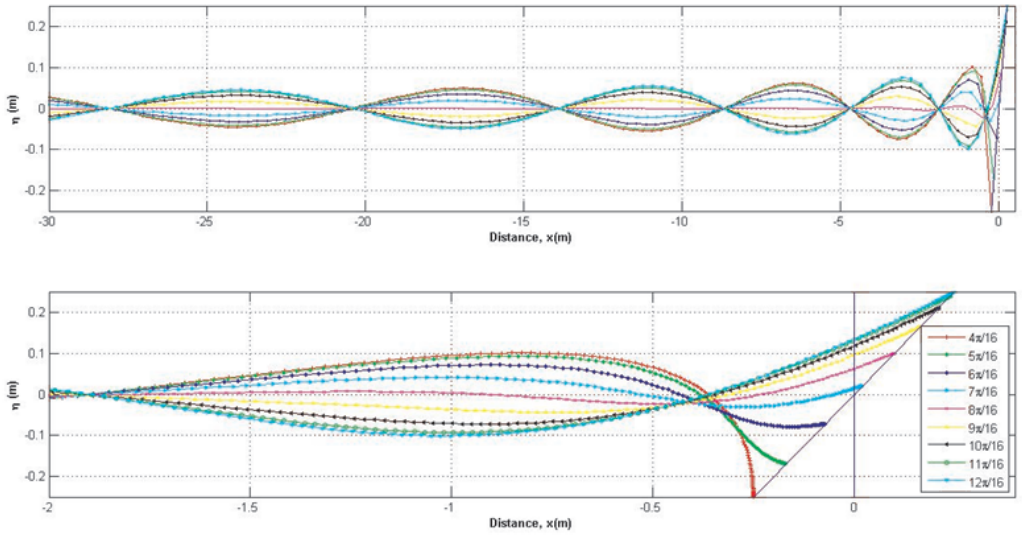

Figure 5.1. Variation of the Free Surface According to the Carrier and Greenspan (1958) Exact Solution.

The analytical solutions of Carrier and Greenspan (1958) (including Equation 5.41 to Equation 5.44) have been used by various researchers to test many numerical models such as Bokhove (2005), Cheng *et al.*, (1993), Dietrich *et al.*, (2004), Hibberd and Peregrine (1978), Johns (1982), Kowalik and Murty (1985), Lewis and Adams (1983), Pearson (1980), Prasad and Svensen (2003), Runchal (1975), Siden and Lynch (1988), Sielecki and Wurtele (1970), Vincent *et al.*, (2001), Zelt and Raichlen (1991), and Zhang (1996).

A number of other analytical solutions have been found that are modifications of Carrier and Greenspan's solutions. Ball (1964) found exact moving boundary solutions of the nonlinear shallow water equations in Lagrangian form. Sielecki and Wurtele (1970) tested their numerical model against these solutions. Keller and Keller (1964) obtained moving boundary analytical solutions of the LSWE for a periodic water wave traveling across an ocean of constant depth then running up a uniform plane beach. Shuto (1967) found exact moving boundary solutions of the linearized shallow water equations in Lagrangian form for flow on a sloping beach. His results for run-up height were found to be in close agreement with experimental results. Tuck and Hwang

(1972) investigated the generation of waves on a linear slope to simulate a tsunami due to seismic disturbances, using linearized equations. They also considered run-up using nonlinear equations which they transformed into linear equations which they solved.

Thacker (1981), using Eulerian equations, obtained exact moving boundary frictionless solutions of the shallow water wave equations similar to those obtained by Ball (1964) using Lagrangian equations. A number of numerical models have been tested against Thacker's exact solutions to name few; Balzano (1998), Holdahl *et al.*, (1998), Lewis and Adams (1983), Peterson *et al.*, (1984), Yoon and Cho (2001). Sachdev *et al.*, (1996) built on Thacker's work, producing periodic solutions for frictionless flow involving the Coriolis force.

Johns (1982) expressed Carrier and Greenspan's (1958) exact solution for moving boundary periodic flow in a simpler form, which involved periodic forcing at the open sea boundary. Li and Raichlen (2001) studied the run-up of solitary waves on a uniform plane beach connected to an open beach of constant depth. They obtained an analytical nonlinear solution using an approach based on that of Carrier and Greenspan (1958). The solution was in close agreement to experimental results, giving slightly better results for maximum run-up than the approximate linear theory of Synolakis (1987). Kanoğlu (2004) solved analytically Carrier and Greenspan's equations for the evolution of waves climbing sloping beaches for a number of different initial waveforms.

5.2. Theoretical Development of the Long Wave Propagation and run-up Model for case studies 1 and 2

The nonlinear, nondispersive shallow water model is based on the assumptions of hydrostatic pressure and uniform velocity distribution. The governing equations, the continuity and momentum equations in the Eulerian form, for one dimension in space and one dimension in time,(1+1), or 1D long wave propagation and run-up in the physical plane are

$$\frac{\partial \eta}{\partial t} + \frac{\partial}{\partial x}\left[u\left(h+\eta\right)\right] = 0 \tag{5.45}$$

$$\frac{\partial u}{\partial t} + u\frac{\partial u}{\partial x} + g\frac{\partial \eta}{\partial x} = 0 \tag{5.46}$$

In the case of moving boundary problems, the Lagrangian-Eulerian method was first introduced by Bellos and Sakkas (1987) for a dam-break flood- wave propagation problem. This solution exactly captured the moving shoreline by combining the Lagrangian description for the moving shoreline with the Eulerian description for the interior flow field. The solution domain extends from a fixed point ($x = -L$) at sea to the waterline which changes its position with time on the shore slope. If we denote by $\chi(t)$ the location of the waterline, then the velocity of the waterline is

$$\frac{d\chi(t)}{dt} = u\left(\chi(t), t\right) = U_0(t) \tag{5.47}$$

where $U_0(t)$ is the Lagrangian velocity of the mass at the waterline.

Consider the geometric transformation from the (x, t)-coordinates to the (ζ, τ)-coordinates given by

$$x = \left(1 + \frac{\chi(t)}{L}\right)\zeta + \chi(t) \tag{5.48}$$

This transformation maps the time varying domain $-L \leq x \leq \chi(t)$ to the fixed domain $-L \leq \zeta \leq 0$. Note that $t \equiv \tau$. To transform the continuity and momentum equations to the (ζ, τ)-coordinates, we have the following

$$\frac{\partial}{\partial t} = \frac{\partial}{\partial \tau}\frac{\partial \tau}{\partial t} + \frac{\partial}{\partial x}\frac{\partial x}{\partial \tau} \tag{5.49}$$

$$\partial x = \left(1 + \chi(t)/L\right)\partial\zeta \rightarrow \frac{\partial}{\partial x} = c_2(t)\frac{\partial}{\partial \zeta} \tag{5.50}$$

where $c_2\left(t\right)$ is defined as $\left(1 + \chi(t)/L\right)^{-1}$

$$\frac{\partial x}{\partial \tau} = \frac{\partial}{\partial \tau}\left[(1+\chi(t)/L)\zeta + \chi(t)\right] = \frac{\zeta}{L}\frac{\partial \chi}{\partial \tau}\frac{\partial \tau}{\partial t} + \frac{\partial \chi}{\partial \tau}\frac{\partial \tau}{\partial t} = \left(1+\frac{\zeta}{L}\right)\frac{\partial \chi}{\partial \tau} \tag{5.51}$$

Since $t \equiv \tau$

$$\frac{\partial \tau}{\partial t} = 1 \tag{5.52}$$

and

$$\frac{\partial \eta}{\partial t} = \frac{\partial \eta}{\partial \tau}\frac{\partial \tau}{\partial t} + \frac{\partial \eta}{\partial x}\frac{\partial x}{\partial \tau} = \frac{\partial \eta}{\partial \tau} + \left(\frac{1}{(1+\chi/L)}\frac{\partial \eta}{\partial \zeta}\right)\left[\left(1+\frac{\zeta}{L}\right)\frac{\partial \chi}{\partial \tau}\right] \tag{5.53}$$

Using Equation 5.47 and defining $(1+\zeta/L)/(1+\chi/L) = c_1(t)$ yields

$$\frac{\partial \eta}{\partial t} = \frac{\partial \eta}{\partial \tau} + c_1 U_0 \frac{\partial \eta}{\partial \zeta} \tag{5.54}$$

or

$$\frac{\partial \eta}{\partial \tau} = \frac{\partial \eta}{\partial t} - c_1 U_0 \frac{\partial \eta}{\partial \zeta} \tag{5.55}$$

Similarly

$$\frac{\partial u}{\partial \tau} = \frac{\partial u}{\partial t} - c_1 U_0 \frac{\partial u}{\partial \zeta} \tag{5.56}$$

Using Equation 5.50, Equation 5.55 and Equation 5.56 to transform the continuity and momentum equations gives,

$$\frac{\partial \eta}{\partial t} - c_1 U_0 \frac{\partial \eta}{\partial \zeta} + c_2 \frac{\partial}{\partial \zeta}\left[u(h+\eta)\right] = 0 \tag{5.57}$$

and

$$\frac{\partial u}{\partial t} - c_1 U_0 \frac{\partial u}{\partial \zeta} + c_2 \left[u \frac{\partial u}{\partial \zeta} + g \frac{\partial \eta}{\partial \zeta} \right] = 0 \tag{5.58}$$

5.3. Analytical Solution For Long wave Run-up On A Sloping Beach (Case Study 1)

Due to the difficulties of this nonlinear problem, only very few theoretical studies have been presented since Carrier-Greenspan's theory (1958). Other theories are more or less extensions of this theory.

In the analytical benchmark problem, 1D run-up of periodic long wave on a beach of uniform slope, α, is considered as seen in Figure 5.2 where α= 1. Carrier and Greenspan's solution (1958) to Equation 5.45 and Equation 5.46 for periodic wave of elevation $\eta(x,t)$ and horizontal velocity $u(x,t)$ can be expressed in parametric form as in Equation 5.40, Equation 5.44. On a sloping beach, this solution is a time-periodic wave for $0 < A \leq 1$, breaks (with infinite slope) at the waterline at the run-down extreme for the critical case of $A = 1$, and becomes multivalued for $A > 1$. Figure 5.3 to Figure 5.16 show Carrier-Greenspan's exact solution for the case of periodic waves and the corresponding numerical results of the present Lagrangian-Eulerian numerical method, both based on Equation 5.45 and Equation 5.46.

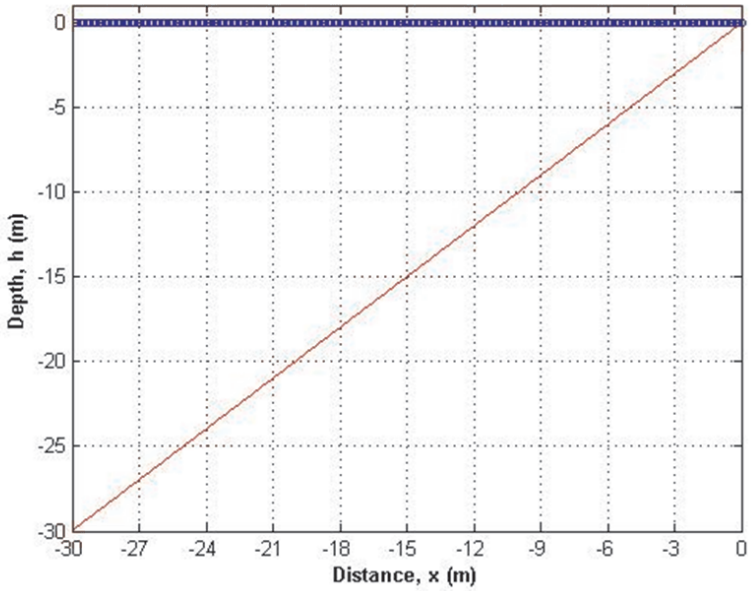

Figure 5.2. Geometry of the Solution Domain, 221 Collocation Nodes were Used in the Simulations.

For this numerical work, two initial conditions are required. From the Carrier-Greenspans solution Equation 5.41- Equation 5.44 at the $t_0 = \lambda/2 = 4\pi/16$ instant, $\eta(x, t_0)$ (implicitly by Equation 5.42), and $u(x, t_0)$ (implicitly by Equation 5.43) are the two initial conditions used for the warm start, respectively. As for the boundary condition on the ocean side the Sommerfeld radiation boundary condition is applied so that no disturbances are reflected back from the open boundary during the numerical experiment. In this numerical experiment MQRBF is used, and no optimization is required for the shape parameter, c, which is explained in Section 4.2.2 and is taken to be constant as $4r_{min}$ as suggested by Hon *et al.*, (1997; 1999).

By comparison, the present numerical results are found to be in excellent agreement with the exact analytical solution. Taking 220 collocation points over a 30 meter length of domain and a time increment of $\pi/8000$, the RMS error for the deviations of the η values from the analytical solution seem to be a most of order 10^{-4}. For the same time increment but with 101 nodes, the RMS error is 4 times greater as seen in Table 5.1. This excellent accuracy surpasses any other numerical methods known for solving this problem i.e. Zhang, (1996). Further, a CPU time of only 0.15 seconds per

time step is required on an Intel(R) Core (TM)2 Duo CPU E8400, 3.00 GHz processor. The entire runtime is 10 minutes.

For the run-up, Figure 5.3 Figure 5.11 are the comparisons at the fixed time instants, $t = 4\pi16, 5\pi/16, 6\pi/16, 7\pi/16, 8\pi/16, 9\pi/16, 10\pi/16, 11\pi/16$, and $12\pi/16$. Also, their RMS error for n=220 and n=101 collocation nodes can be found in Table 5.1.

Table 5.1. RMS Error for Run-Up at the Given Time Instants.

Time instant	RMS error (10^{-4}) n=220	RMS error (10^{-4}) n=101
$4\pi/16$	1.98	9.8
$5\pi/16$	2.08	10.5
$6\pi/16$	2.16	10.8
$7\pi/16$	2.28	11.2
$8\pi/16$	2.37	11.7
$9\pi/16$	2.41	11.4
$10\pi/16$	2.47	11.9
$11\pi/16$	2.51	12.1
$12\pi/16$	2.46	10.1
RMS error:	2.31	11.2

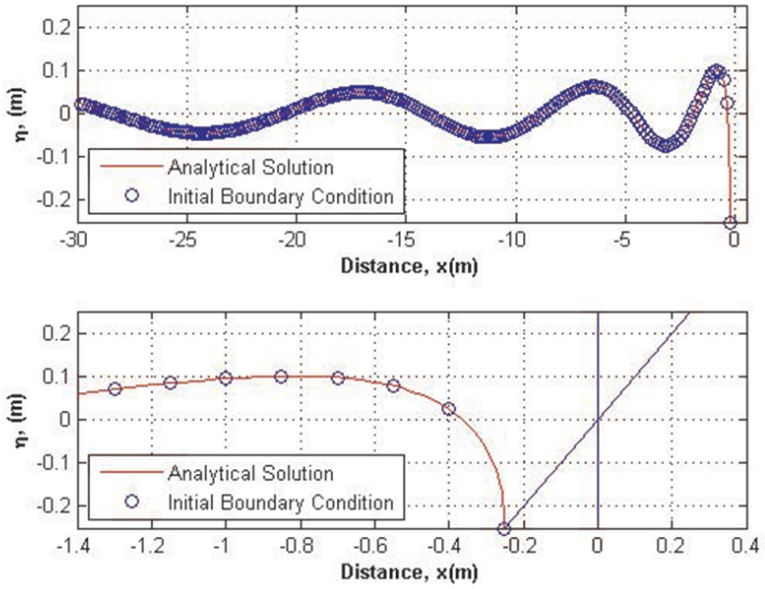

Figure 5.3. Comparison of the Initial Boundary Condition with the Carrier-Greenspan (1958) Exact Solution for Run-up of a Periodic Wave on a Sloping Beach, A=1.0, Initial Condition at $t = 4\pi/16$.

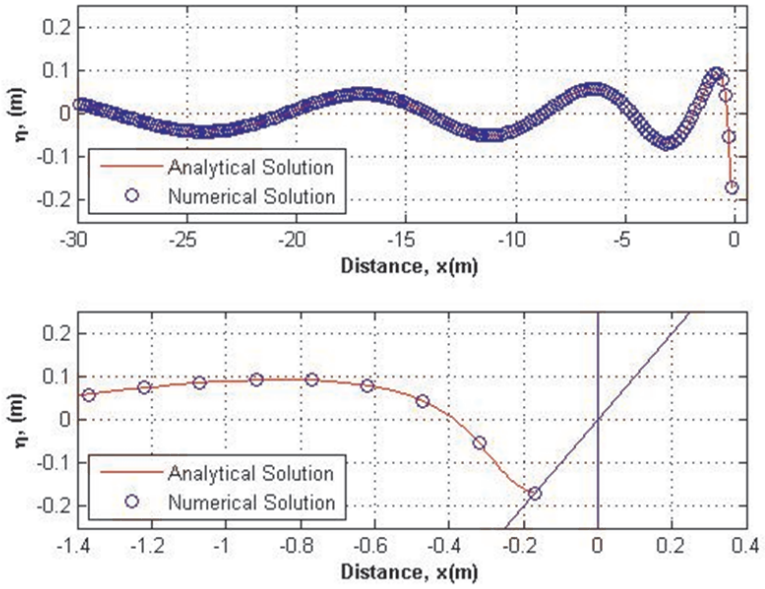

Figure 5.4. Comparison of the Numerical Results with the Carrier-Greenspan (1958) Exact Solution for Run-up of a Periodic Wave on a Sloping Beach, A=1.0, Computed at t=$5\pi/16$.

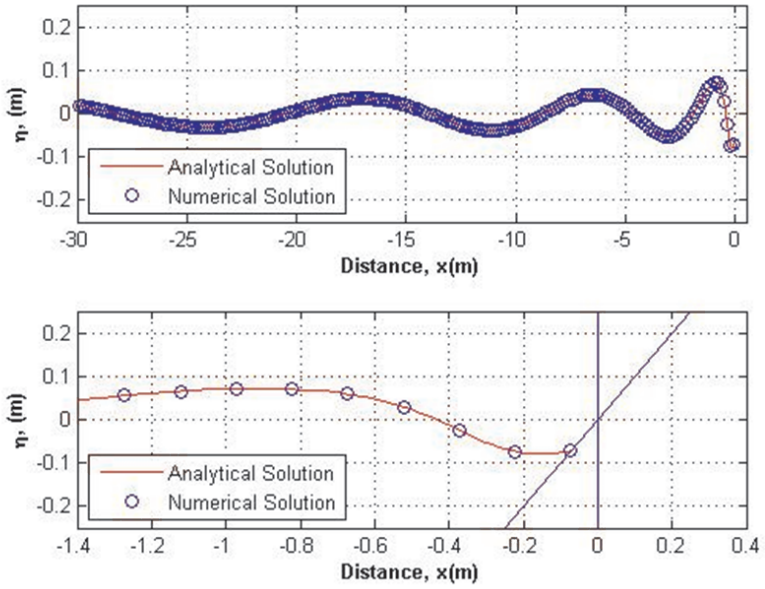

Figure 5.5. Comparison of the Numerical Results with the Carrier-Greenspan (1958) Exact Solution for Run-up of a Periodic Wave on a Sloping Beach, A=1.0, Computed at t=$6\pi/16$.

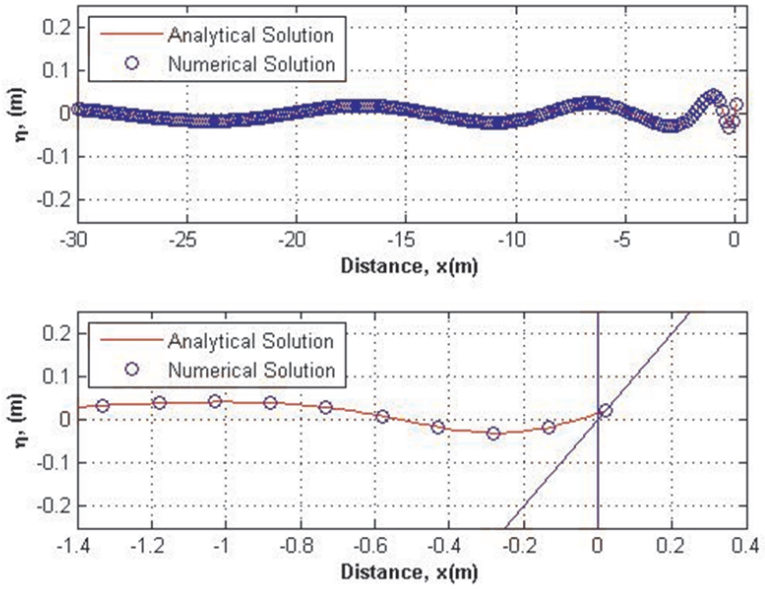

Figure 5.6. Comparison of the Numerical Results with the Carrier-Greenspan (1958) Exact Solution for Run-up of a Periodic Wave on a Sloping Beach, A=1.0, Computed at t=$7\pi/16$.

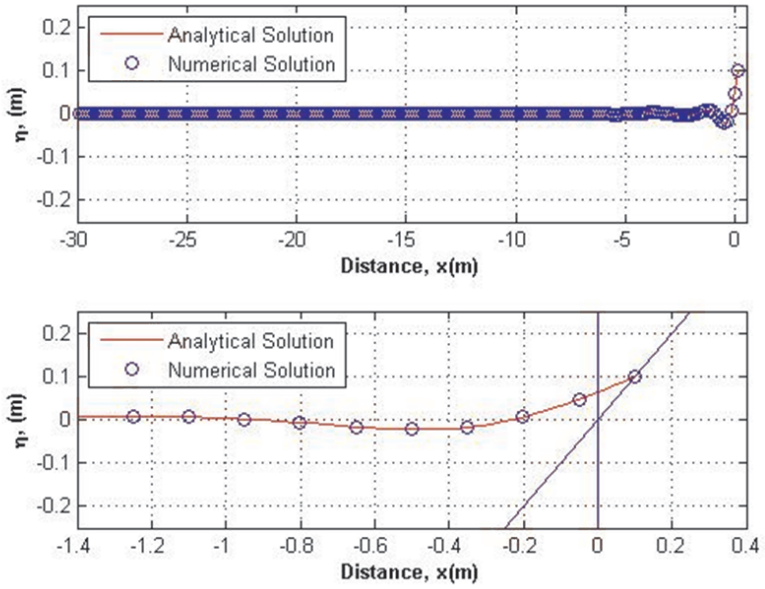

Figure 5.7. Comparison of the Numerical Results with the Carrier-Greenspan (1958) Exact Solution for Run-up of a Periodic Wave on a Sloping Beach, A=1.0, Computed at t=$8\pi/16$.

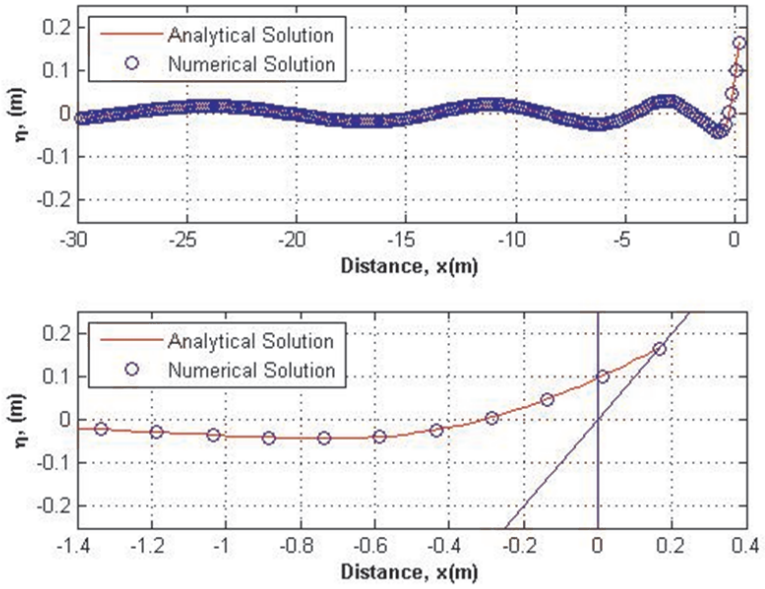

Figure 5.8. Comparison of the Numerical Results with the Carrier-Greenspan (1958) Exact Solution for Run-up of a Periodic Wave on a Sloping Beach, A=1.0, Computed at t=$9\pi/16$.

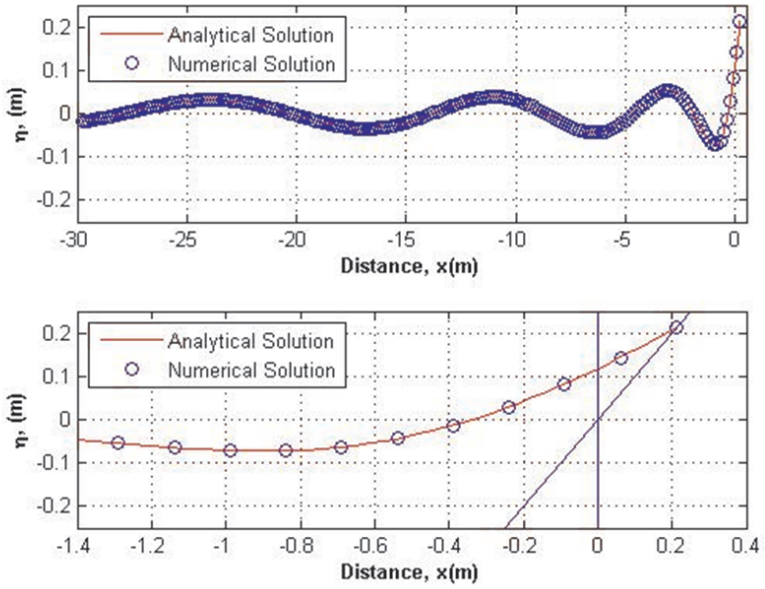

Figure 5.9. Comparison of the Numerical Results with the Carrier-Greenspan (1958) Exact Solution for Run-up of a Periodic Wave on a Sloping Beach, A=1.0, Computed at t=$10\pi/16$.

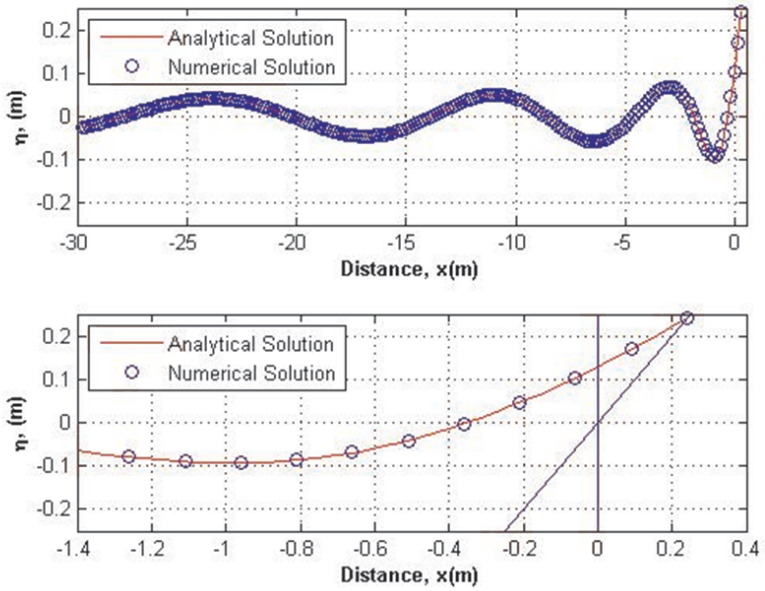

Figure 5.10. Comparison of the Numerical Results with the Carrier-Greenspan (1958) Exact Solution for Run-up of a Periodic Wave on a Sloping Beach, A=1.0, Computed at t=$11\pi/16$.

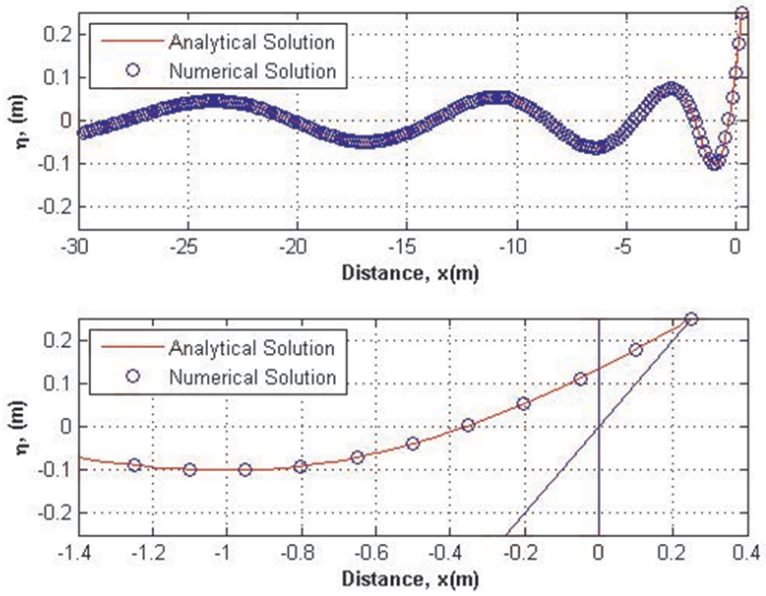

Figure 5.11. Comparison of the Numerical Results with the Carrier-Greenspan (1958) Exact Solution for Run-up of a Periodic Wave on a Sloping Beach, A=1.0, Computed at t=$12\pi/16$.

The present numerical results are found to be in excellent agreement with the analytical solution. Taking 220 collocation points over a 30 meter length of domain and with a time increment of $\pi/8000$, the RMS error is uniformly less then 2.29x10^{-4}. For the same time increment with 101 nodes, the RMS error is 4 times greater and 1.09x 10^{-3} thus qualifying the scheme as being of the second order.

Figure 5.12- Figure 5.16 are for a fixed time instant, $t = 12\pi/16, 14\pi/16, 16\pi/16, 18\pi/16,$ and $20\pi/16$, for the run-down. Also, their RMS error norms both for a loose collocation node and a dense collocation node cases can be found in Table 5.2.

Table 5.2. RMS Error for Run-Down at the Given Time Instants.

Time instant	RMS error (10^{-4}) n=220	RMS error (10^{-4}) n=101
$12\pi/16$	2.45	10.2
$14\pi/16$	2.49	12.1
$16\pi/16$	2.36	11.6
$18\pi/16$	2.17	11.0
$20\pi/16$	1.99	9.7
RMS error:	2.29	10.9

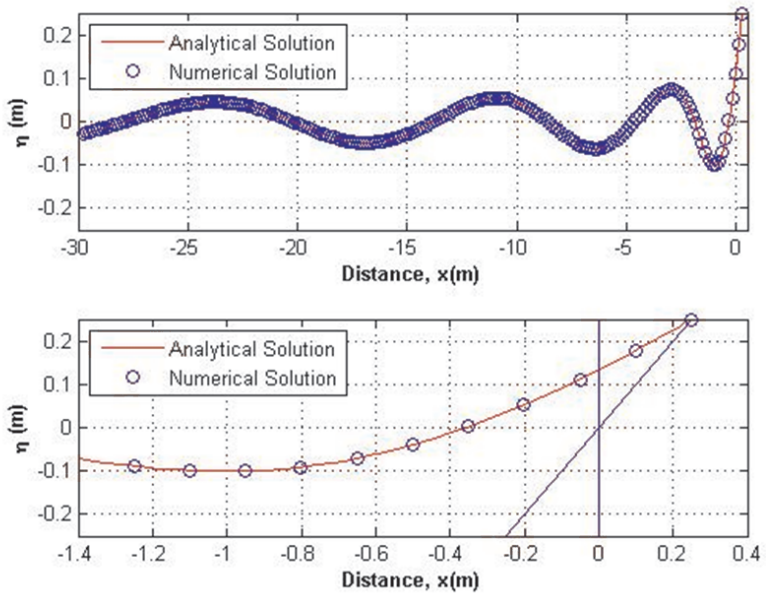

Figure 5.12. Comparison of the Initial Boundary Condition with the Carrier-Greenspan (1958) Exact Solution for Run-down of a Periodic Wave on a Sloping Beach, A=1.0, Computed at t=$12\pi/16$.

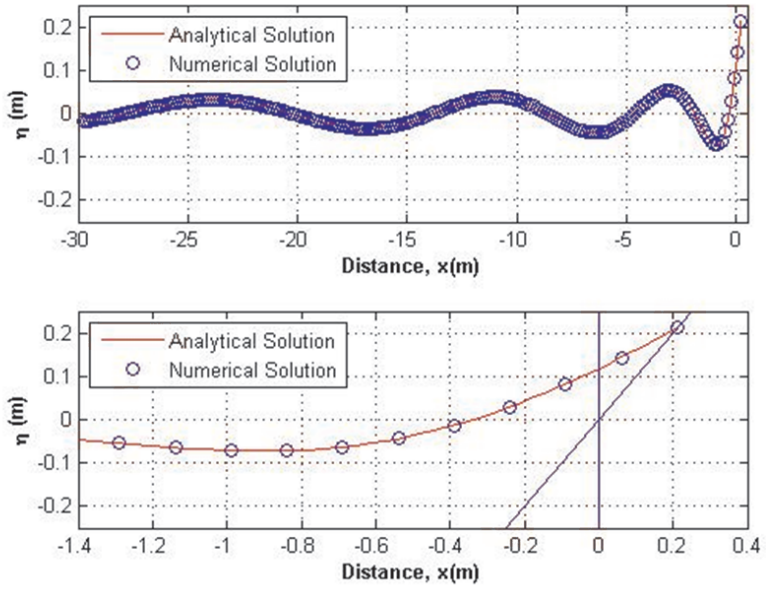

Figure 5.13. Comparison of the Numerical Results with the Carrier-Greenspan (1958) Exact Solution for Run-down of a Periodic Wave on a Sloping Beach, A=1.0, Computed at t=14π/16.

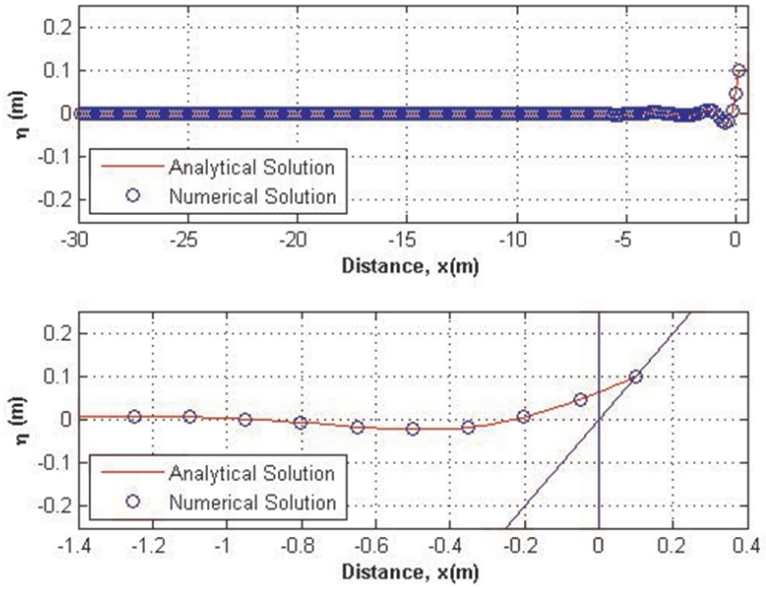

Figure 5.14. Comparison of the Numerical Results with the Carrier-Greenspan (1958) Exact Solution for Run-down of a Periodic Wave on a Sloping Beach, A=1.0, Computed at t=16π/16.

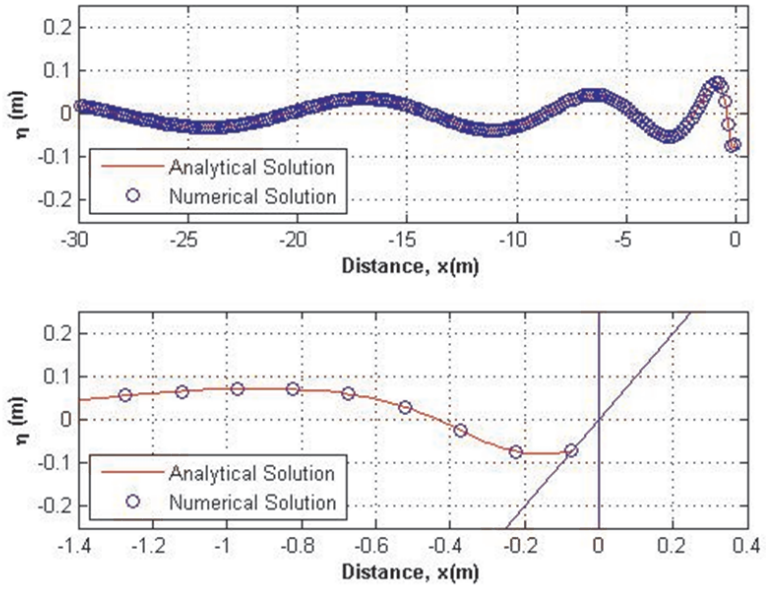

Figure 5.15. Comparison of the Numerical Results with the Carrier-Greenspan (1958) Exact Solution for Run-down of a Periodic Wave on a Sloping Beach, A=1.0, Computed at t=18π/16.

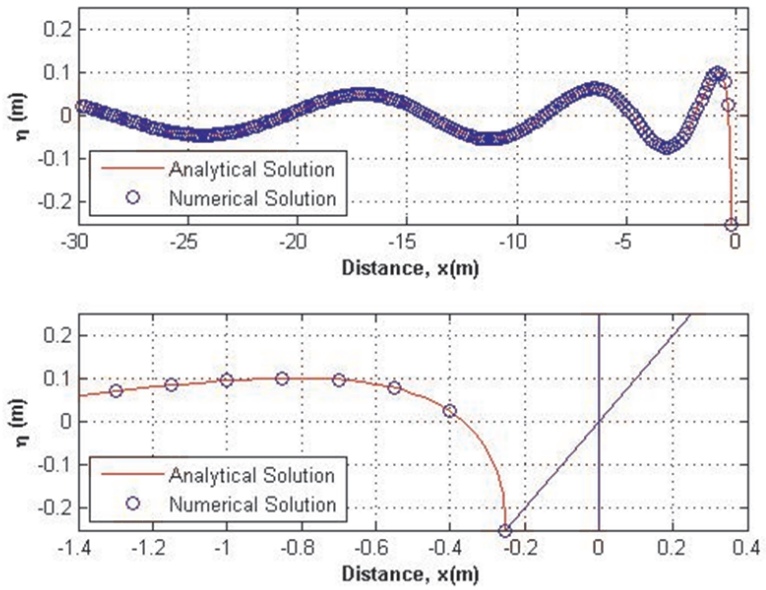

Figure 5.16. Comparison of the Numerical Results with the Carrier-Greenspan (1958) Exact Solution for Run-down of a Periodic Wave on a Sloping Beach, A=1.0, Computed at t=20π/16.

5.4. Long Wave Run-up On A Sloping Beach (Case Study 2)

A meshless method based on the RBFs is used to solve the nonlinear, nondispersive shallow water equations. The one dimensional initial value problem has a moving free surface boundary. As stated in Section 5.2, the formulation employs a Lagrangian-Eulerian scheme to track the movement of the free boundary and transforms the problem to a time-independent domain. The results obtained from the numerical simulations in case study 1 using the RBFCM provided motivation to compare the two numerical codes of Zhou *et al.*, (2004) and this study. In the former, the Wilson-θ method, in the latter developed code, the Adams-Basforth-Moulton method is used to advance the solution in time and RBF evaluates the spatial derivatives.

The RBFCM was applied to simulate the wave run-up and run-down of a long wave propagating from an open ocean of depth h_0 onto a uniformly sloping plane beach as depicted Figure 5.17. The water depth taken to vary as

$$h = \begin{cases} \alpha\zeta, & -\frac{h_0}{\alpha} \leq \zeta \leq 0 \\ h_0, & x < -\frac{h_0}{\alpha} \end{cases} \tag{5.59}$$

where ζ represents the spatial horizontal coordinate and α denotes the slope of the plane beach. The fixed domain is $[-L, 0]$. The wave in the fixed domain is given as;

$$U_0(t) = A\sin(\omega t) \tag{5.60}$$

which is originally located L meters from the shoreline of the beach. The boundary conditions are,

$$\eta\,(0,t) = \alpha\chi\,(t)\,, \quad u(-L,t) = U_0(t) \tag{5.61}$$

The initial conditions, a cold start, are taken to be,

$$\eta\,(x,0) = 0, \quad u(x,0) = 0 \tag{5.62}$$

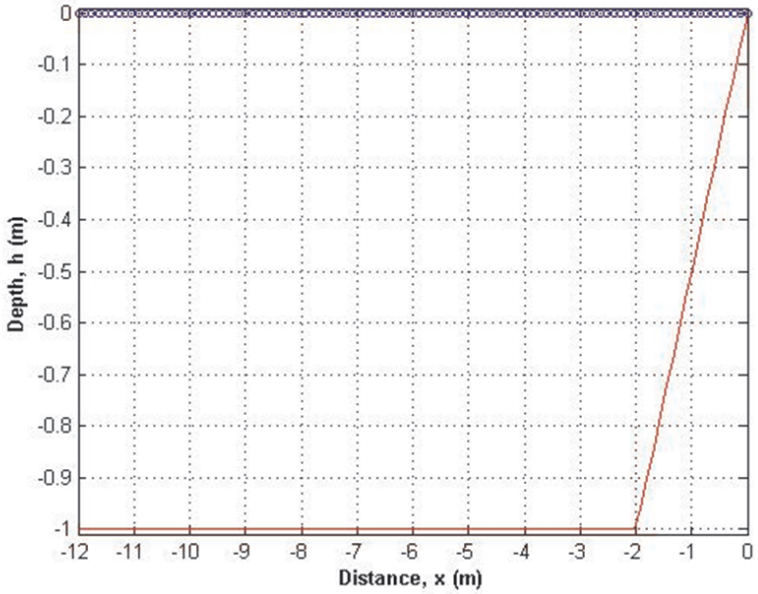

Figure 5.17. Geometry of the Solution Domain, 101 Collocation Nodes were Used in the Simulations.

The parameters used in the simulations are given in the Table 5.3.

Table 5.3. Comparison of Wave and Domain Parameters.

Parameters	Zhou *et al.*, (2004)	This study
Depth, h_0 [m]	1	1
Slope, α	0.5	0.5
Velocity Amplitude, A [m]	0.06	0.06
Wave Frequency, ω	$\sqrt{g}$	$\sqrt{g}$
Domain Length, L	12m	12m
Time domain, [sec]	[0-10]	[0-10]
The total number of time steps	500	10000
The total number of the points used, n	101	101
Shape parameter, c^2 [m^2]	16	0.0576

The results of the numerical simulation are shown in Figure 5.18. The horizontal lines, A=0.06, in Figure 5.18 show the maximum vertical amplitude of the wave run-

up problem. For the same accuracy with Zhou *et al.*, (2004)'s model, my simulation needs more time steps with a small shape parameter which plays an important role for the accuracy of the method. In most papers the authors end up choosing this shape parameter by trial and error or some other ad-hoc means. An unwelcome aspect appears when the linear systems are solved by the shape parameter they used, the matrix turned out to be ill-conditioned. When the value of shape parameter increases more increasingly flat basis functions occur, this leads to a severely ill-conditioned problem as stated in Buhmann (2003). From Figure 5.19 Figure 5.23 it can be observed that the RBFCM was successful in simulating the wave run-up phenomena. RMS error is $2.7\text{x}10^{-4}$.

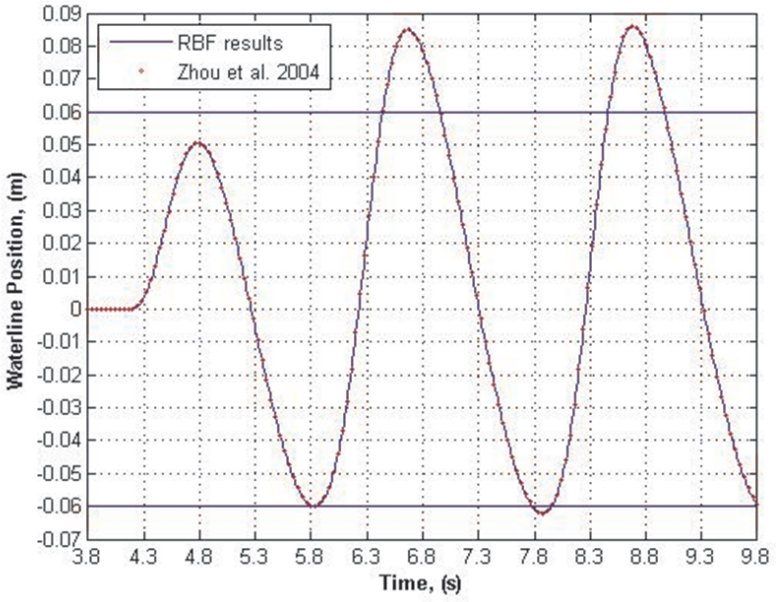

Figure 5.18. Vertical Amplitude of the Wave in the Run-up Problem.

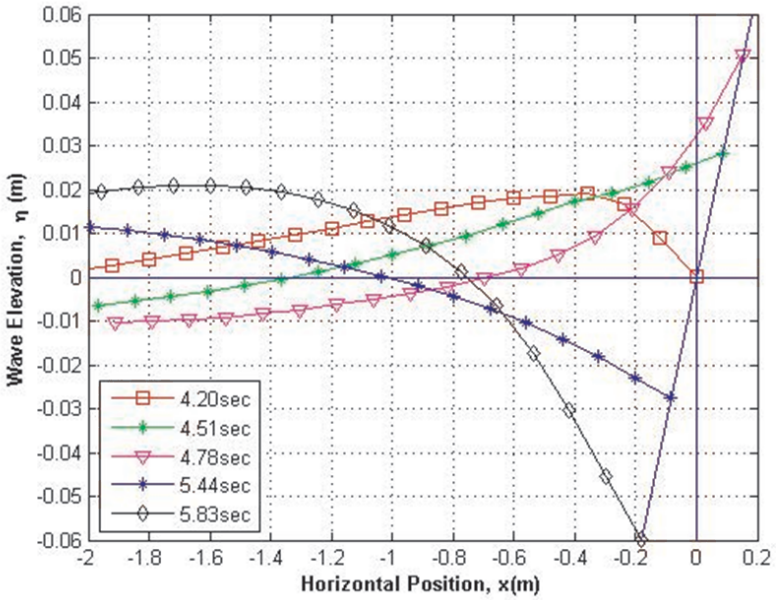

Figure 5.19. Wave Run-Up and Run-Down Profile Between 4.20 and 5.83 Seconds on the Sloping Plane Beach.

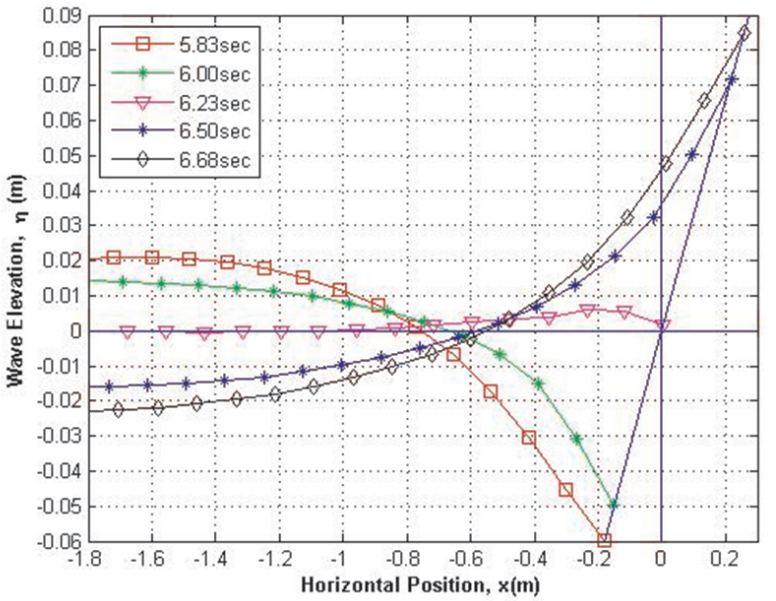

Figure 5.20. Wave Run-Up Profile Between 5.83 and 6.68 Seconds on the Sloping Plane Beach.

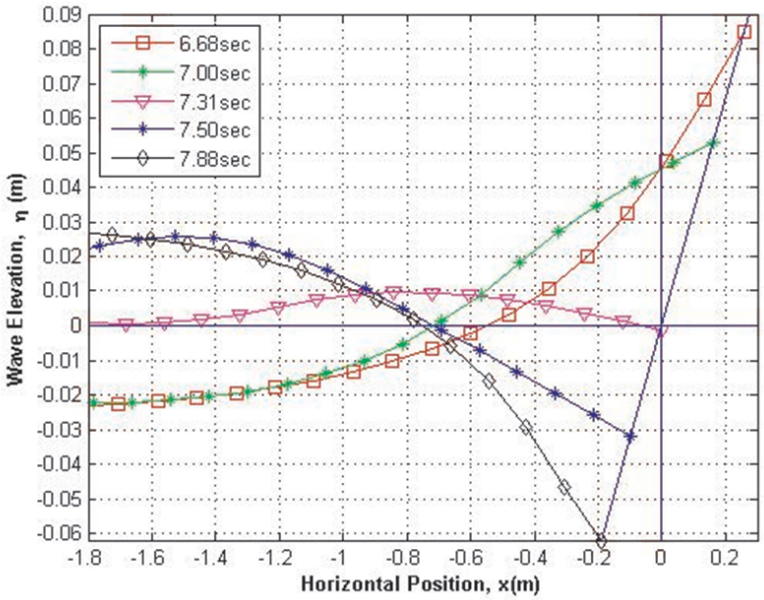

Figure 5.21. Wave Run-Down Profile Between 6.68 and 7.88 Seconds on the Sloping Plane Beach.

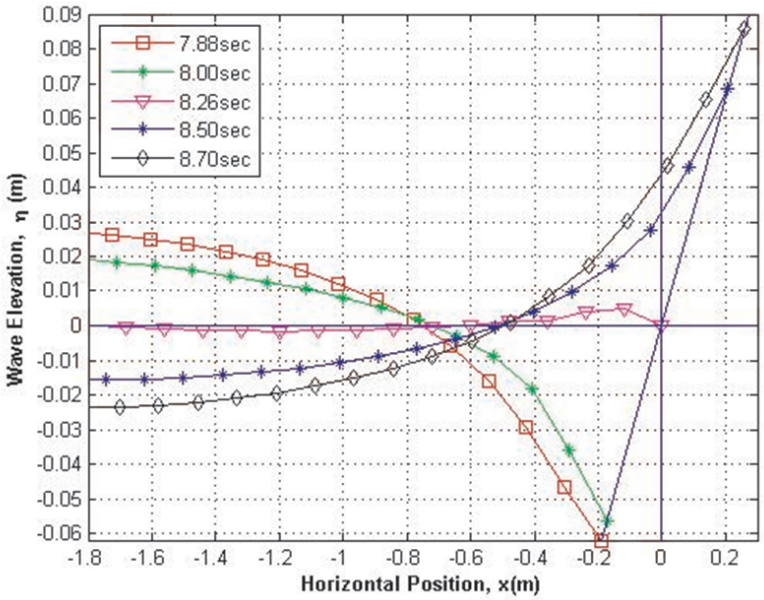

Figure 5.22. Wave Run-Up Profile Between 7.88 and 8.70 Seconds on the Sloping Plane Beach.

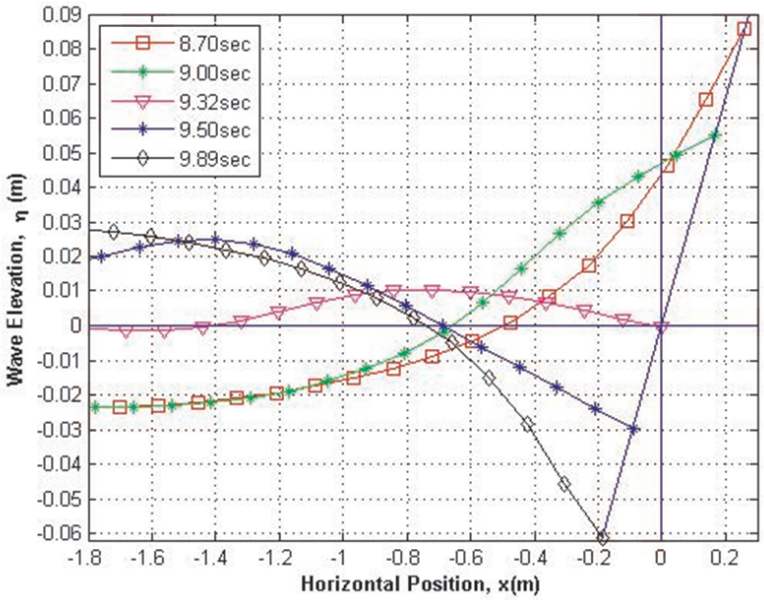

Figure 5.23. Wave Run-Down Profile Between 8.70 and 9.89 Seconds on the Sloping Plane Beach.

5.5. Long Wave Propagation Problems with Sponge Treatment

The results of some selected numerical tests are given and compared with the linear and one dimensional nonlinear solution in terms of the normalized free surface displacements. There are several parameters involved in the problem. These are input wave parameter such as wave steepness, period and Ursell number (UN) (Ursell, 1953), problem dimensions such as the length, width of the domain and the sponge layer, computationally necessary parameters such as the time step, the shape parameter and the Courant-Friedrichs-Lewy (CFL) condition (Courant *et al.*, 1967). UN indicates the nonlinearity in the long wave limit of shallow water and simply stated as the ratio of the amplitudes of the second-order to the first-order term in the free surface elevation.

When model runs were being performed, experiments on the accuracies associated with using different time steps were analyzed. It was decided to take a rule of thumb type of time step and apply the same approach on all of the models. CFL condition states that the computational speed of the wave should not be greater than the physical speed of the wave. Time step for the computational wave should be less than the time

for the wave to travel to the next time step. To avoid any such violation, for all of the models, the time increments were in the order of one-thousandth of a second was chosen and better results obtained. Time steps of smaller that one-thousandth of a second were tried and found not to contribute toward increasing accuracy of the results and also consume computational time. Each case that was run is for 20-24 simulation periods.

On the other hand, wave steepness criterion which is one of the most critical parameters to construct stabilized numerical solution is overcomed for the LSWE. Also, for the NSWE model, the steeper the wave, the less accurate results are obtained. The numerical tests in this study have shown that beyond a limiting steepness and UN, the accuracy of the results worsens. The test cases for comparison are selected according to wave steepness and UN which for linear wave solution and nonlinear wave solution of the given data in Table 5.4. The highest UN that the developed code can solve for the test cases are shown in all Figure. The largest UN that the NSWE code can handle is approximately 50.

Table 5.4. Test Cases Wave Parameters.

T (s)	H (m)	h (m)	ω (s^{-1})	$L_0(m)$	h/L_0	kh	L (m)	a/h	h/L	UN
2	0.01	1	3.142	6.245	0.16012	1.205	5.22	0.005	0.192	0.136
	0.02	1	3.142	6.245	0.16012	1.205	5.22	0.010	0.192	0.272
	0.03	1	3.142	6.245	0.16012	1.205	5.22	0.015	0.192	0.408
	0.04	1	3142	6.245	0.16012	1.205	5.22	0.020	0.192	0.544
4	0.01	1	1.571	24.981	0.04003	0.524	12,00	0.005	0.083	0.720
	0.02	1	1.571	24.981	0.04003	0.524	12.00	0.010	0.083	1.440
	0.03	1	1.571	24.981	0.04003	0.524	12.00	0.015	0.083	2.160
	0.04	1	1.571	24.981	0.04003	0.524	12.00	0.020	0.083	2.881
8	0.01	1	0.785	99.924	0.01001	0.253	24.79	0.005	0.040	3.074
	0.02	1	0.785	99.924	0.01001	0.253	24.79	0.010	0.040	6.147
	0.03	1	0.785	99.924	0.01001	0.253	24.79	0.015	0.040	9.221
	0.04	1	0.785	99.924	0.01001	0.253	24.79	0.020	0.040	12.295
16	0.01	1	0.393	399.695	0.0025	0.126	49.98	0.005	0.020	12.491
	0.02	1	0.393	399.695	0.0025	0.126	49.98	0.010	0.020	24.982
	0.03	1	0.393	399.695	0.0025	0.126	49.98	0.015	0.020	37.474
	0.04	1	0.393	399.695	0.0025	0.126	49.98	0.020	0.020	49.965

The placement density of the centers is an important factor in obtaining accurate results. High density not only results in long computational times but also leads to ill-conditioned systems matrices and non-converging schemes.

5, 9, 17, 33 and 65 collocation points per wave length were tested both for the LSWE solution and the NSWE solution. As seen from Figure 5.24, the best results were obtained for 33 and 65 collocation nodes per wave length in the NSWE solution where the shape parameter, c, is taken to equal as $4r_{min}$ as suggested by Hon *et al.*, (1997; 1999) vertical lines in the Figure 5.24 drawn at $\pm 3L$ where the sponge layer starts. For the rest of the test cases collocation nodes per wave length was fixed to 33 nodes to save memory and to decrease the computational time.

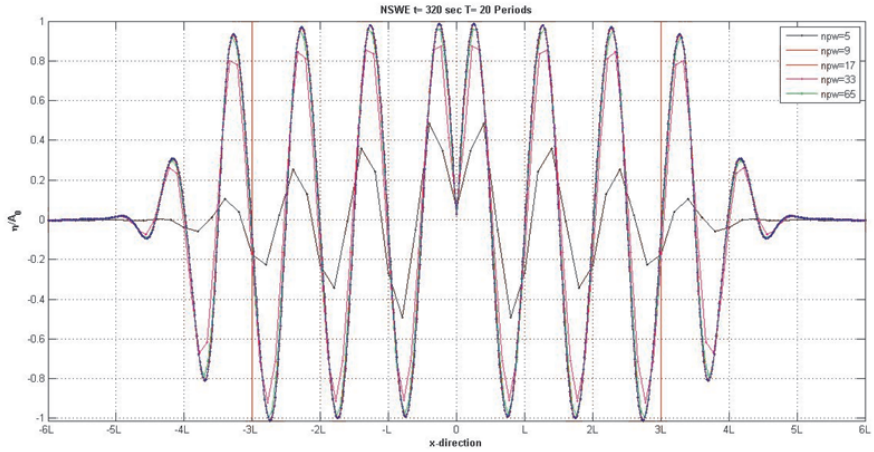

Figure 5.24. Comparison of NSWE Solutions for Different Choices of Nodes per Wave Length, c=$4r_{min}$ following Hon *et al.*, (1997).

Another adjustment necessary to obtain accurate solution is shape parameter. Although, there are several studies on the selection of the shape parameter as explained in Chapter 4, there is no common agreement for the optimum value. Therefore, the strategy adopted here is to start with the suggested values, then, to refine this value by trail and error. To achieve this different shape parameters are used and the percentage reflection from the sponge layer is investigated. In the tests single half positive wave, single half negative wave, single wave and airy wave are tested. Figure 5.25 shows the periodic wave's shape parameter optimization to minimize the reflection from the sponge layers. All the other wave types have the same trait. Due to the fluctuations at the end of the sponge layers, the optimum shape parameter is not the one where the minimum reflection occurs. To overcome this problem, Sommerfeld radiation boundary condition is employed at both ends of sponge layers. As a result of the tests conducted,

the optimum square of the shape parameter, c^2, was found to be between 80-100 cm^2. In an expressional form shape parameter, c, can be taken as $2\pi r_{min}$ where r_{min} is between 0.1 and 1.9 meters.

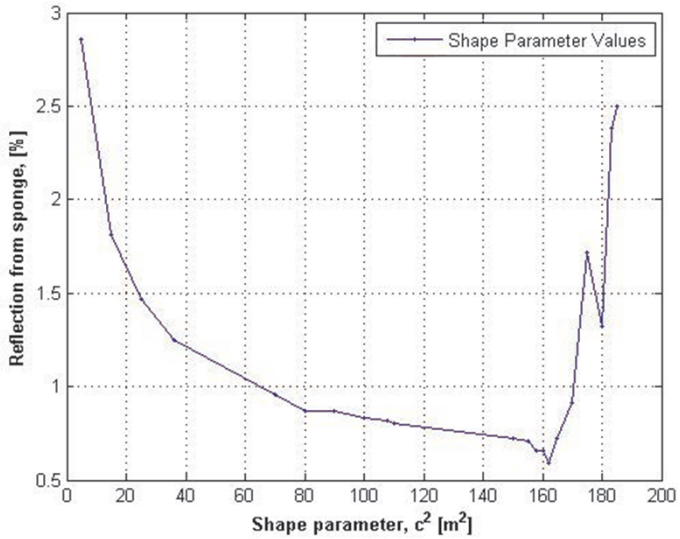

Figure 5.25. Optimizing Shape Parameter with Sponge Layers and RBC at the Ends.

Once the adequate resolution and optimum shape parameter are obtained, time integrator tests are done. All the time integrators as seen from the figure have the same order of accuracy to illustrate this observation Figure 5.26 is given, nevertheless, they have different computational time. More detailed of Figure 5.26 is shown in Figure 5.27 for wave amplitudes, their UN and RMS error by ABM O(4) integrator.

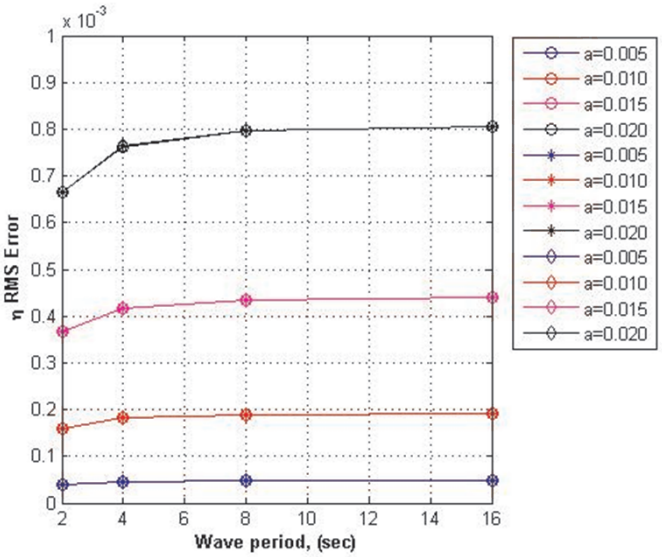

Figure 5.26. Comparison of RMS Error of Different Time Integrators, ABM O(4) (Circles), MH O(4) (Stars), RK O(4)(Diamonds), and for a Linear Wave of Different Wave Amplitudes.

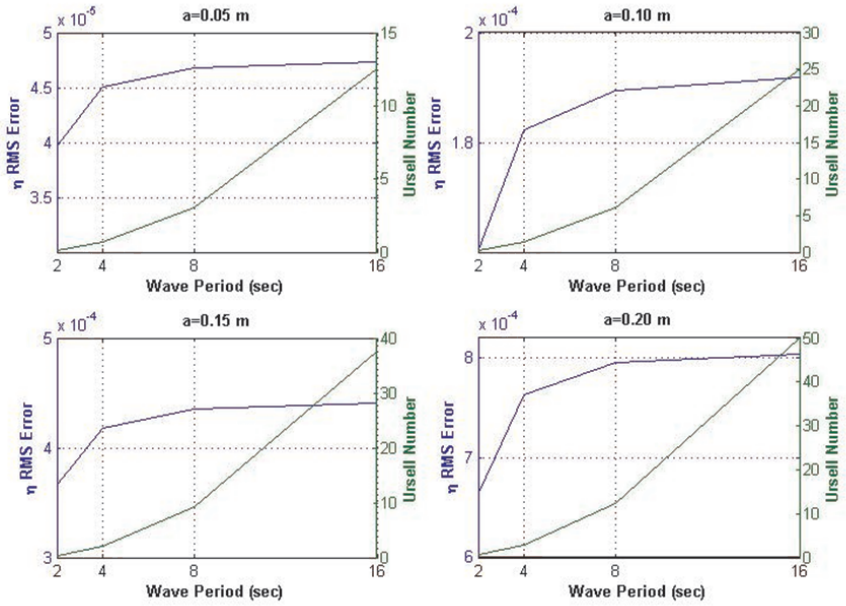

Figure 5.27. Comparison of UN and RMS Error with Wave Amplitudes.

Another important adjustment necessary to obtain accurate solutions is on the sponge layer coefficients. Despite the fact that there are few studies that suggest the values of sponge coefficients, again by trail and error the damping coefficients can easily

be determined by the type of the wave used in the simulations. The sponge layer length in this case is three times the wavelength in both the positive and in the negative x directions.

Recalling the x direction momentum Equation 4.32 and the sponge layer Equation 4.33 and rearranging them for 1D yield ;

$$\frac{\partial u}{\partial t} + u\frac{\partial u}{\partial x} = -g\frac{\partial \eta}{\partial x} \underbrace{-w_1(x)u - w_2(x)u_{xx}}_{inside\,the\,sponge\,layer\,on\,the\,x-axis} \tag{5.63}$$

and

$$\left.\begin{aligned} -w_1(x) &= \begin{cases} 0 & ,x < x_s \\ \alpha_1 \omega f(x) & ,x \geq x_s \end{cases} \\ -w_2(x) &= \begin{cases} 0 & ,x < x_s \\ \alpha_2 \upsilon f(x) & ,x \geq x_s \end{cases} \end{aligned}\right\} f(x) = \frac{\exp\left(\frac{x-x_s}{x_l-x_s}\right)^n}{\exp(1)-1} \tag{5.64}$$

The variation of the sponge layer coefficients, $w_1(x)$ and $w_2(x)$, with constant α_1 and α_2 coefficients shown in Figure 5.28. When power, n of the sponge layer coefficient increases the wave enters the sponge layer more, less reflection occurs, nevertheless, the stability problems arises even for one dimensional problems. Thus, in the simulations n is selected to be 2. The variation of the sponge layer coefficients, $w_1(x)$ and $w_2(x)$, with constant n=2, and α_2=0.1 coefficients shown in Figure 5.29. The change in the α_1 term has no effect on $w_2(x)$. As seen in Figure 5.30 this time, the change in the α_2 term has no effect on $w_1(x)$. The moderate coefficients selected as α_1=10 and α_2 is 0.1 to avoid computational instabilities.

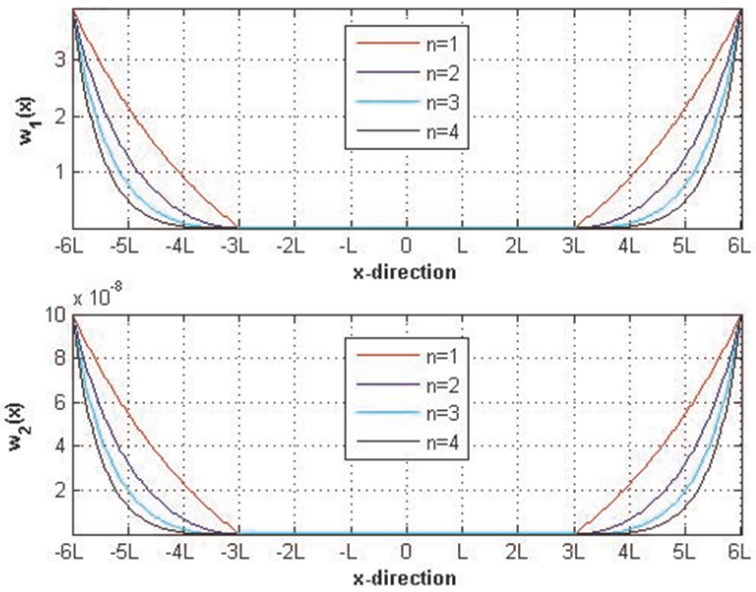

Figure 5.28. Variation of Sponge Layer Coefficients $w_1(x)$ and $w_2(x)$ (α_1=10 and α_2=0.1).

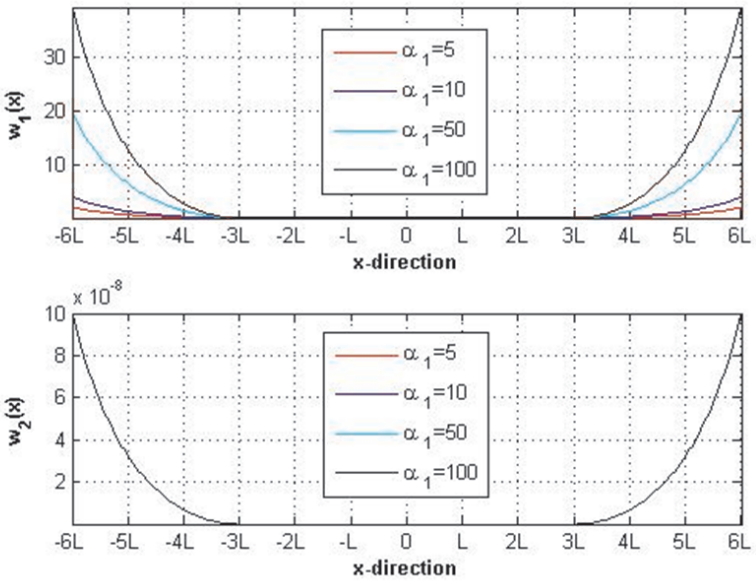

Figure 5.29. Variation of Sponge Layer Coefficients $w_1(x)$ and $w_2(x)$ (n=2 and α_2=0.1).

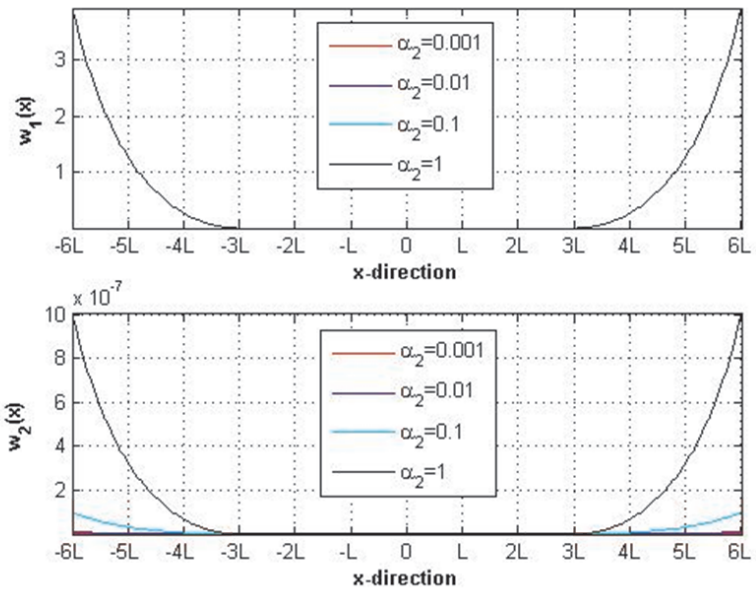

Figure 5.30. Sponge Layer Coefficients $w_1(x)$ and $w_2(x)$ (n=2 and α_1=10).

The improvement in the accuracy of the results directly effected by the sponge layer coefficients and the shape parameter due to the slight reflection from the sponge layer. The propagation and reflection of a single positive wave, a single negative wave and a single full wave can be seen in the Figure 5.31 Figure 5.38 for 0.5, 1, 3, 3.5, 4, 5, 6, and 12 simulation periods. The reflection diminishes in time since the reflected wave from left sponge layer captured by the right sponge layer in time. The reflection can be minimized in the half waves by changing the wave parameters to have small UN. Thus, the difficulty of using sponge layer arises from the coefficients to be used needs to be changed according to the type of the input wave.

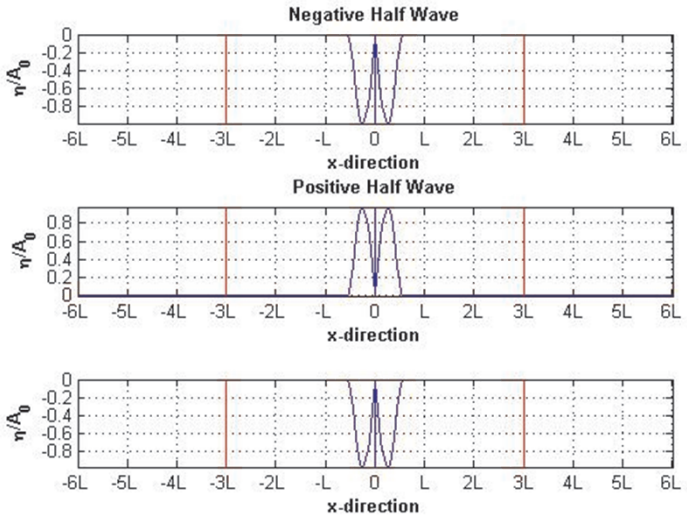

Figure 5.31. The Propagation and Reflection of a Single Negative Half Wave, a Single Positive Half Wave and a Single Full Wave by Using NSWE at t=0.5T.

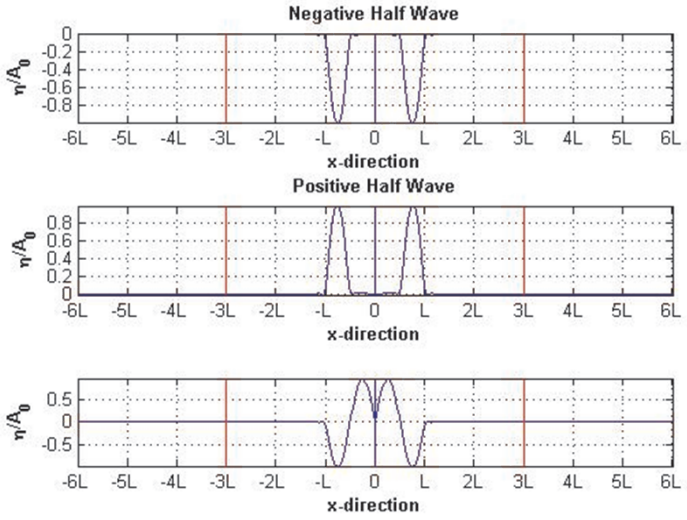

Figure 5.32. The Propagation and Reflection of a Single Negative Half Wave, a Single Positive Half Wave and a Single Full Wave by Using NSWE at t=T.

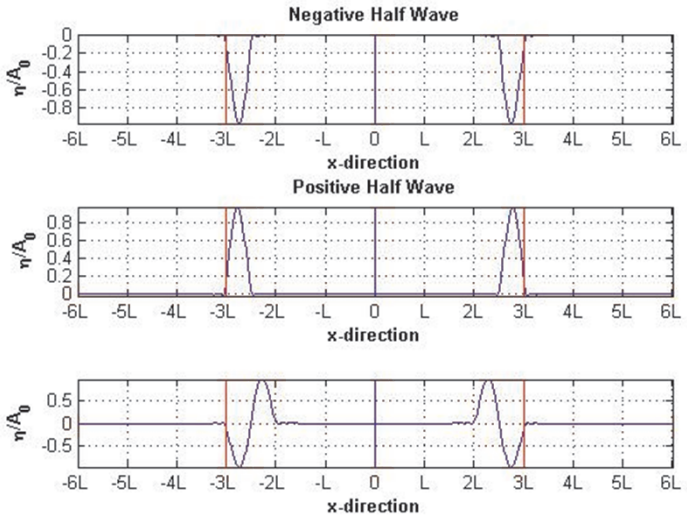

Figure 5.33. The Propagation and Reflection of a Single Negative Half Wave, a Single Positive Half Wave and a Single Full Wave by Using NSWE at t=3T.

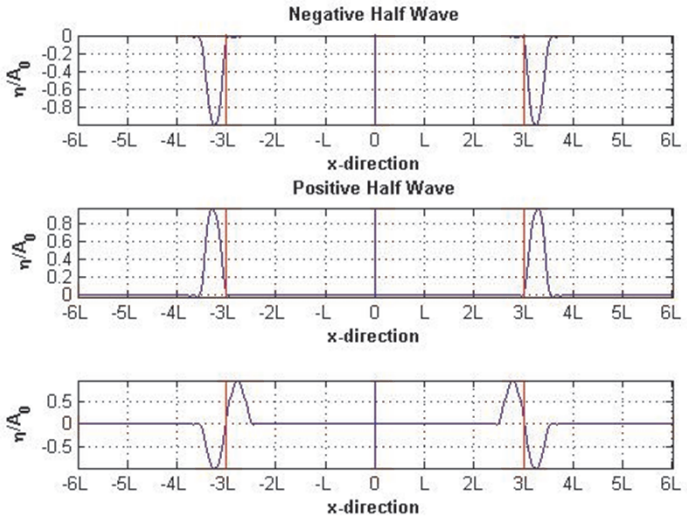

Figure 5.34. The Propagation and Reflection of a Single Negative Half Wave, a Single Positive Half Wave and a Single Full Wave by Using NSWE at t=3.5T.

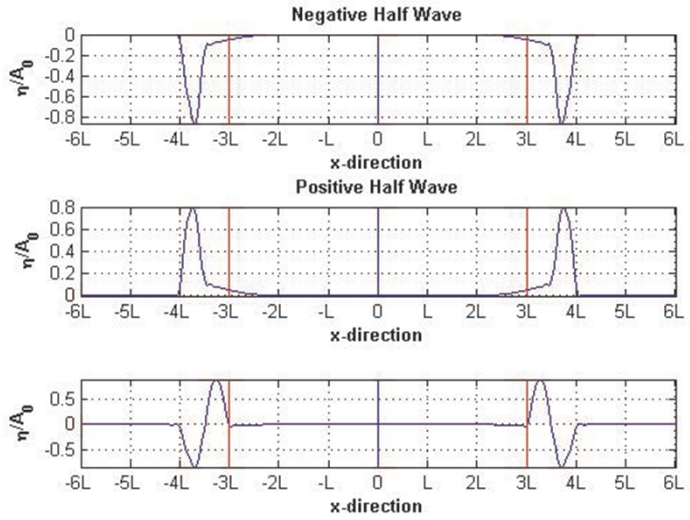

Figure 5.35. The Propagation and Reflection of a Single Negative Half Wave, a Single Positive Half Wave and a Single Full Wave by Using NSWE at t=4T.

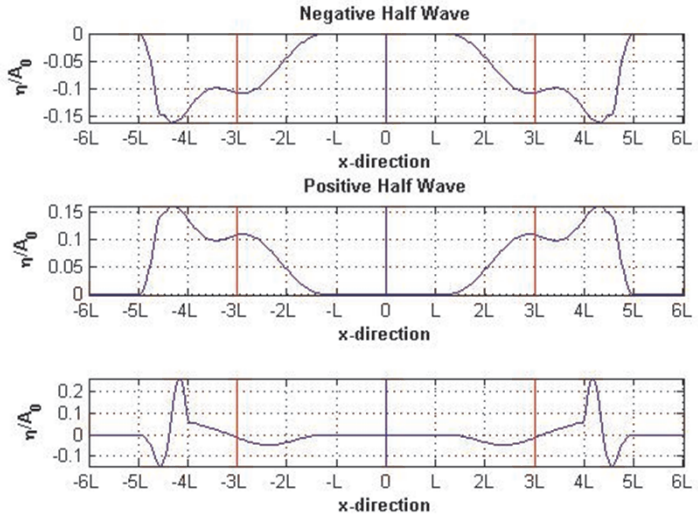

Figure 5.36. The Propagation and Reflection of a Single Negative Half Wave, a Single Positive Half Wave and a Single Full Wave by Using NSWE at t=5T.

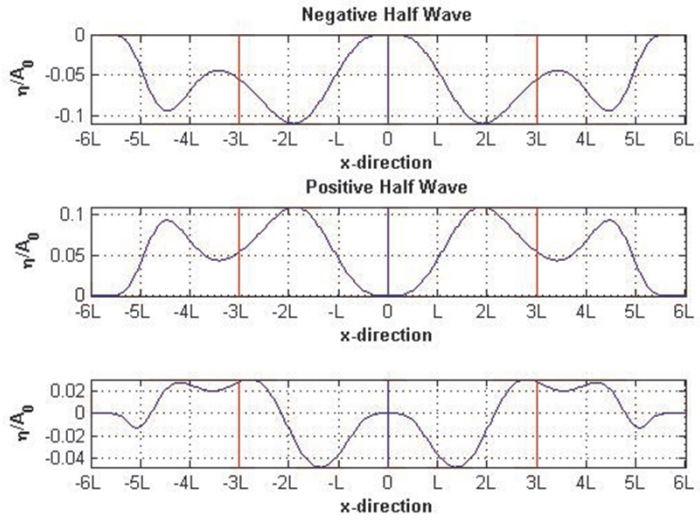

Figure 5.37. The Propagation and Reflection of a Single Negative Half Wave, a Single Positive Half Wave and a Single Full Wave by Using NSWE at t=6T.

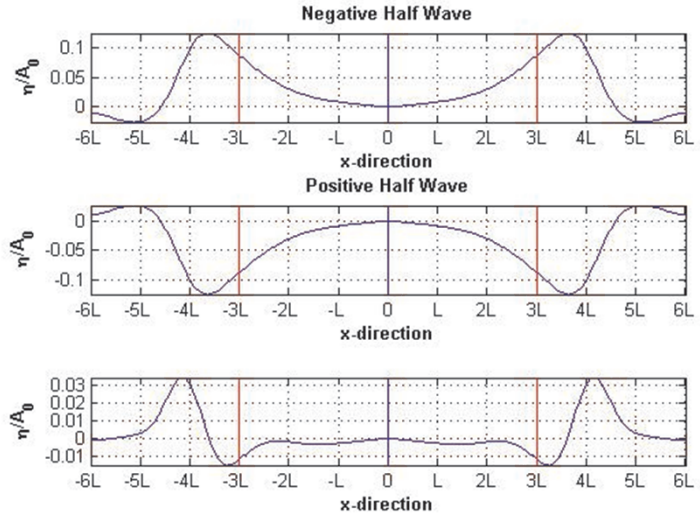

Figure 5.38. The Propagation and Reflection of a Single Negative Half Wave, a Single Positive Half Wave and a Single Full Wave by Using NSWE at t=12T.

FFT analysis gave some valuable information regarding the performance of the numeric models. For this reason some numerical gage locations were selected along the channel. The locations where the free surface displacements were analyzed are in the middle of the domain, x=0 where influx boundary condition is specified, at distances of L, 2L where GE are valid and 3L where is the beginning of the sponge layer. The data

collected on the numerical gage locations are for horizontal bottom and for the UN of 50 by using NSWE model. FFT analyze is applied to the collected data in terms of amplitude and mean water level (MWL) locations. The fluctuation of the MWL is tabulated in Table 5.5 where each analysis involved 2^n data and good results are obtained. In Table 5.6 FFT results of amplitude spectrum is given. Figure 5.39 shows the FFT results of different sized sample data at the gage location of $\pm 2L$. The FFT analysis shows the two points on the graphs as expected zero frequency for the MWL and one at the carrier amplitude. In the light of FFT analysis the model with sponge layer and RBC condition is working properly.

Table 5.5. Variation of the Mean Water Level, UN is 50.

	$x = 0$	L	2L	3L
T	1.72E-03	1.22E-03	1.06E-03	1.19E-02
2T	9.76E-04	7.98E-04	7.18E-04	3.13E-02
4T	5.52E-04	5.53E-04	1.58E-02	2.74E-02
8T	4.39E-05	6.16E-03	7.67E-03	7.90E-03
16T	1.81E-04	1.86E-03	3.03E-03	3.41E-03

Table 5.6. Amplitude Spectrum.

	$x = 0$	L	2L	3L
T	9.98E-01	9.98E-01	9.97E-01	9.84E-01
2T	9.98E-01	9.97E-01	9.97E-01	9.87E-01
4T	9.98E-01	9.97E-01	9.92E-01	9.94E-01
8T	9.97E-01	9.99E-01	9.98E-01	9.97E-01
16T	9.97E-01	9.97E-01	9.96E-01	9.95E-01
Avr.	9.98E-01	9.98E-01	9.96E-01	9.91E-01

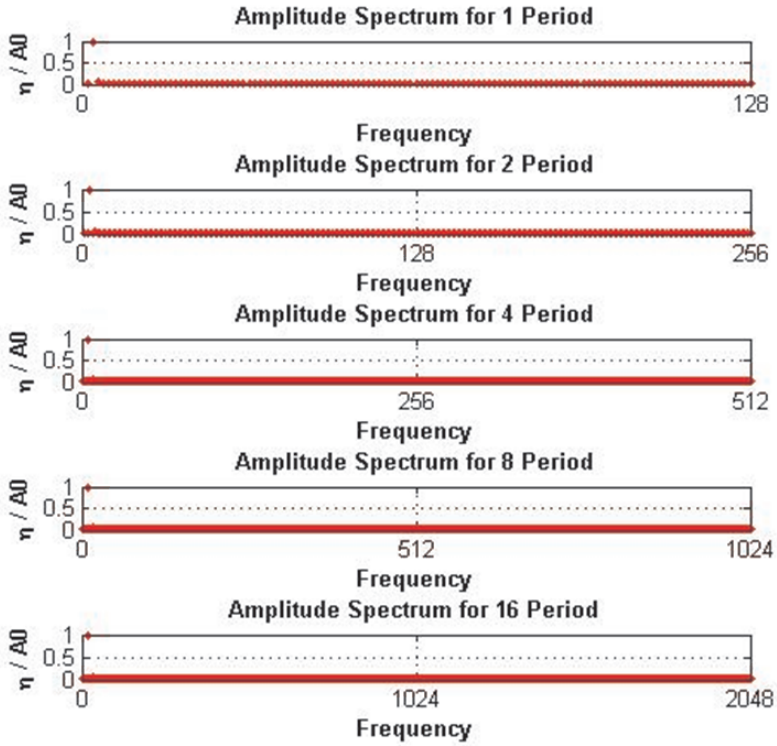

Figure 5.39. FFT Results of Normalized Free Surface at ±2L.

5.5.1. One Dimensional Solutions of SWE (Case Study 3)

5.5.1.1. LSWE Solution and NSWE Solution in 1D. Numerical tests were conducted to determine which integration method, RK O(4), MH O(4) or ABM O(4), gives the best performance. Different wave steepnesses were selected to obtain the maximum UN to be used in the one dimensional NSWE model. The horizontal length of the solution domain was selected as 12 wave lengths of the selected wave. The Sommerfeld radiation boundary condition was symmetrically applied at the ends of the solution domain to minimize the reflection and fluctuations at the end of sponge layers. The wave properties and the RMS error in time are summarized in Table 5.7 for an intermediate water wave and in Table 5.8 for a shallow water wave. The simulation times of the tests range from 30-253 sec. for LSWE solutions and from 35-326 sec. for NSWE solutions. Common skewed wave traits are observed the more the UN is the more RMS error involve in the solution. Best performance is observed for time integration by using

the ABM O(4) in terms of intermediate time steps needed per integration time step, required storage and run time.

Figure 5.40 and Figure 5.41 show the variation of the normalized free surface in the shallow water at the 3T where waves enter the sponge layer and 24T for the UN of 50, respectively. In Appendix B.1., the variation of the normalized free surface in the shallow water are given for horizontal bathymetry at the 0.5T, T, 3T, 5T, 6T, 7T, 8T, and 24T, respectively. In Appendix B.2., the variation of the normalized free surface in the shallow water are given for the sloped bathymetry at the 0.5T, T, 3T, 5T, 6T, 7T, 8T, and 24T, respectively.

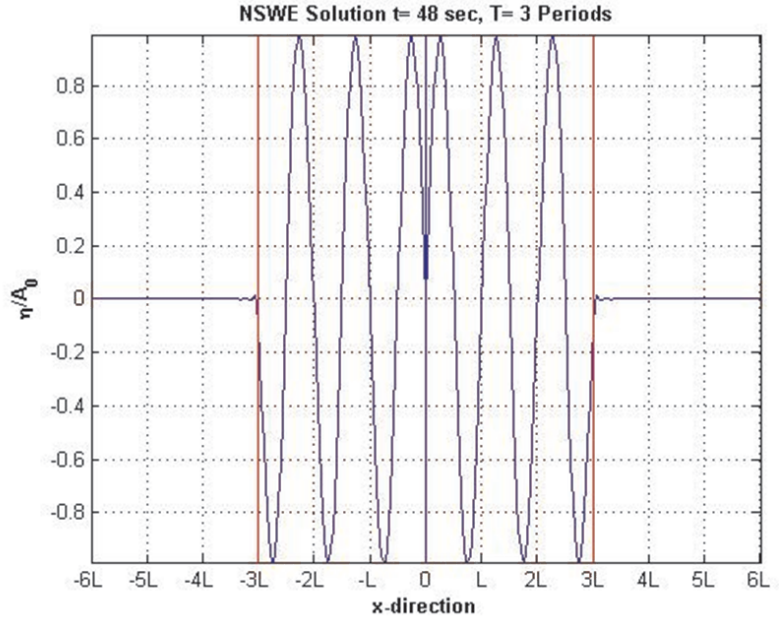

Figure 5.40. Variation of the Normalized Free Surface in Shallow Water by Using NSWE at t=3T.

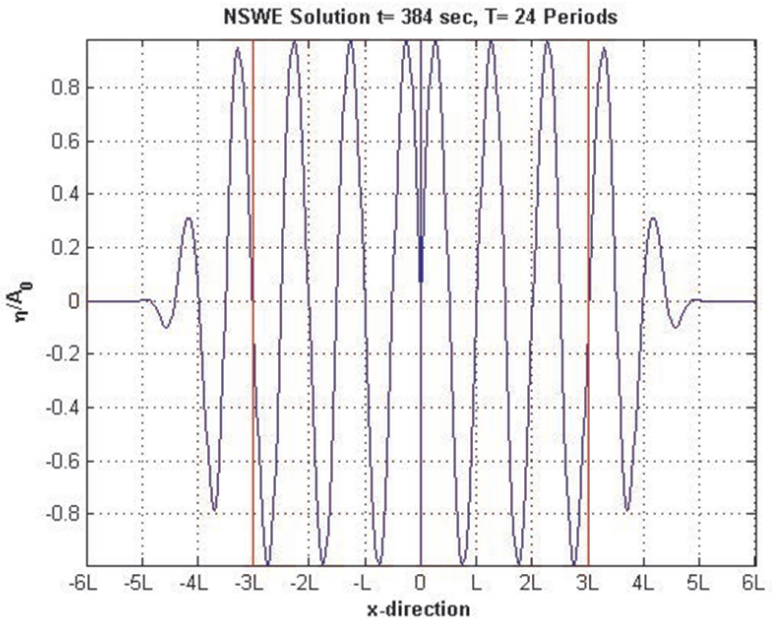

Figure 5.41. Variation of the Normalized Free Surface in Shallow Water by Using NSWE at t=24T.

From Figure 5.42- Figure5.49, Comparison of LSWE vs. NSWE solution with its RMS error at the time instants of 3T, 5T, 6T, 9T, 10T, 12T 15T, 18T and 24T, respectively. The model has negligible reflection traits as seen in the Figure 5.42-Figure5.49. The fluctuations maybe attributed to the fact that in a NSWE solution a linear wave is given on the influx boundary. The nonlinear wave whose UN greater then 1, skew the wave crest and trough, thus, when comparing with the linear wave solution fluctuations occurred. The maximum RMS error is with the fourth order RK $8.042\text{x}10^{-4}$, MH $8.0427\text{x}10^{-4}$ and ABM $8.0417\text{x}10^{-4}$ time integrators, respectively.

Table 5.7. Maximum RMS Error for Intermediate Wave.

T (s)	A_0 (m)	Max. Error (10^{-4})	Method of Integration	Linear Solver Run Time (s)	Nonlinear Solver Run Time (s)
2	0.005	0.39685	ABM O(4)	30	35
	0.010	1.60220			
	0.015	3.65650			
	0.020	6.63830			
	0.005	0.39725	MH O(4)	31	38
	0.010	1.60380			
	0.015	3.65990			
	0.020	6.64450			
	0.005	0.39688	RK O(4)	39	41
	0.010	1.60230			
	0.015	3.65670			
	0.020	6.63890			
4	0.005	0.45041	ABM O(4)	59	67
	0.010	1.82190			
	0.015	4.17480			
	0.020	7.63110			
	0.005	0.45064	MH O(4)	65	70
	0.010	1.82280			
	0.015	4.17700			
	0.020	7.63510			
	0.005	0.45045	RK O(4)	70	82
	0.010	1.82200			
	0.015	4.17510			
	0.020	7.63160			

Table 5.8. Maximum RMS Error for Long Wave.

T (s)	A_0 (m)	Max. Error (10^{-4})	Method of Integration	Linear Solver Run Time (s)	Nonlinear solver Run Time (s)
8	0.005	0.46815	ABM O(4)	124	134
	0.010	1.89490			
	0.015	4.35070			
	0.020	7.95570			
	0.005	0.46829	MH O(4)	128	140
	0.010	1.89550			
	0.015	4.35200			
	0.020	7.95810			
	0.005	0.46818	RK O(4)	142	164
	0.010	1.89500			
	0.015	4.35090			
	0.020	7.95610			
16	0.005	0.47377	ABM O(4)	243	265
	0.010	1.91790			
	0.015	4.40320			
	0.020	8.04170			
	0.005	0.47384	MH O(4)	252	273
	0.010	1.91820			
	0.015	4.40390			
	0.020	8.04270			
	0.005	0.47379	RK O(4)	312	326
	0.010	1.91800			
	0.015	4.40340			
	0.020	8.04200			

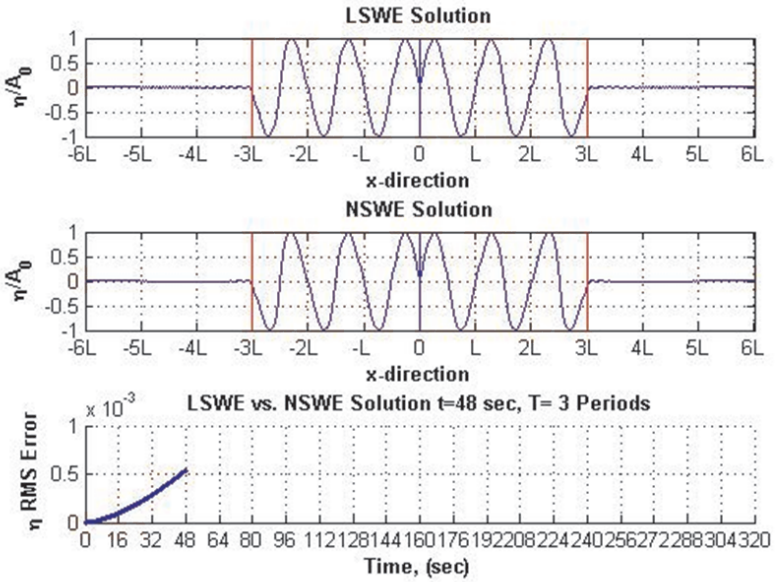

Figure 5.42. Comparison of LSWE vs. NSWE Solution at t=3T.

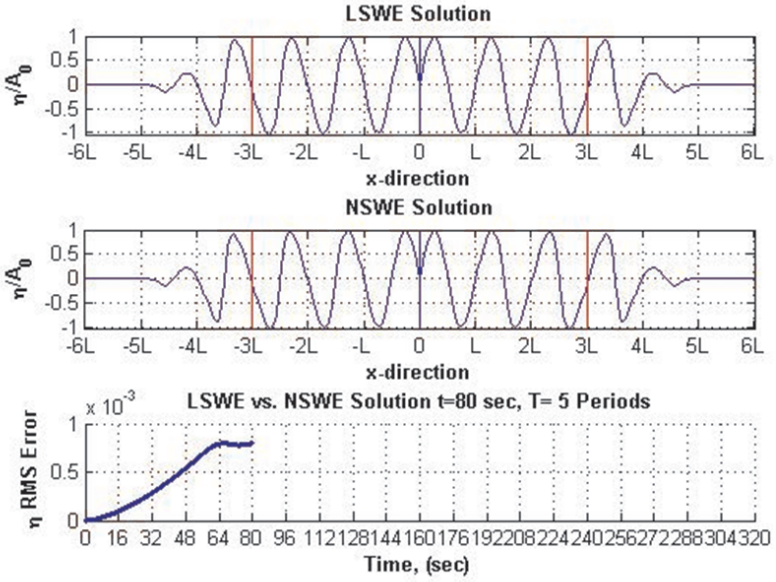

Figure 5.43. Comparison of LSWE vs. NSWE Solution at t=5T.

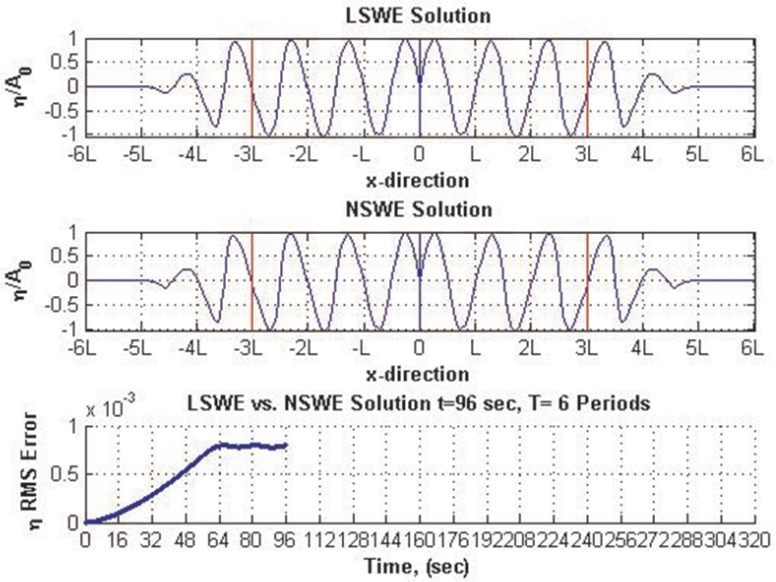

Figure 5.44. Comparison of LSWE vs. NSWE Solution at t=6T.

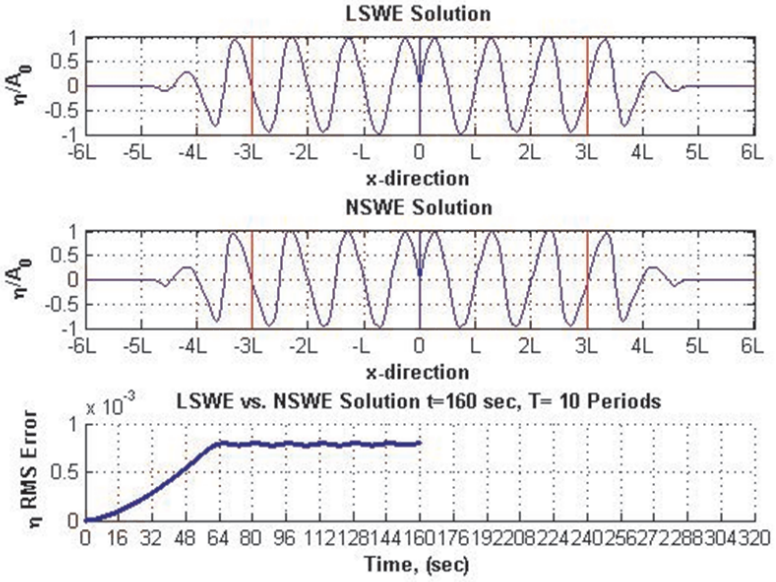

Figure 5.45. Comparison of LSWE vs. NSWE Solution at t=10T.

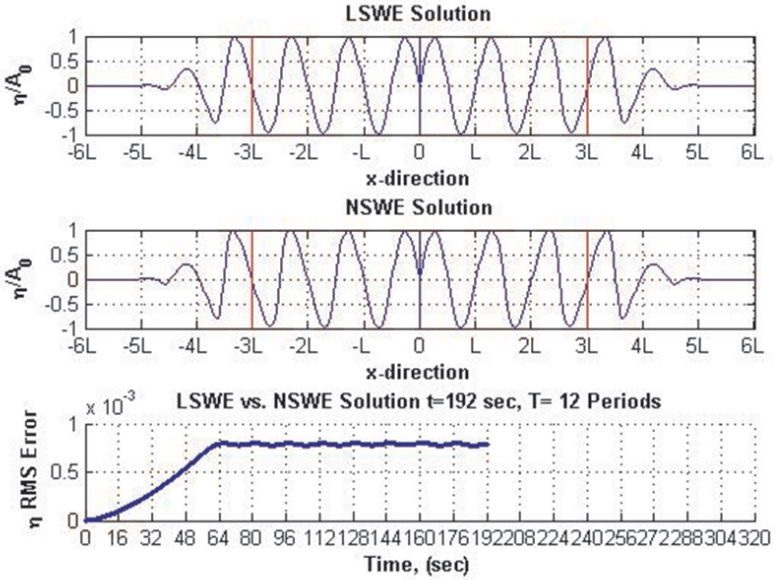

Figure 5.46. Comparison of LSWE vs. NSWE Solution at t=12T.

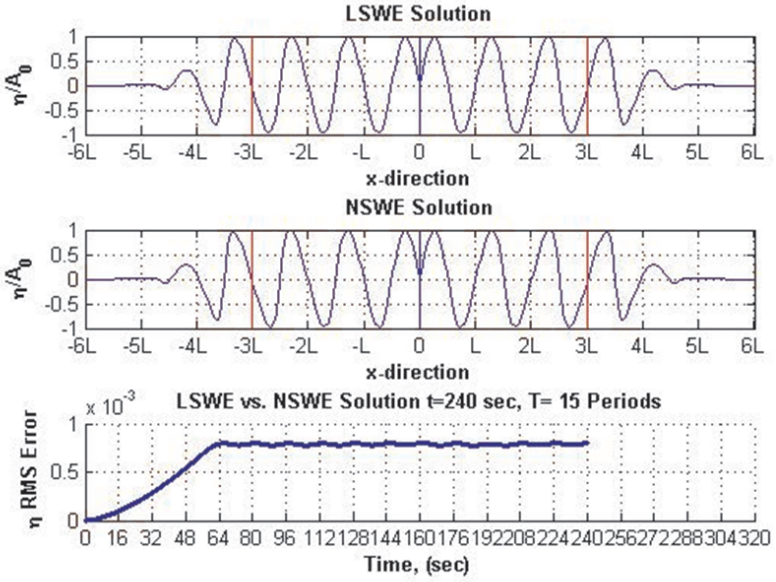

Figure 5.47. Comparison of LSWE vs. NSWE Solution at t=15T.

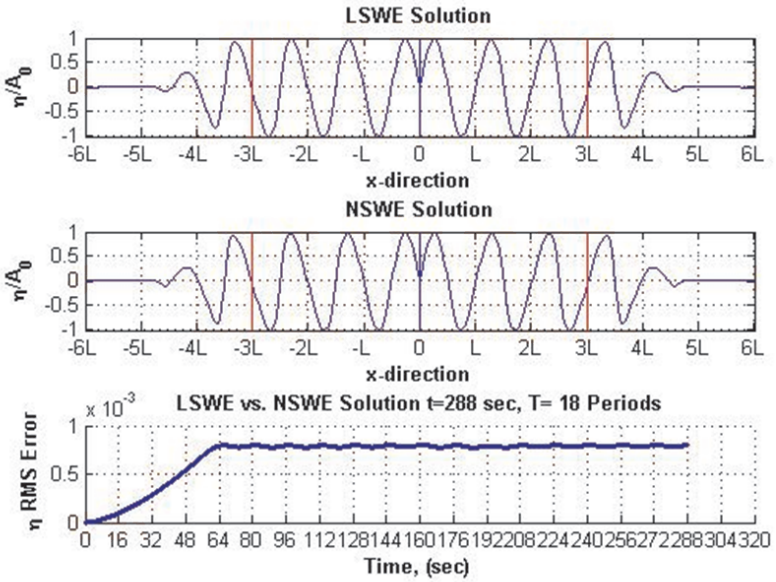

Figure 5.48. Comparison of LSWE vs. NSWE Solution at t=18T.

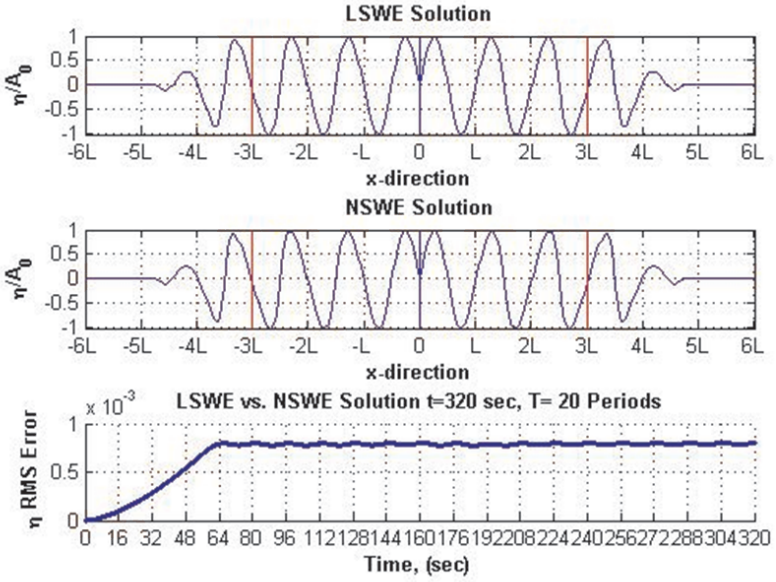

Figure 5.49. Comparison of LSWE vs. NSWE Solution at t=20T.

5.5.2. Two Dimensional Solutions of NSWE (Case Study 4)

The advantages of the meshless RBFs method will be demonstrated by applying the method from 1D solutions to successfully obtain the numerical approximations of

2D solutions. Numerical simulation of 2D model was performed on the horizontal and sloped bathymetry by using NSWE model with sponge layers to show the model also works properly in 2D.

Node placement in the x, propagation direction and y, cross direction can be seen in Figure 5.50. In the middle of the propagation direction at x=0, the wave maker is placed as influx boundary. The sponge layers start at x=3L and x=-3L till the end of the domain. Collocation node placement is the same for the horizontal and the sloped bathymetry. In the propagation direction, there are 12 wave length. Each wave length has 33 collocation nodes. In the cross direction, there are 5 transects placed half the wave length each, each has 397 collocation nodes and 1985 total collocation nodes in the domain. In Subsection 5.5.2.1., the solutions are obtained on the horizontal bathymetry and in Subsection 5.5.2.2, the solutions are obtained on the sloped bathymetry by 2D NSWE model.

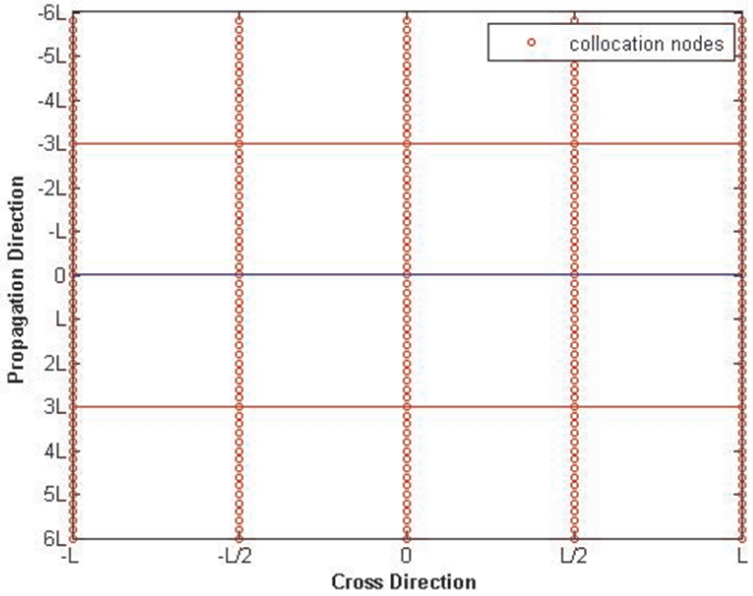

Figure 5.50. Node Placement in the Propagation and Cross Direction, Influx Boundary (Blue Line) and Sponge Layers (Red Lines).

5.5.2.1. 2D NSWE Solution on the Horizontal Bathmetry. In the horizontal plane, the depth is set to 1 meter so that for future studies a comparison can be done by the model

and laboratory studies. To show how RBF works well in 2D solutions a comparison of 1D NSWE Solution to Midtransect of 2D NSEW Solution on the horizontal bathmetry is done. In Figure 5.51 and Figure 5.52, the variation of the normalized free surface in shallow water can be seen at 3T and 24T, respectively. In Appendix C.1., the variation of the normalized free surface in the shallow water are figured at 0.5T, T, 3T, 5T, 6T, 7T, 15T and 24T.

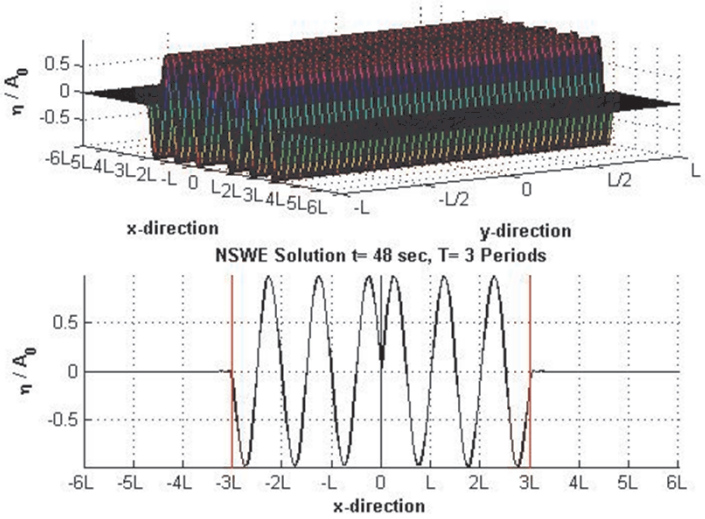

Figure 5.51. Variation of the Normalized Free Surface in Shallow Water by Using NSWE at t=3T.

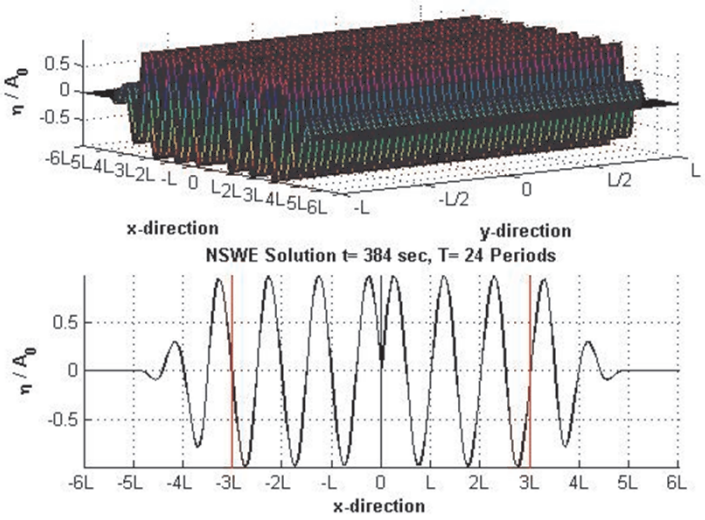

Figure 5.52. Variation of the Normalized Free Surface in Shallow Water by Using NSWE at t=24T.

Variation of the maximum RMS error with time for intermediate and long wave can be seen in Table 5.9 and Table 5.10. When the wave steepness increases the error increases. Time marching in the model is carried out by the ABM O(4) method. The maximum RMS error is 4.74×10^{-5} for UN 50.

Table 5.9. Maximum RMS Error in Time for Intermediate Waves.

T (s)	A_0 (m)	Max RMS error	2D Nonlinear Solver Run Time (s)
2	0.005	2.34E-06	8669
	0.01	9.44E-06	
	0.015	2.16E-05	
	0.02	3.91E-05	
4	0.005	2.66E-06	16596
	0.01	1.07E-05	
	0.015	2.46E-05	
	0.02	4.50E-05	

Table 5.10. Maximum RMS Error in Time for Long Waves.

T (s)	A_0 (m)	Max RMS error	2D Nonlinear Solver Run Time (s)
8	0.005	2.76E-06	33192
	0.01	1.12E-05	
	0.015	2.56E-05	
	0.02	4.69E-05	
16	0.005	2.79E-06	65640
	0.01	1.13E-05	
	0.015	2.60E-05	
	0.02	4.74E-05	

The model results shown in Figure 5.53- Figure 5.61 comparison of 1D and 2D midtransect NSWE solution with this maximum relative error at the time instants of 3T, 5T, 6T, 9T, 10T, 12T 15T, 18T and 24T. The model results indicate that the sponge layers are functioning properly with Sommerfeld radiation boundary condition at the ends for the horizontal bathymetry.

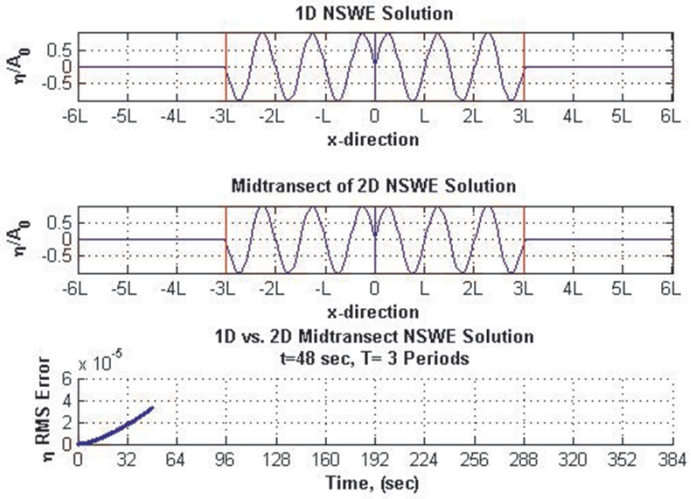

Figure 5.53. Comparison of 1D vs 2D Midtransect NSWE Solution at t=3T.

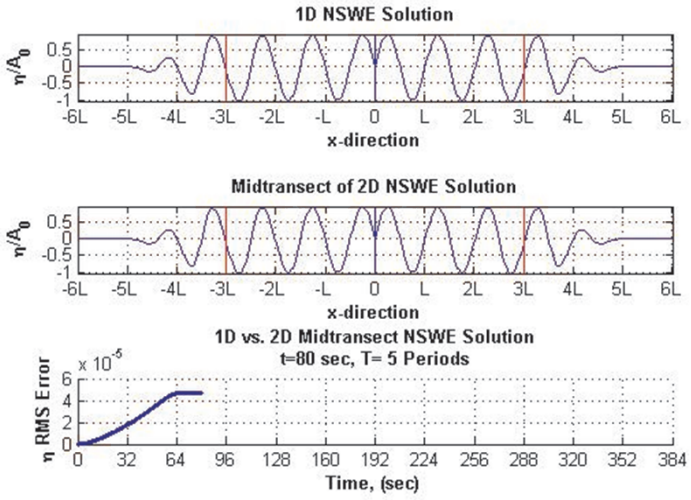

Figure 5.54. Comparison of 1D vs 2D Midtransect NSWE Solution at t=5T.

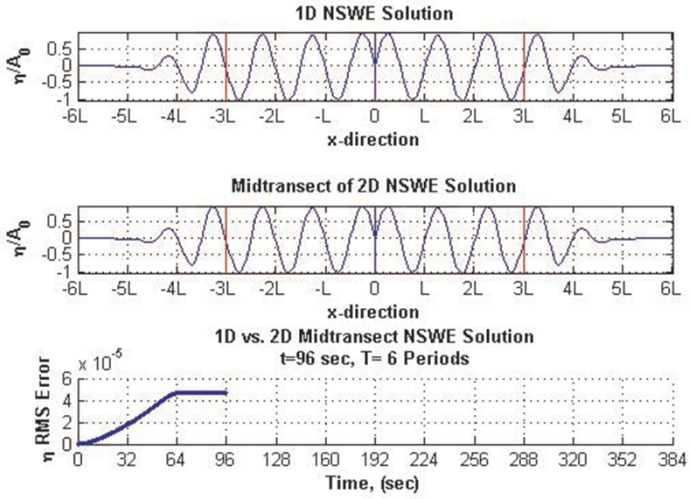

Figure 5.55. Comparison of 1D vs 2D Midtransect NSWE Solution at t=6T.

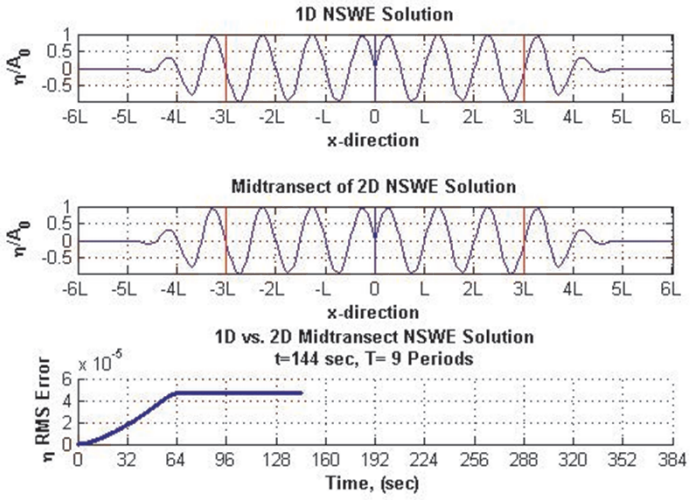

Figure 5.56. Comparison of 1D vs 2D Midtransect NSWE Solution at t=9T.

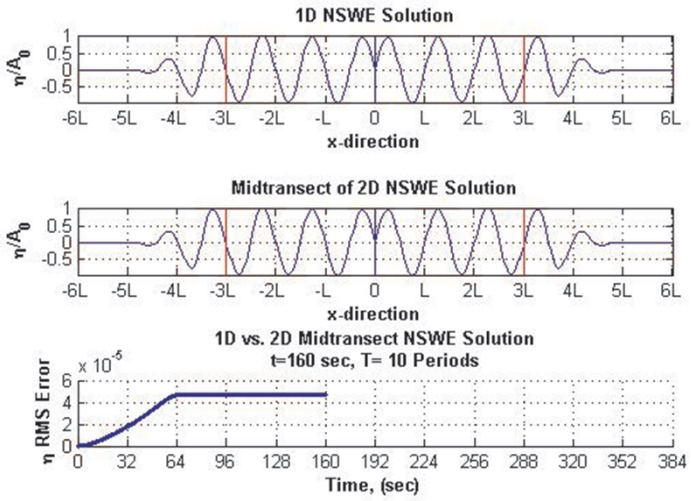

Figure 5.57. Comparison of 1D vs 2D Midtransect NSWE Solution at t=10T.

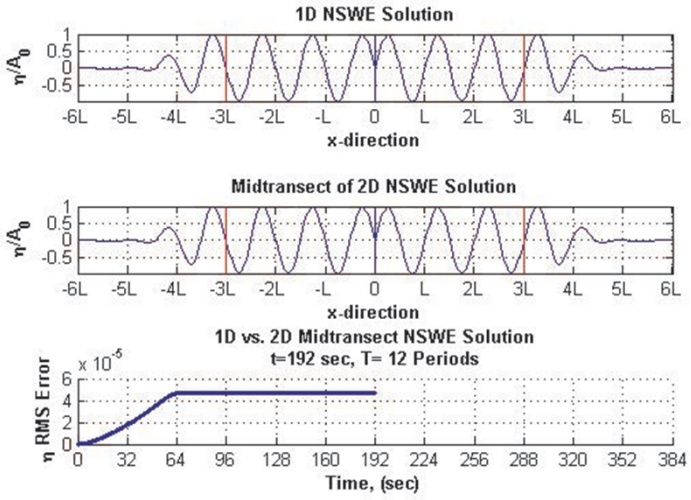

Figure 5.58. Comparison of 1D vs 2D Midtransect NSWE Solution at t=12T.

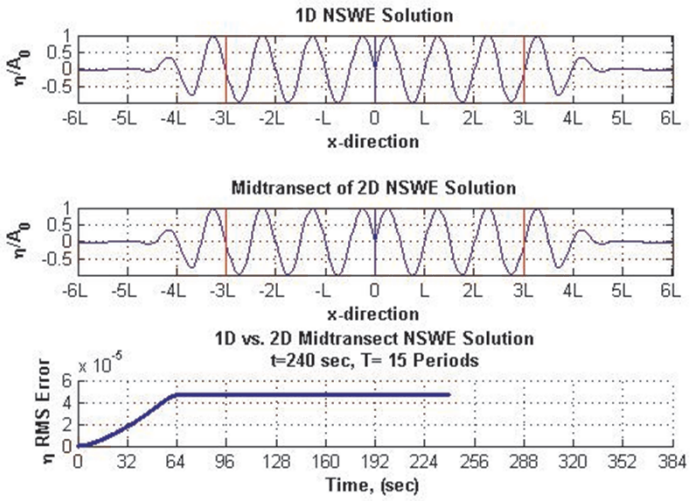

Figure 5.59. Comparison of 1D vs 2D Midtransect NSWE Solution at t=15T.

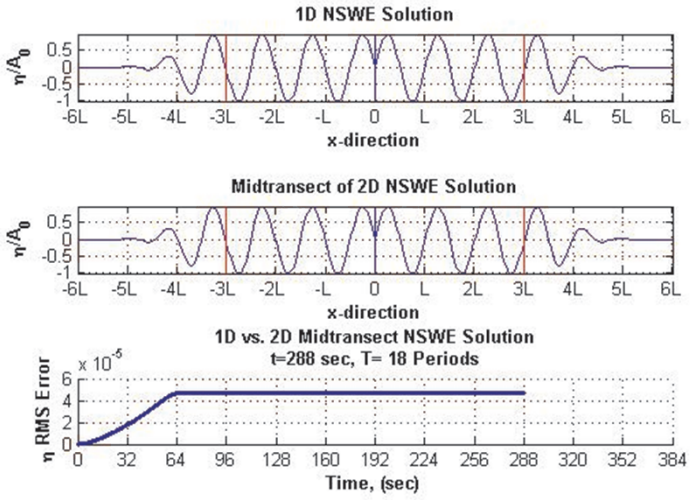

Figure 5.60. Comparison of 1D vs 2D Midtransect NSWE Solution at t=18T.

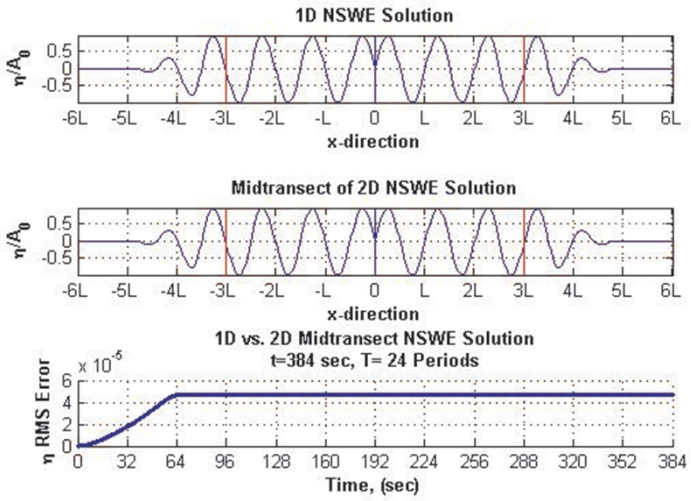

Figure 5.61. Comparison of 1D vs 2D Midtransect NSWE Solution at t=24T.

5.5.2.2. 2D NSWE Solution on the Sloped Bathmetry. Comparison of 1D NSWE to Midtransect of 2D NSWE Sloped Solution

Node placement in the x, propagation direction and y, cross direction can be seen in Figure 5.62. In the middle of the propagation direction at x=0, the wave maker is placed as influx boundary. The sponge layers start at x=3L and x=-3L till the end of the domain. Between ±L and ±2L the sloped bathymetry is set. Collocation node placement is the same for the horizontal and the sloped bathymetry. Nodes for the sloped bathymetry on the propagation direction, x, 12 wave length distance is set and each wave length has a 33 collocation nodes. There are 5 transect each has 397 collocation points on the cross direction, y and 1985 total collocation on the domain.

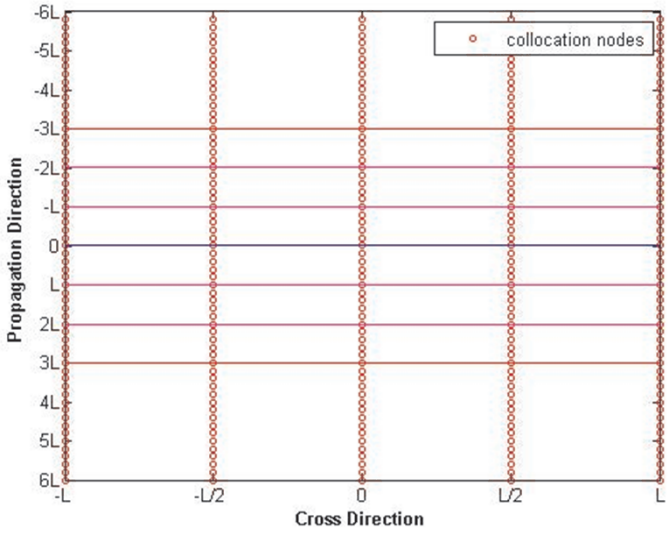

Figure 5.62. Node Placement in the Propagation and Cross Direction, Influx Boundary (Blue Line at x=0), Sponge Layers (Red Lines at x=±3, Sloped Bathymetry Starts at x=±L and Ends at x=±2L).

The bathymetry of the domain as seen in Figure 5.63. The depth is set to 1 meter between L and -L and 0.5 meter between 2L to 6L in the positive x direction (-2L to -6L in the negative x direction). Between L and 2L (and -L and-2L) there is a constant slope of 1/100.

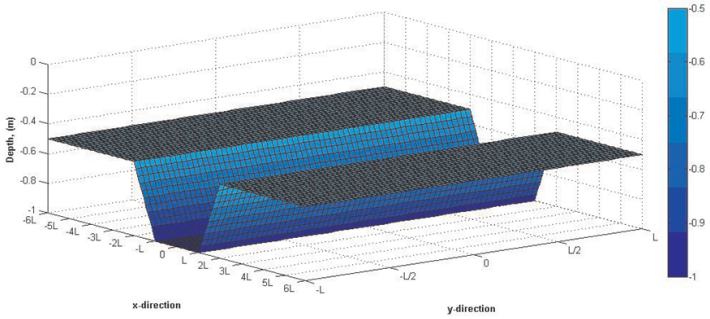

Figure 5.63. Bathymetry of the Sloped Domain.

In Figure 5.65 and Figure 5.66, the variation of the normalized free surface in the shallow water are figured at the 3T and 24T time instants, respectively. In Appendix C.2., the variation of the normalized free surface in the shallow water are figured at the 0.5T, T, 3T, 5T, 6T, 7T, 8T, 15T and 24T time instants, respectively.

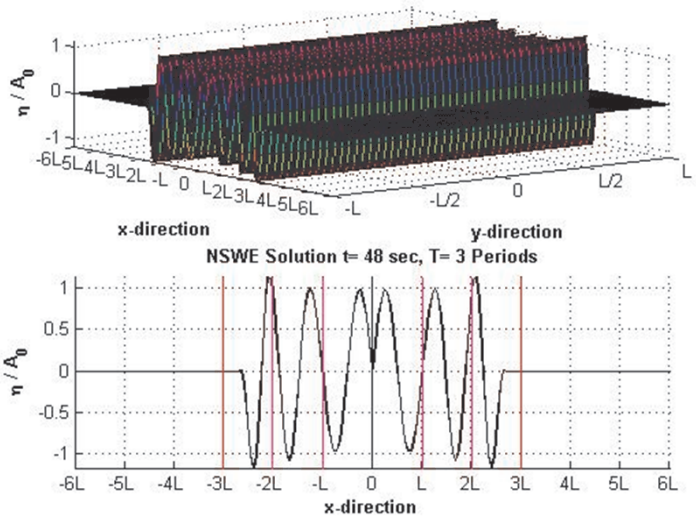

Figure 5.64. Variation of the Normalized Free Surface in Shallow Water by Using NSWE at t=3T.

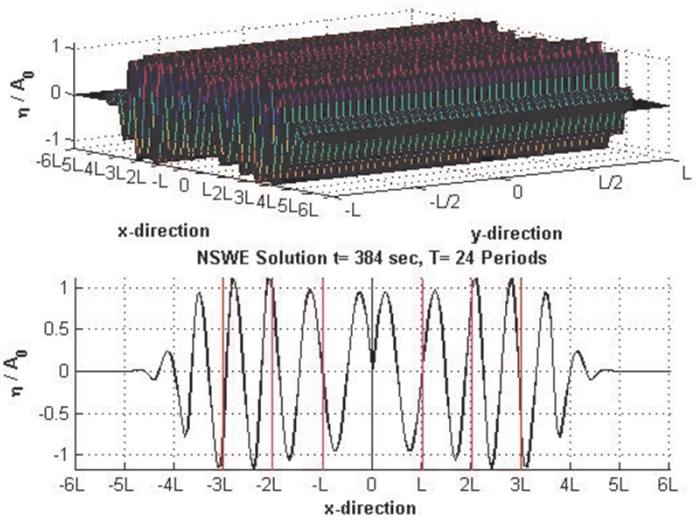

Figure 5.65. Variation of the Normalized Free Surface in Shallow Water by Using NSWE at t=24T.

Maximum RMS error in time for intermediate and long wave values can be seen in Table 5.11 and Table 5.12. When the wave steepness increases the error increases. The time integration is done by ABM since all the studied time integration methods have the same order from the point of computational times ABM is selected not to consume too much time.

Table 5.11. Maximum RMS Error in Time for Intermediate Wave.

T (s)	A_0 (m)	Max. RMS error	2D Nonlinear Solver Run Time (s)
2	0.005	2.78E-06	8669
	0.010	1.12E-05	
	0.015	2.56E-05	
	0.020	4.66E-05	
4	0.005	3.16E-06	16596
	0.010	1.28E-05	
	0.015	2.93E-05	
	0.020	5.35E-05	

Table 5.12. Maximum RMS Error in Time for Long Wave.

T (s)	A_0 (m)	Max. RMS error	2D Nonlinear Solver Run Time (s)
8	0.005	3.28E-06	33192
	0.010	1.33E-05	
	0.015	3.05E-05	
	0.020	5.58E-05	
16	0.005	3.32E-06	65640
	0.010	1.34E-05	
	0.015	3.09E-05	
	0.020	5.64E-05	

From Figure 5.66-5.74, comparison of 1D and 2D midtransect NSWE solution with this maximum relative error at the time instants of 3T, 5T, 6T, 9T, 10T, 12T 15T, 18T and 24T respectively. The developed code has negligible reflection traits as seen in Figure 5.66- Figure 5.74.

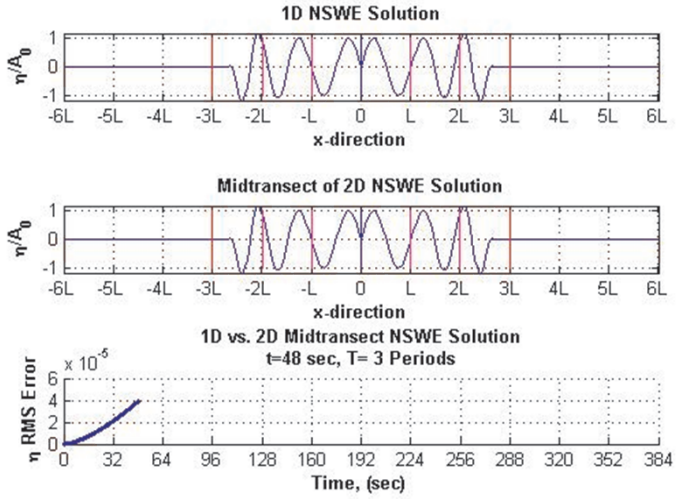

Figure 5.66. Comparison of 1D vs 2D Midtransect NSWE Solution at t=3T.

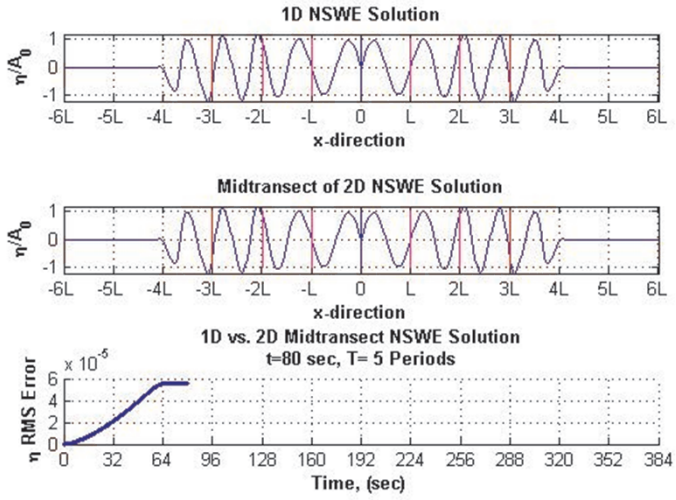

Figure 5.67. Comparison of 1D vs 2D Midtransect NSWE Solution at t=5T.

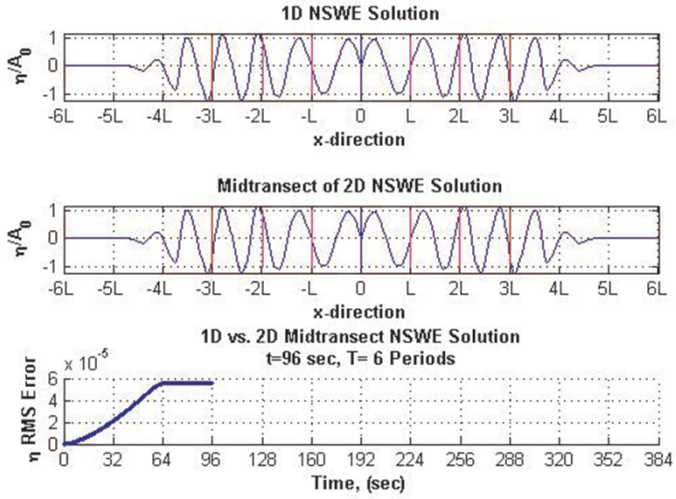

Figure 5.68. Comparison of 1D vs 2D Midtransect NSWE Solution at t=6T.

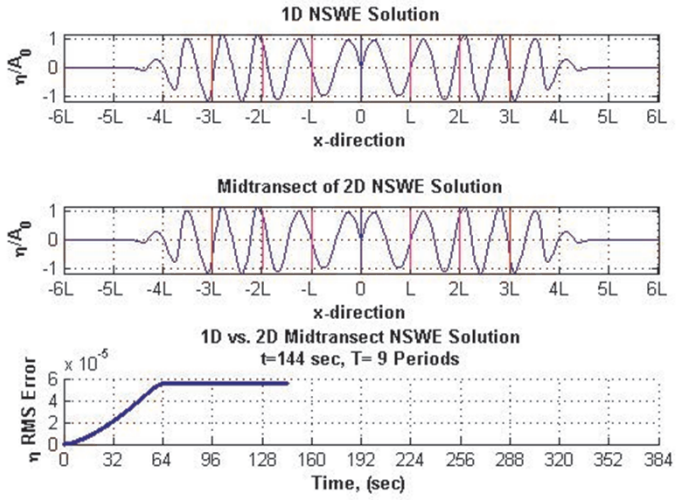

Figure 5.69. Comparison of 1D vs 2D Midtransect NSWE Solution at t=9T.

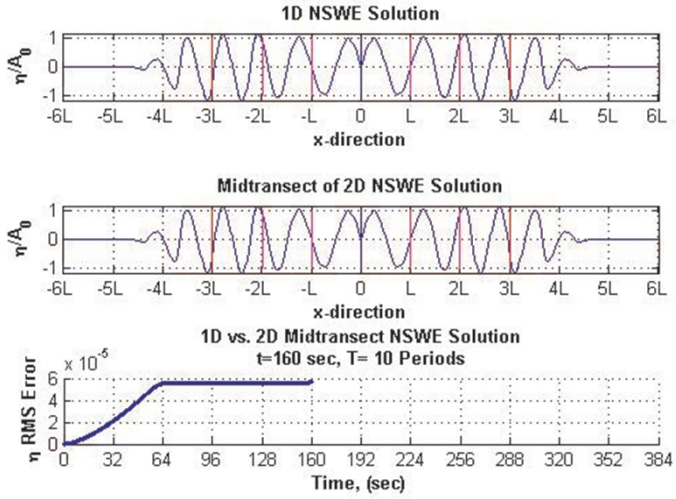

Figure 5.70. Comparison of 1D vs 2D Midtransect NSWE Solution at t=10T.

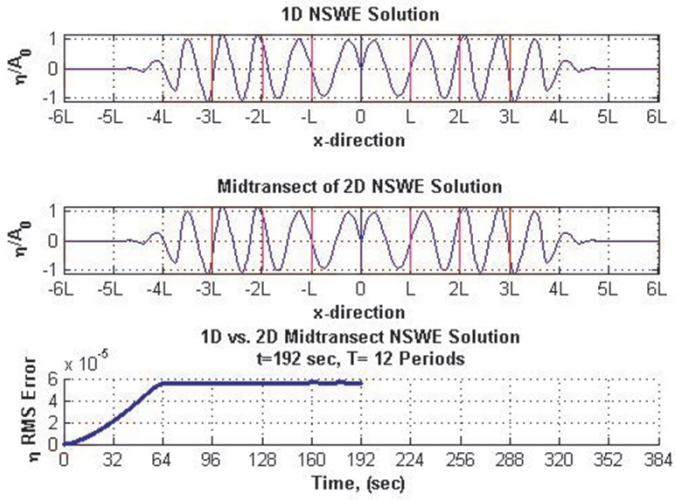

Figure 5.71. Comparison of 1D vs 2D Midtransect NSWE Solution at t=12T.

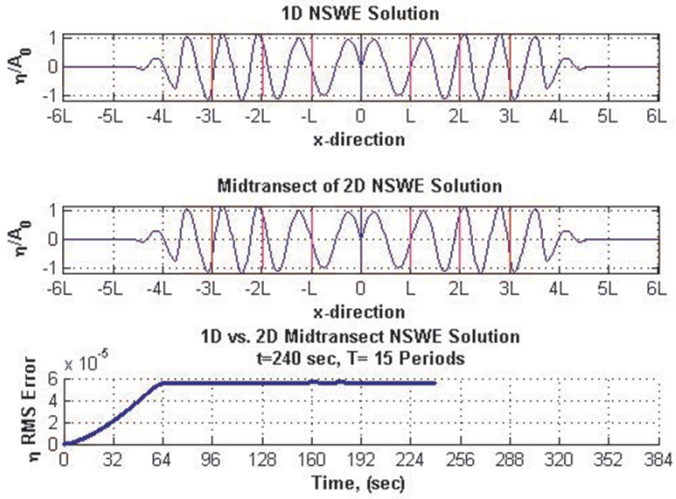

Figure 5.72. Comparison of 1D vs 2D Midtransect NSWE Solution at t=15T.

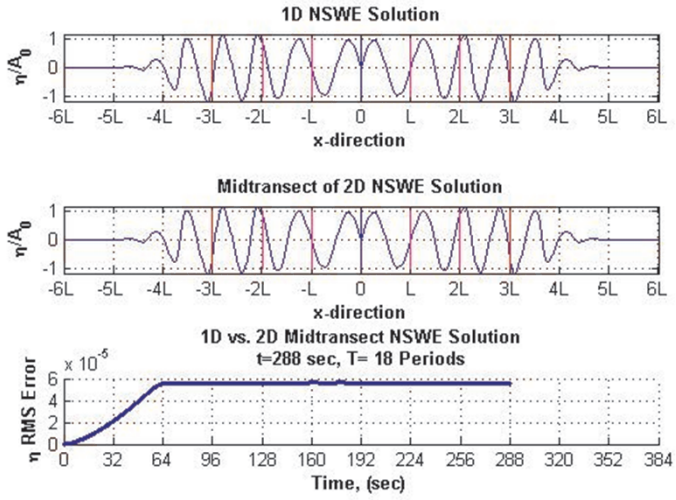

Figure 5.73. Comparison of 1D vs 2D Midtransect NSWE Solution at t=18T.

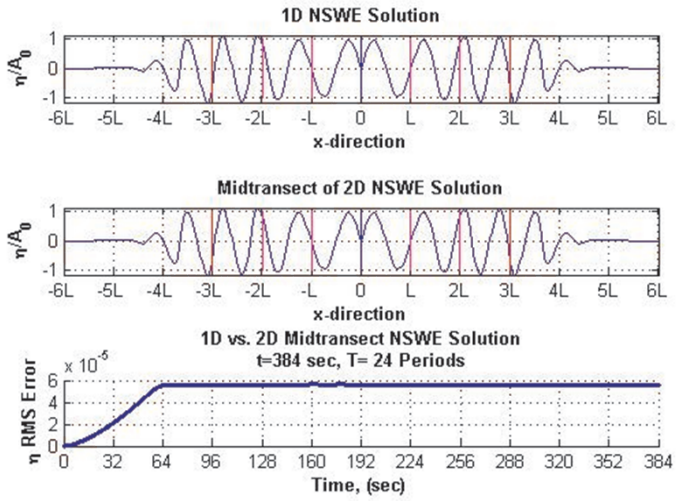

Figure 5.74. Comparison of 1D vs 2D Midtransect NSWE Solution at t=24T.

6. CONCLUSIONS

The applications of the RBFCM to provide a solution for the unsteady, nondispersive NSWE are considered in case studies. Thus, the first conclusion of this thesis is that successful numerical solutions of the SWE are developed for four case studies. In case studies 1 and 2, the performance of the model is evaluated against the analytical and numerical solutions of the problems. In case study 3 and 4 unbounded domain solutions with sponge treatment is devised.

In case study 1, the meshless RBFCM combined with the Lagrangian-Eulerian scheme is devised with moving boundary. The advantages of the meshless method are demonstrated in the numerical solutions of a water wave climbing a linearly sloping beach. RBFCM solution compared with the analytical solution for long wave run-up on a sloping beach, Carrier-Greenspan's theory (1958). The RBFCM produces accurate results comparable to the analytic solution. Transforming the boundary value problem to a time invariant domain approach, however, leads to several new nonlinear terms in the governing equations that render the numerical computation considerably more complicated. Corresponding numerical results of the present Lagrangian-Eulerian numerical method with additional terms are easily formulated and applied by RBFCM without any stability problems. MQ RBF, which is globally supported, infinitely differentiable, smooth and even with a shape parameter, outperforms best regarding its accuracy, stability, efficiency, memory requirement, simplicity and straightforwardness of its implementation.

In case study 2, long wave run-up on a sloping beach with different bathymetry then case study 1 is compared with a numerical test of Zhou *et al.*, (2004). Good numerical solutions obtained in this case both for run-up and run down profiles and also in good agreement with the observed waterline position. The use of the RBFCM with Lagrangian-Eulerian scheme saves the computational time. This representation brings the benefit of spatial independence and flexible data structure. Numerical experiments show that this meshless method has many advantages over traditional methods.

In case study 3 and 4, Eulerian form of the unsteady, nonlinear, nondispersive SWE with sponge treatment are used to capture variation of free surface in one and two dimensions with constant and sloped bathymetry in unbounded domain of interest. Thus, second conclusion of this thesis, in unbounded domains, sponge treatment is easily applicable to long wave propagation problem by RBFCM in terms of accuracy and simple implementation. The damping terms of sponge layer adds higher derivatives in the governing equations which are easily formulated and applied by RBFCM without any stability problem.

The computations depicted the definite advantages in using this truly meshfree method for solving various initial and boundary value problems. Secondly, The meshfree algorithm's spatial dimension independent which is the triggering motivation for RFB users in the sense that as the spatial dimension of the problem increase, the convergence order also increases and hence fewer collocation points will be needed to maintain the same accuracy. This gives the motivation of more sophisticated two and three dimensional model development for future studies.

The advantages of the meshless RBFs method are demonstrated by applying the method to successfully obtain the numerical approximations of the solutions. The resultant coefficient matrix of the system of equations resulted from RBFs method is usually full and unsymmetric and hence leads to an ill-conditioning problem when a large system of equations is involved. The developed overlapping and multizone domain decomposition method for the RBFs approximation by Wong *et al.*, (1999) and truncated MQ applications by Galperin and Kansa, (2002) may enable the applications of the method to solve larger scale problems for operational purposes. This may be a future extension in the simulation of 2+1 dimension wave run-up problem with a special emphasis of the shape parameter or free parameter. The models' demonstrated performances in solving the case studies also show that they can be used for engineering design purposes especially for tsunami propagation and run-up of a tsunami. Further fields of another study may be to model tsunami propagation and inundation by RBFCM to get fast results with acceptable errors that can be used for operational tsunami modeling.

APPENDIX A: LEIBNITZ'S RULE

When the differentiation of integrals contains a parameter Leibnitz's rule applied. The integral

$$I(\beta) = \int_{a(\beta)}^{b(\beta)} f(x,\beta)dx \tag{A.1}$$

has a function of the parameter which is not a function of x, solely a dummy integration variable.

$$I'(\beta) = \frac{d}{d\beta}\int_{a(\beta)}^{\mathrm{b}(\beta)} f(\mathrm{x},\beta)\,\mathrm{dx} \tag{A.2}$$

In principle, evaluating the integral and then taking have to be done; in practice, however, inverting the order of integration and differentiation can be advantageous. The difference quotient is,

$$\frac{I(\beta+\Delta\beta)-I(\beta)}{\Delta\beta} = \frac{1}{\Delta\beta}\left\{\int_{a+\Delta a}^{b+\Delta b} f(x,\beta+\Delta\beta)\mathrm{dx} - \int_{\alpha}^{\mathrm{b}} \mathrm{f}(\mathrm{x},\beta)\mathrm{dx}\right\} \tag{A.3}$$

$$= \int_{a}^{\mathrm{b}} \frac{\mathrm{f}(\mathrm{x},\beta+\Delta\beta)-f(x,\beta)}{\Delta\beta}\mathrm{dx} + \frac{1}{\Delta\beta}\int_{\mathrm{b}}^{\mathrm{b}+\Delta b} \mathrm{f}(\mathrm{x},\beta+\Delta\beta)\mathrm{dx} - \frac{1}{\Delta\beta}\int_{a}^{\mathrm{a}+\Delta a} \mathrm{f}(\mathrm{x},\alpha+\Delta\alpha)\mathrm{dx} \tag{A.4}$$

$$\approx \int_{\alpha}^{\mathrm{b}} \frac{\mathrm{f}(\mathrm{x},\beta+\Delta\beta)-\mathrm{f}(\mathrm{x},\beta)}{\Delta\beta}\mathrm{dx} + \mathrm{f}(\mathrm{b},\beta+\Delta\beta)\frac{\Delta\mathrm{b}}{\Delta\beta} - \mathrm{f}(\mathrm{a},\beta+\Delta\beta)\frac{\Delta\alpha}{\Delta\beta} \tag{A.5}$$

A Continuous function, f, is constant over the infinitesimal intervals from $b \leq x \leq b+\Delta b$ to $a \leq x \leq a + \Delta a$. Formally, letting $\Delta\alpha \to 0$, the Leibnitz rule is obtained as;

$$I'(\beta) = \int_{\alpha(\beta)}^{b(\beta)} \frac{\partial f(x,\beta)}{\partial \beta} \mathrm{dx} + \mathrm{f}\left[\mathrm{b}(\beta), \beta\right] \frac{\mathrm{db}}{\mathrm{d}\beta} - \mathrm{f}\left[a(\beta), \beta\right] \frac{\mathrm{da}}{\mathrm{d}\beta} \tag{A.6}$$

Equation A.1 is valid if $\partial f/\partial\beta$ be continuous in the rectangular x, and the derivatives $\partial f/\partial\beta$, $\partial b/\partial\beta$ and $\partial a/\partial\beta$ all exist.

APPENDIX B: ONE DIMENSIONAL SOLUTIONS OF NSWE

B.1. Two Sponge Treatment with Horizontal Bathymetry

Figure B.1- Figure B.17 show the variation of the normalized free surface in the shallow water are given for the horizontal bathymetry at 0.5T, T, 3T, 5T, 6T, 7T, 8T, and 24T, respectively.

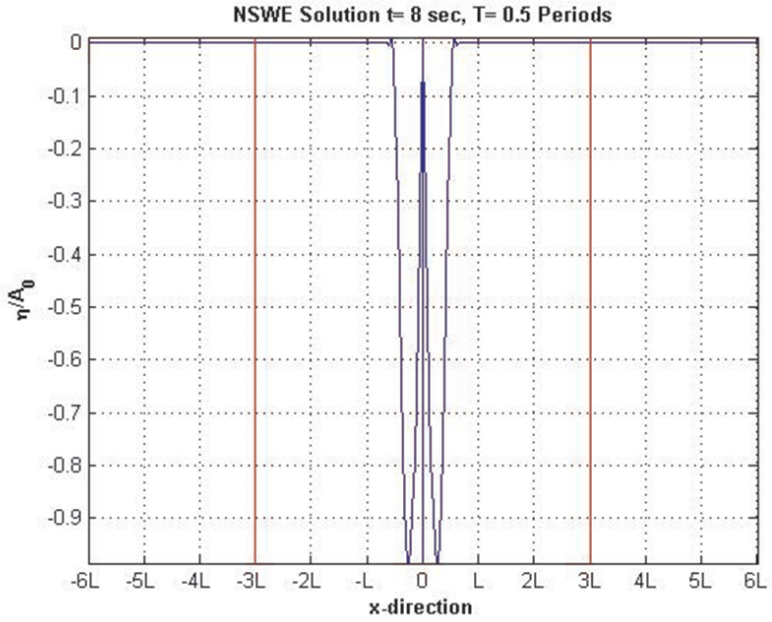

Figure B.1. Variation of the Normalized Free Surface in Shallow Water by Using NSWE at t=0.5T.

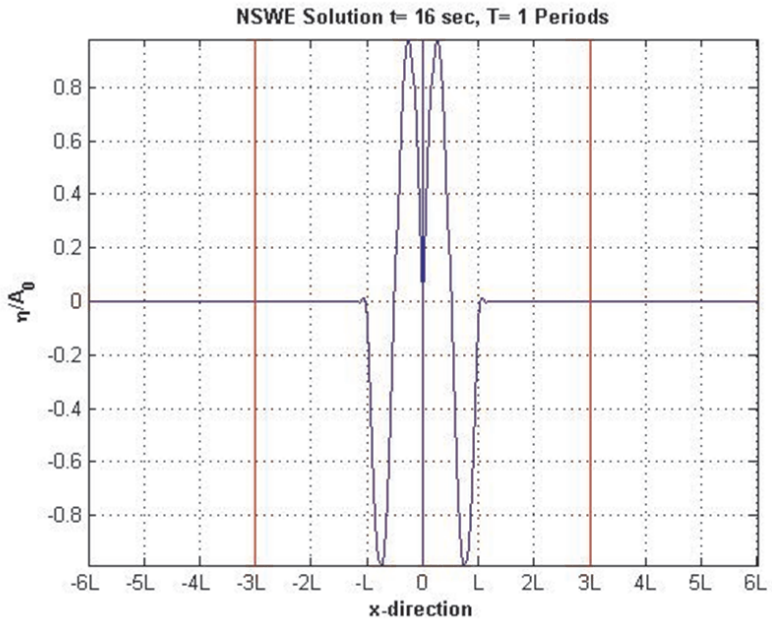

Figure B.2. Variation of the Normalized Free Surface in Shallow Water by Using NSWE at t=T.

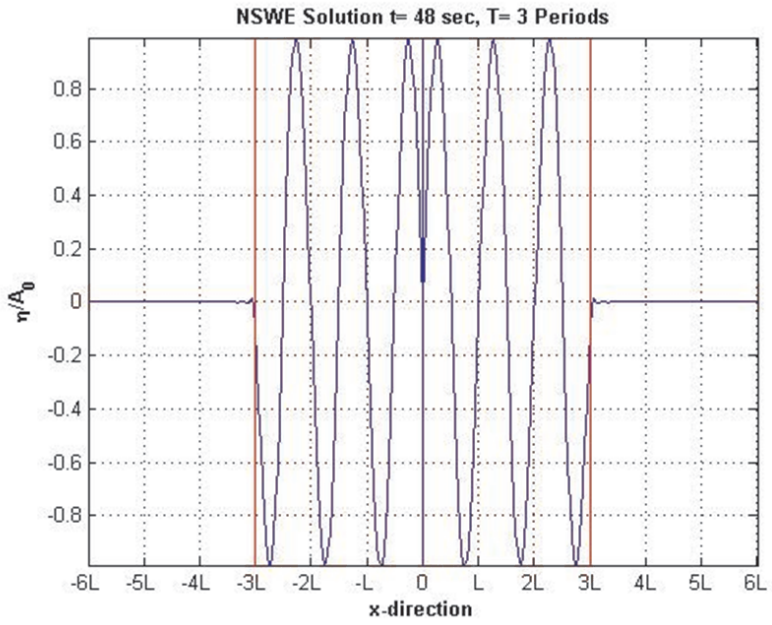

Figure B.3. Variation of the Normalized Free Surface in Shallow Water by Using NSWE at t=3T.

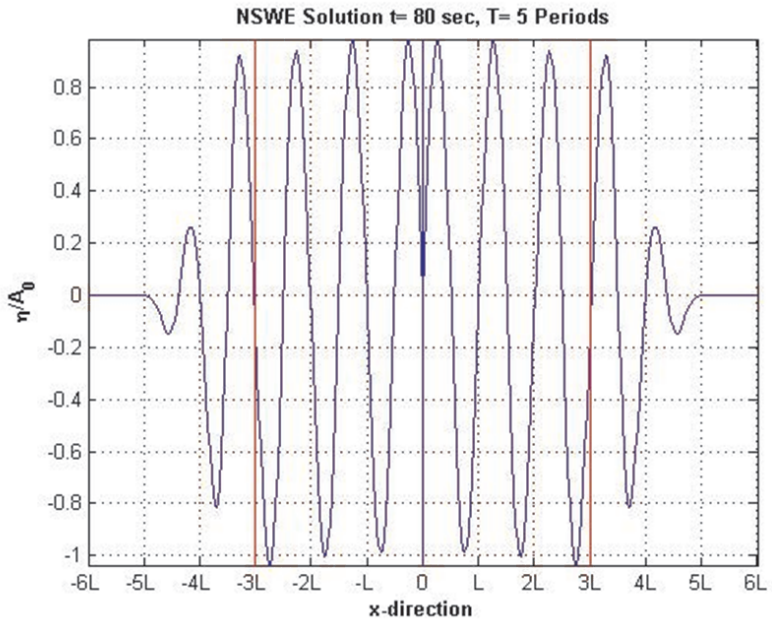

Figure B.4. Variation of the Normalized Free Surface in Shallow Water by Using NSWE at t=5T.

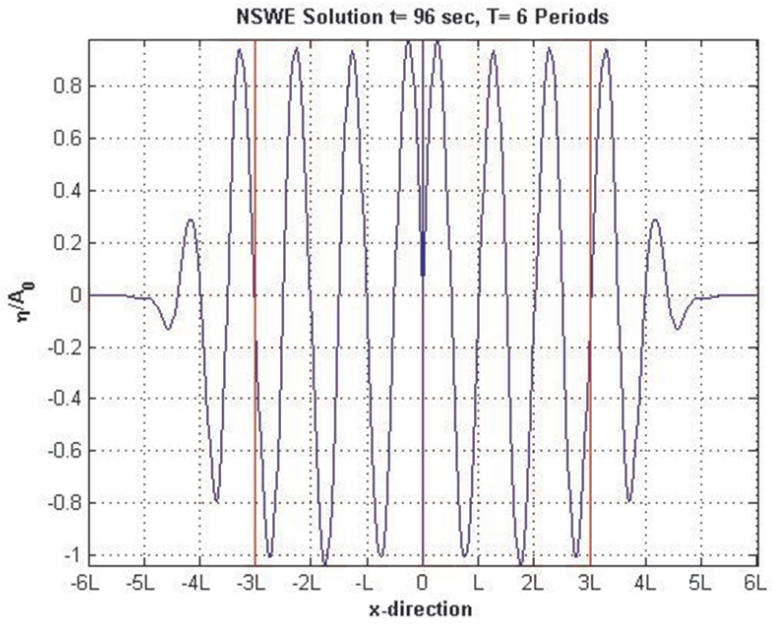

Figure B.5. Variation of the Normalized Free Surface in Shallow Water by Using NSWE at t=6T.

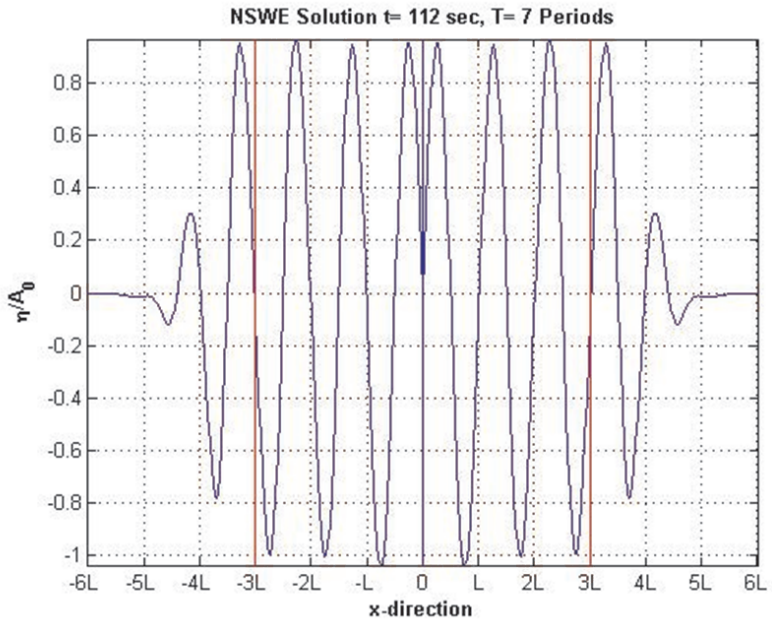

Figure B.6. Variation of the Normalized Free Surface in Shallow Water by Using NSWE at t=7T.

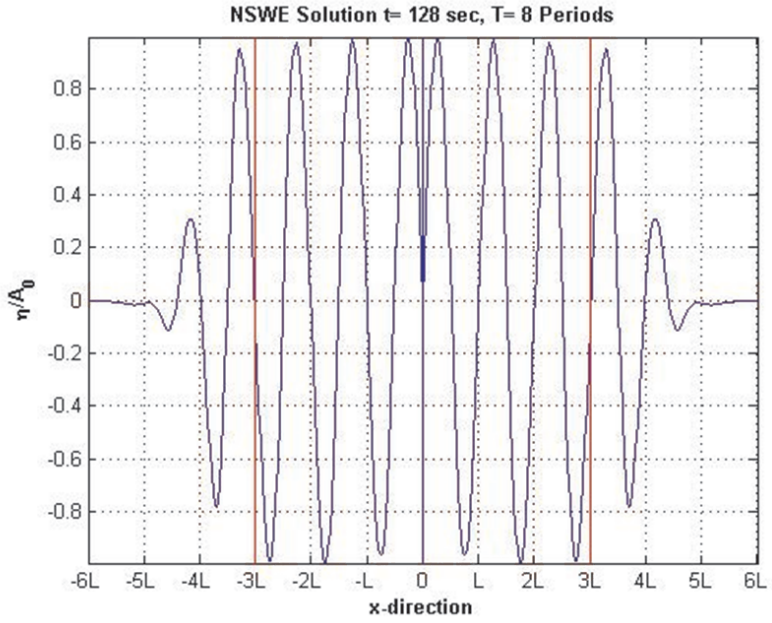

Figure B.7. Variation of the Normalized Free Surface in Shallow Water by Using NSWE at t=8T.

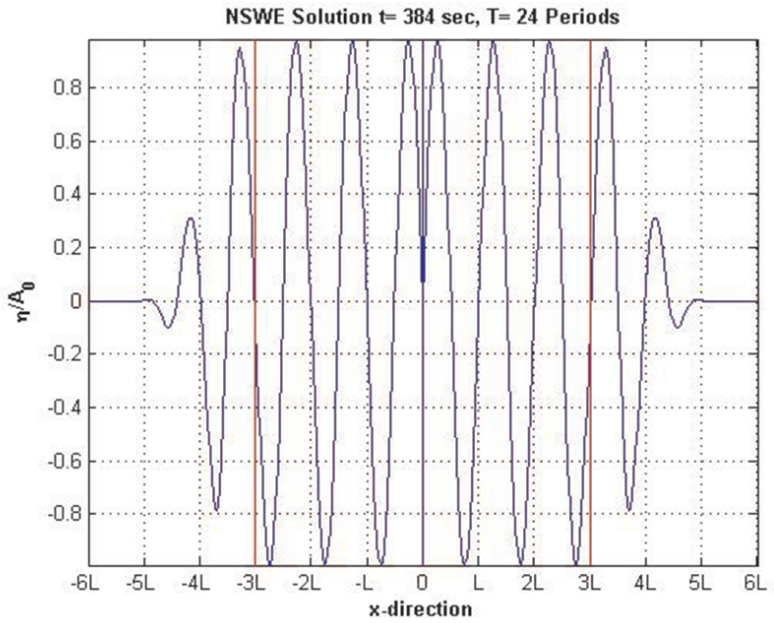

Figure B.8. Variation of the Normalized Free Surface in Shallow Water by Using NSWE at t=24T.

B.2. Two Sponge Treatment with Sloped Bathymetry

Figure B.9- Figure B.17 show the variation of the normalized free surface in the shallow water are given for the sloped bathymetry at 0.5T, T, 3T, 5T, 6T, 7T, 8T, 15T and 24T, respectively.

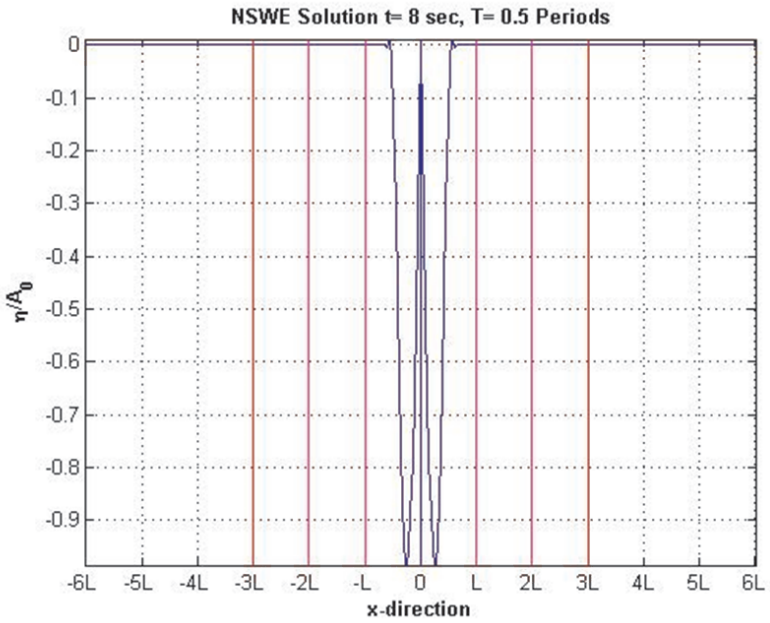

Figure B.9. Variation of the Normalized Free Surface in Shallow Water by Using NSWE at t=0.5T.

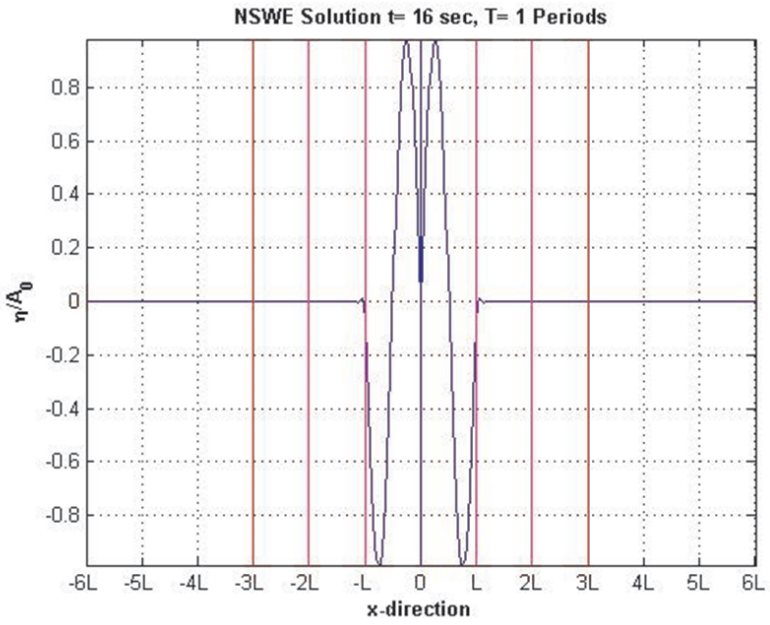

Figure B.10. Variation of the Normalized Free Surface in Shallow Water by Using NSWE at t=T.

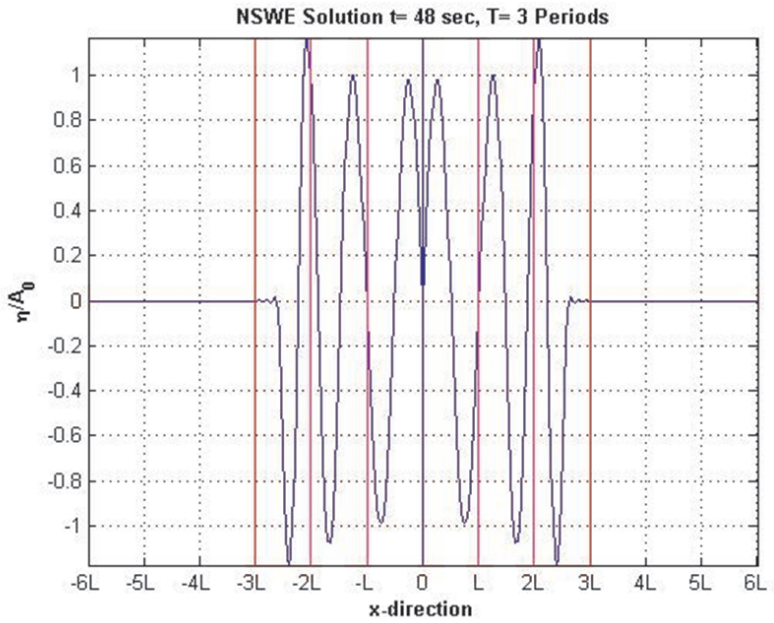

Figure B.11. Variation of the Normalized Free Surface in Shallow Water by Using NSWE at t=3T.

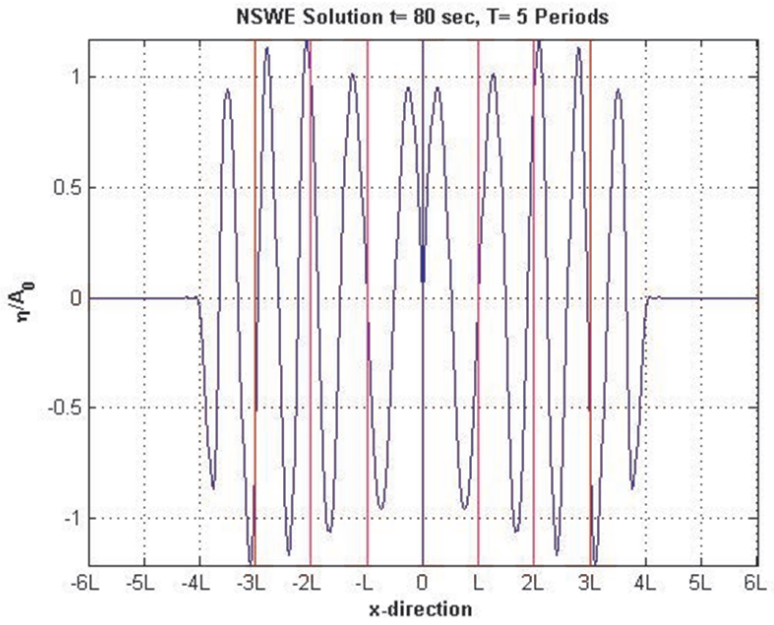

Figure B.12. Variation of the Normalized Free Surface in Shallow Water by Using NSWE at t=5T.

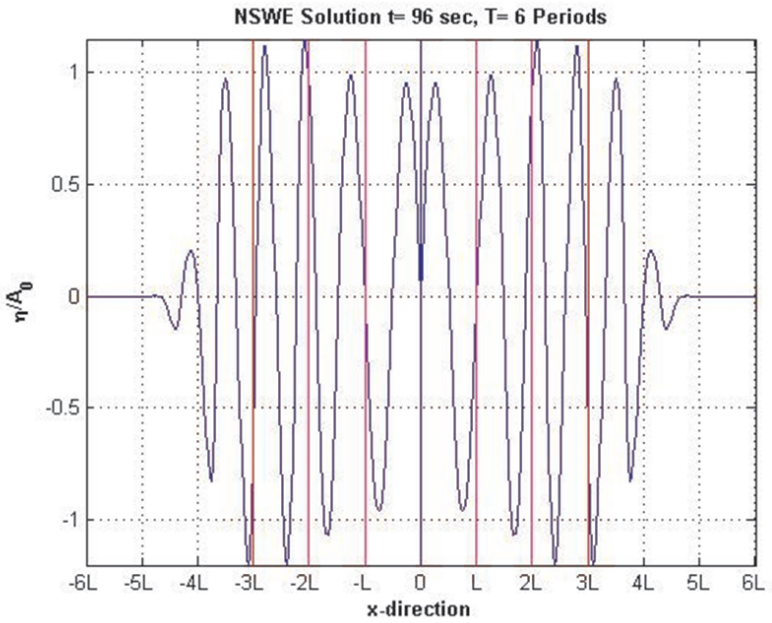

Figure B.13. Variation of the Normalized Free Surface in Shallow Water by Using NSWE at t=6T.

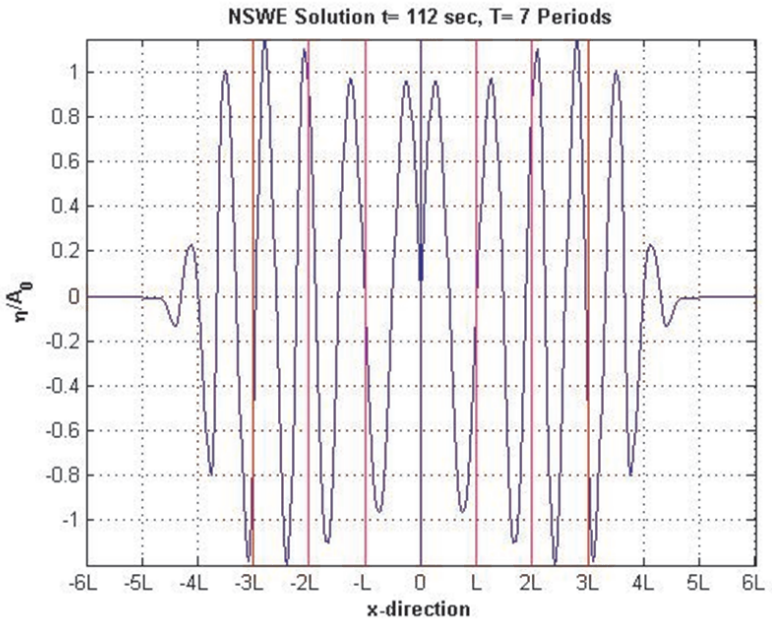

Figure B.14. Variation of the Normalized Free Surface in Shallow Water by Using NSWE at t=7T.

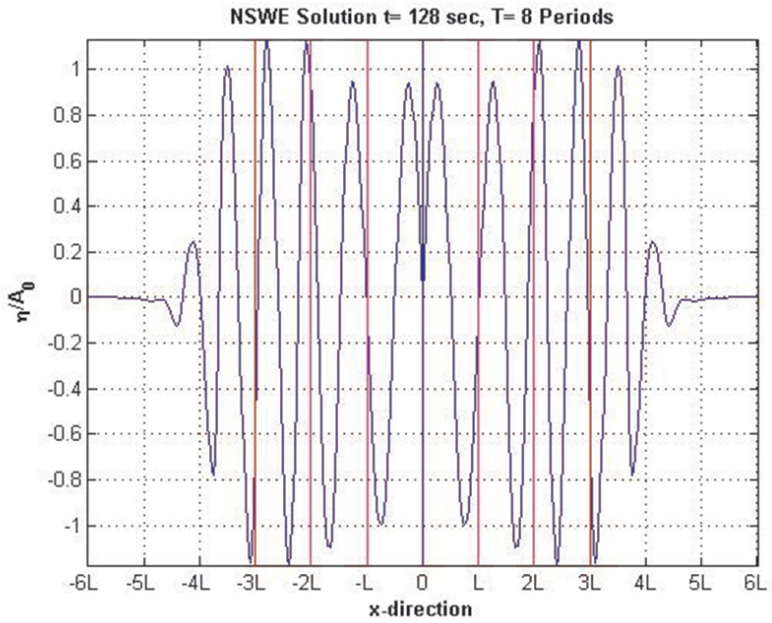

Figure B.15. Variation of the Normalized Free Surface in Shallow Water by Using NSWE at t=8T.

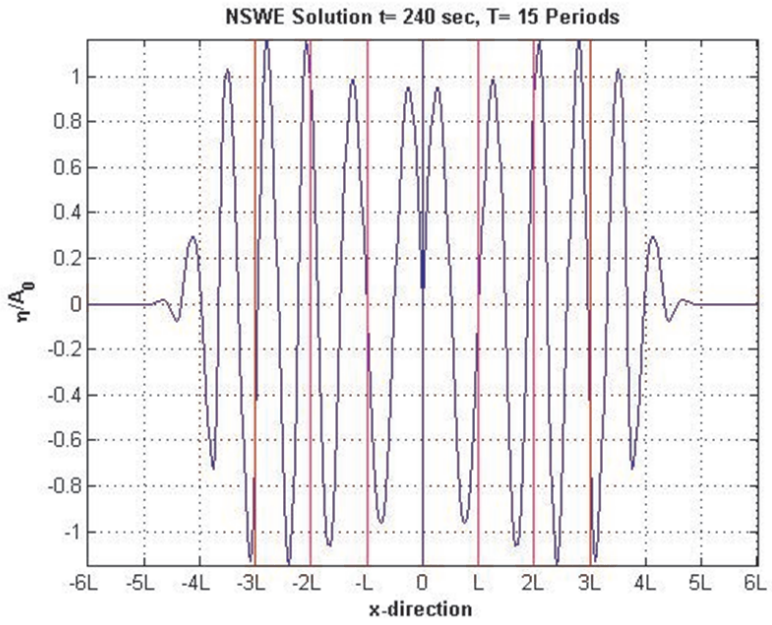

Figure B.16. Variation of the Normalized Free Surface in Shallow Water by Using NSWE at t=15T.

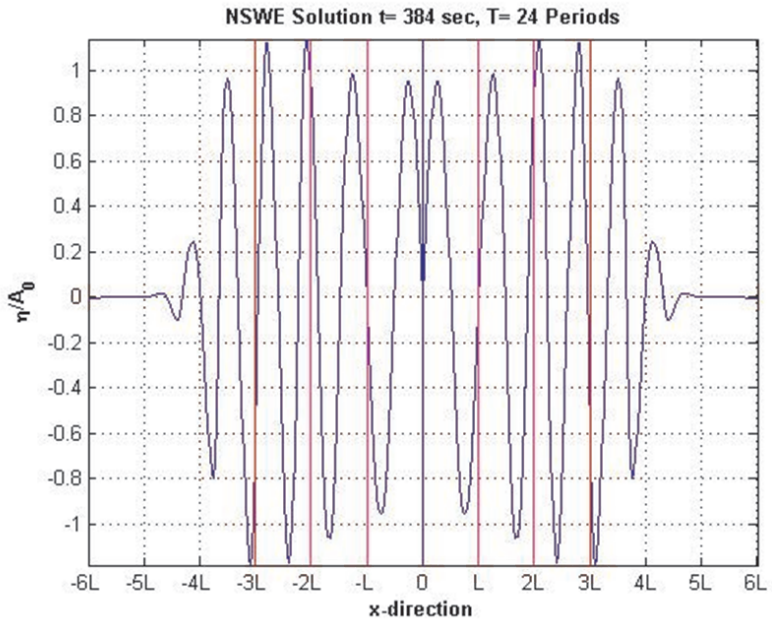

Figure B.17. Variation of the Normalized Free Surface in Shallow Water by Using NSWE at t=24T.

APPENDIX C: TWO DIMENSIONAL SOLUTIONS OF NSWE

C.1. Two Sponge Treatment with Horizontal Bathymetry

Developed numerical code is verified by applying a numerical benchmark problem

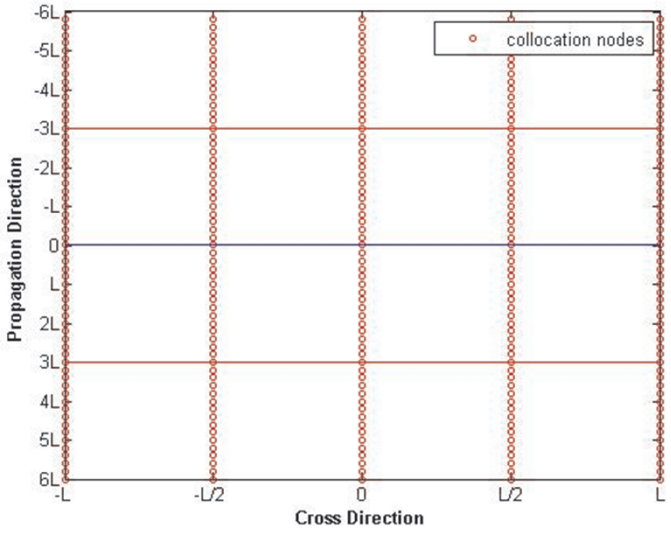

Figure C.1. Node Placement in the Propagation and Cross Direction, Influx Boundary (Blue Line) and Sponge Layers (Red Lines).

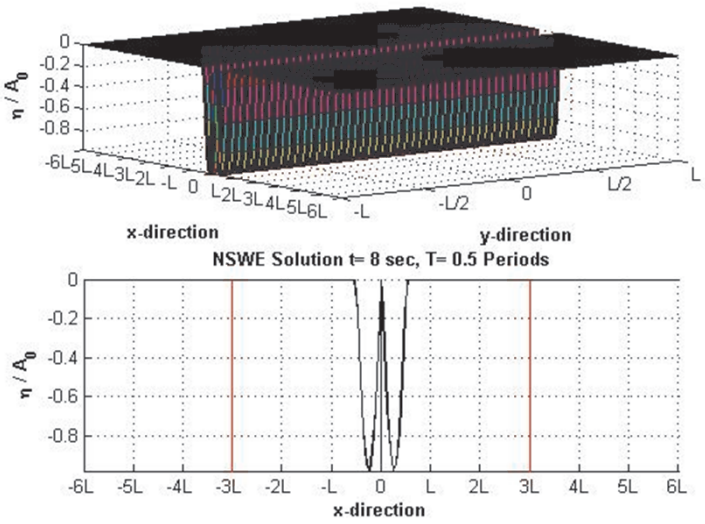

Figure C.2. Variation of the Normalized Free Surface in Shallow Water by Using NSWE at t=0.5T.

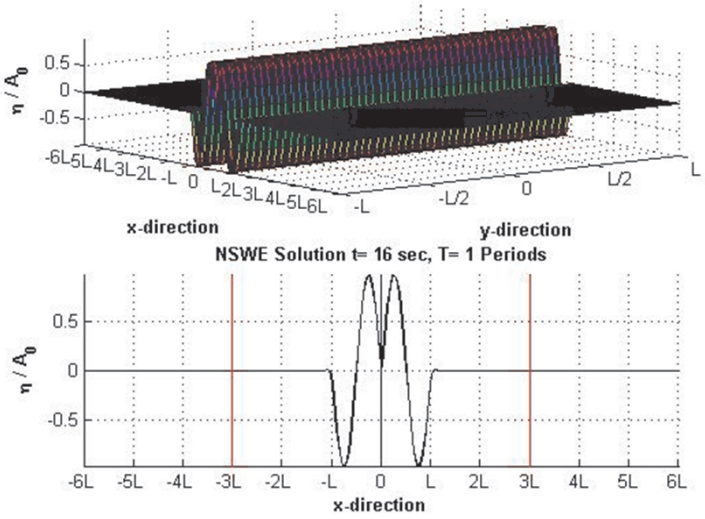

Figure C.3. Variation of the Normalized Free Surface in Shallow Water by Using NSWE at t=T.

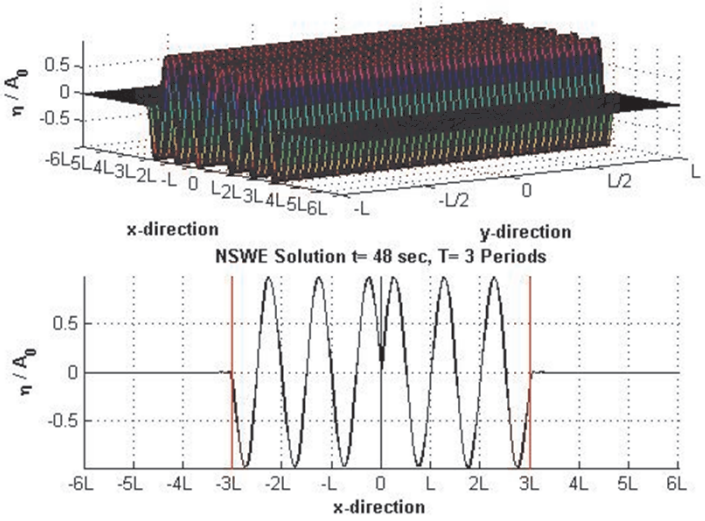

Figure C.4. Variation of the Normalized Free Surface in Shallow Water by Using NSWE at t=3T.

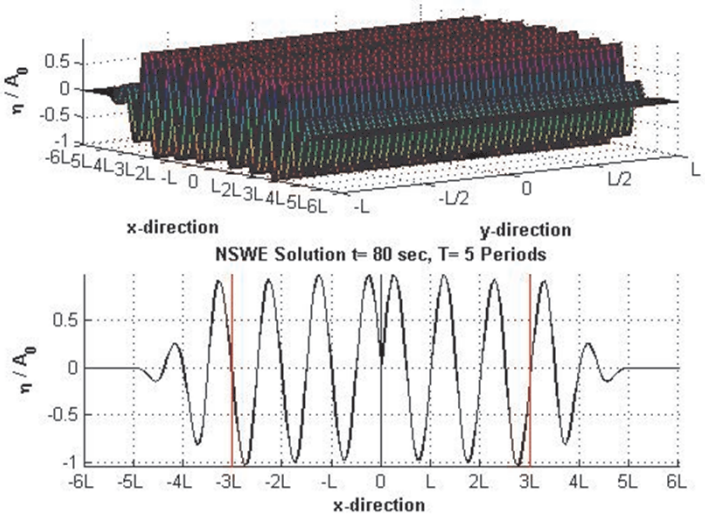

Figure C.5. Variation of the Normalized Free Surface in Shallow Water by Using NSWE at t=5T.

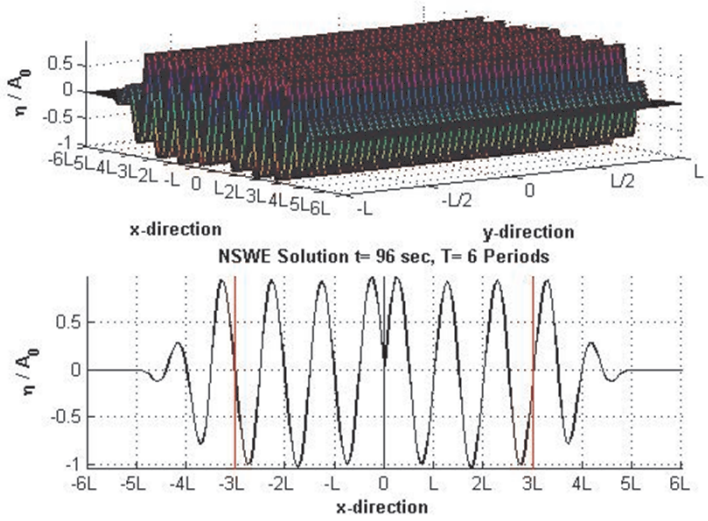

Figure C.6. Variation of the Normalized Free Surface in Shallow Water by Using NSWE at t=6T.

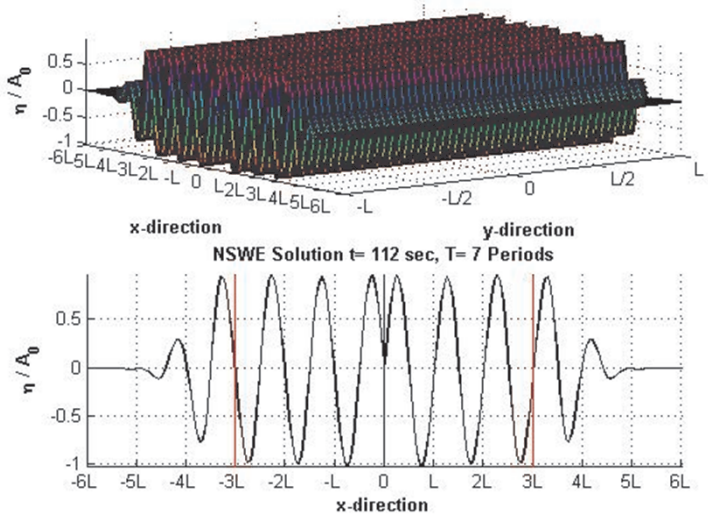

Figure C.7. Variation of the Normalized Free Surface in Shallow Water by Using NSWE at t=7T.

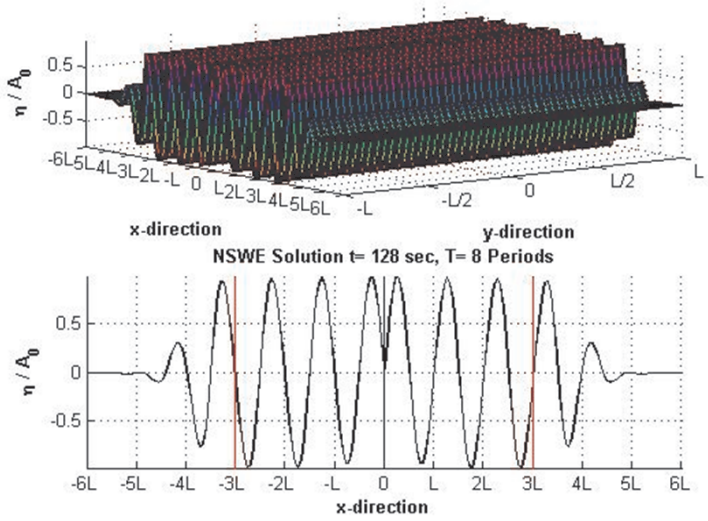

Figure C.8. Variation of the Normalized Free Surface in Shallow Water by Using NSWE at t=8T.

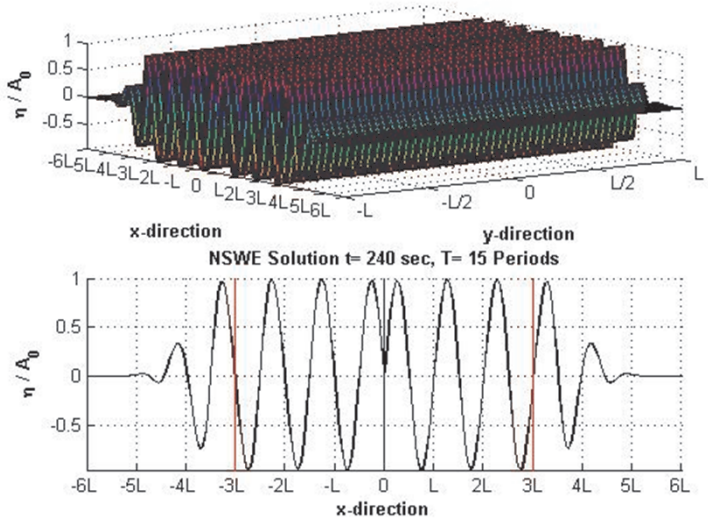

Figure C.9. Variation of the Normalized Free Surface in Shallow Water by Using NSWE at t=15T.

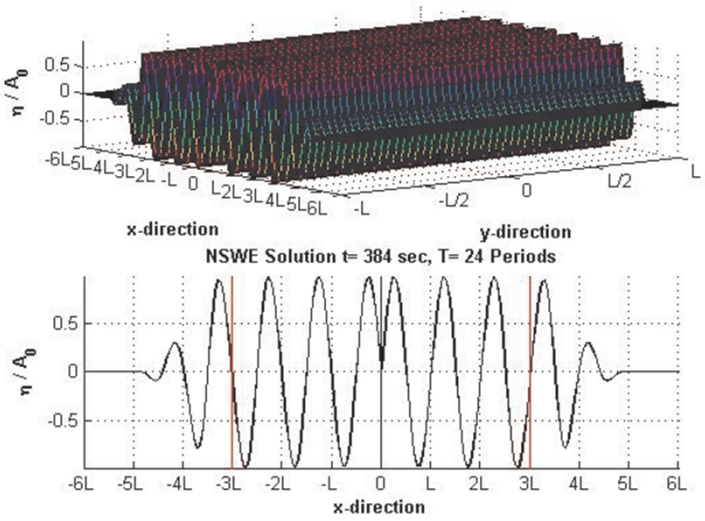

Figure C.10. Variation of the Normalized Free Surface in Shallow Water by Using NSWE at t=24T.

C.2. Two Sponge Treatment with Sloped Bathymetry

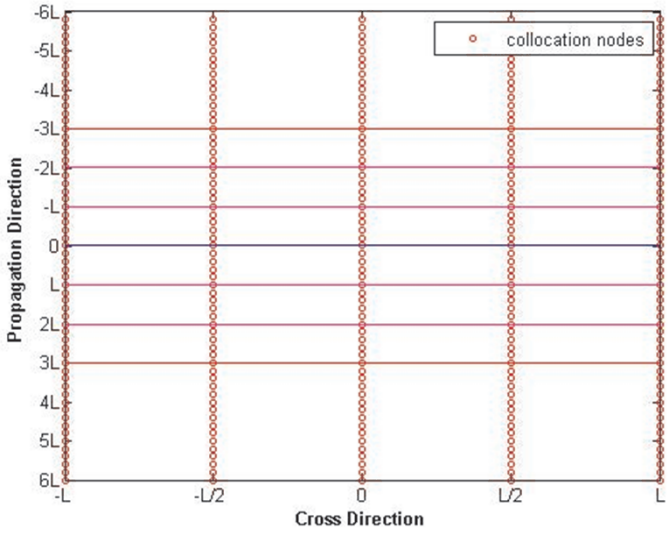

Figure C.11. Node Placement in the Propagation and Cross Direction, Influx Boundary (Blue Line at x=0), Sponge Layers (Red Lines at x=±3L, Sloped Bathymetry Starts at x=±L and Ends at x=±2L).

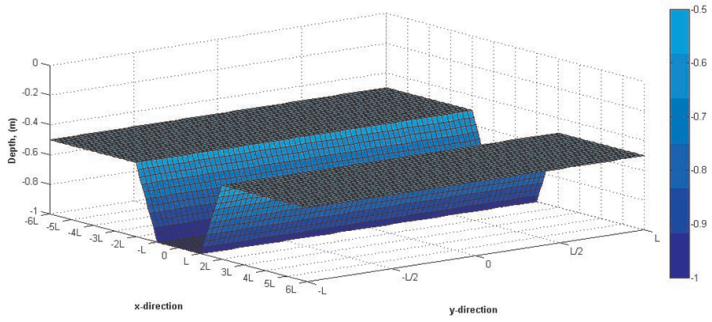

Figure C.12. Bathymetry of the Sloped Domain.

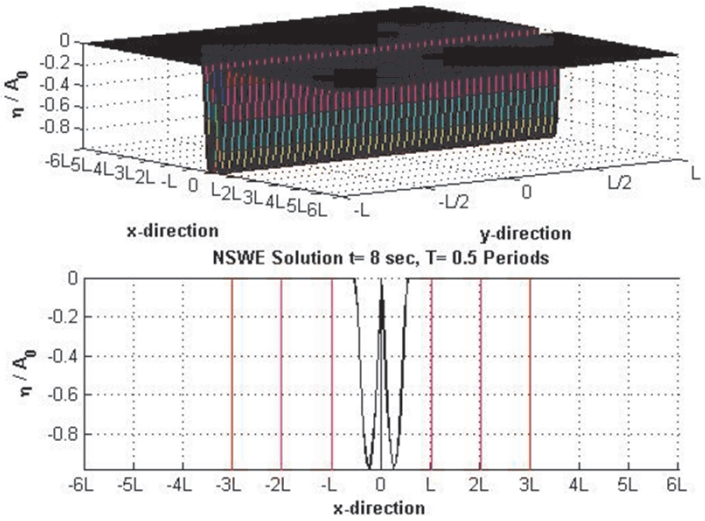

Figure C.13. Variation of the Normalized Free Surface in Shallow Water by Using NSWE at t=0.5T.

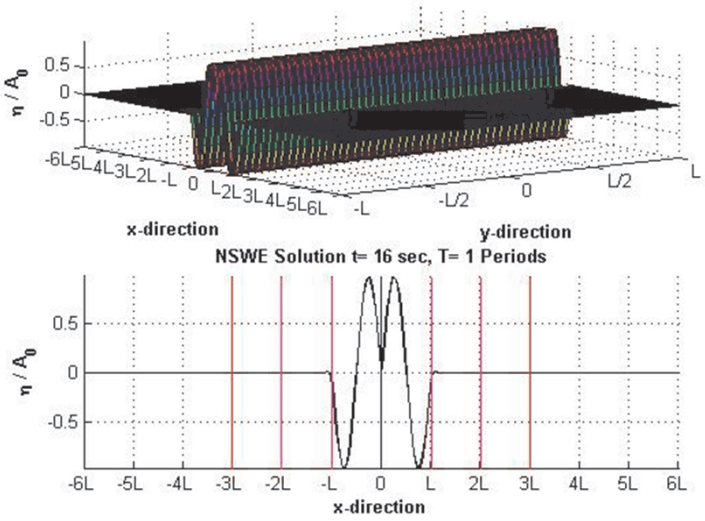

Figure C.14. Variation of the Normalized Free Surface in Shallow Water by Using NSWE at t=T.

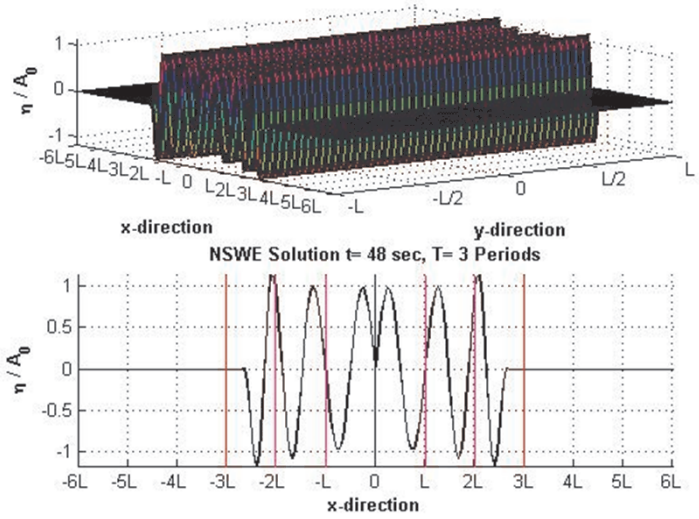

Figure C.15. Variation of the Normalized Free Surface in Shallow Water by Using NSWE at t=3T.

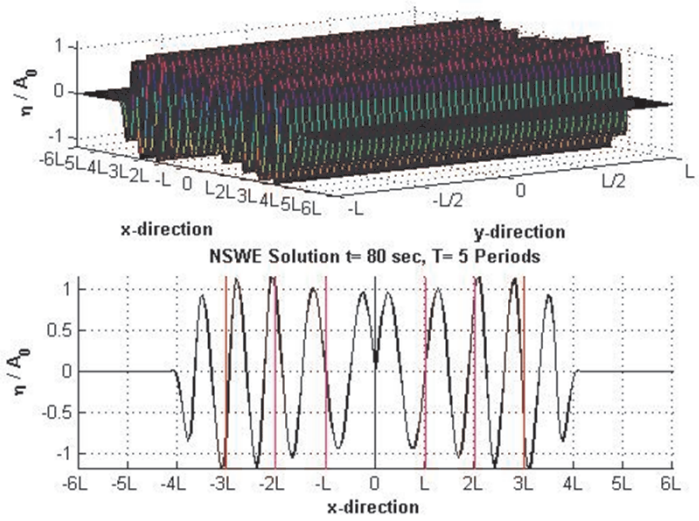

Figure C.16. Variation of the Normalized Free Surface in Shallow Water by Using NSWE at t=5T.

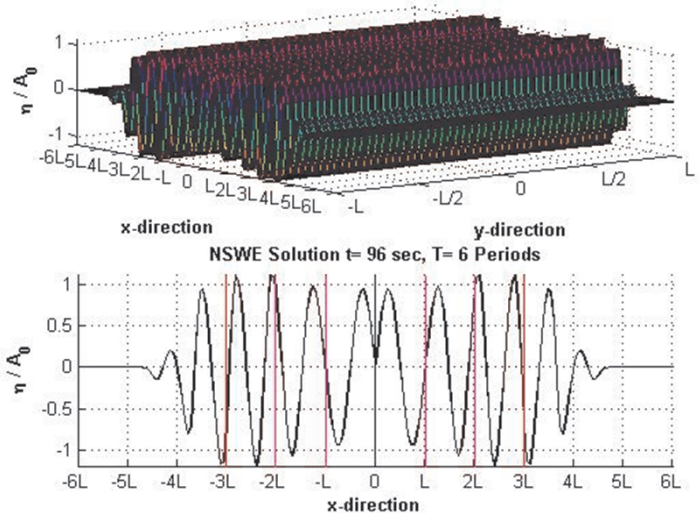

Figure C.17. Variation of the Normalized Free Surface in Shallow Water by Using NSWE at t=6T.

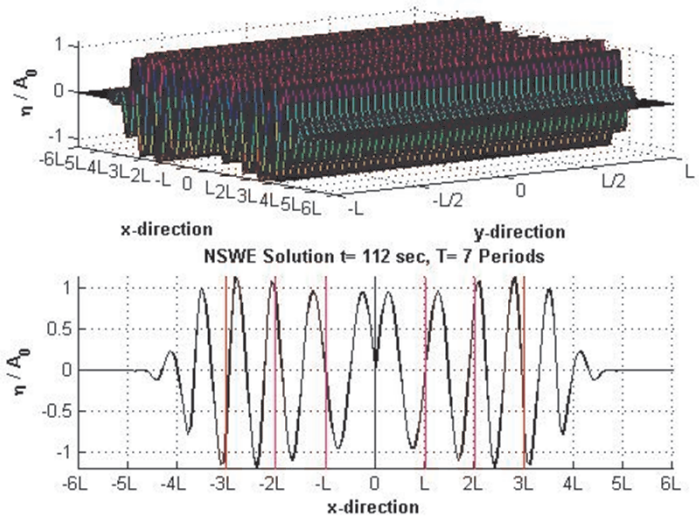

Figure C.18. Variation of the Normalized Free Surface in Shallow Water by Using NSWE at t=7T.

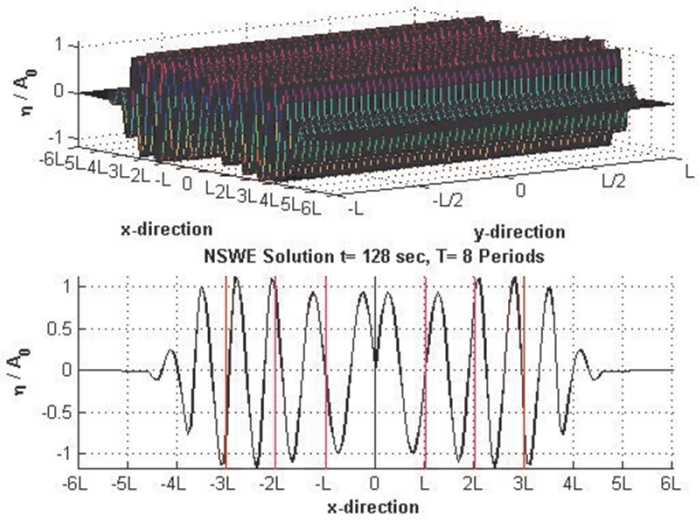

Figure C.19. Variation of the Normalized Free Surface in Shallow Water by NSWE Solution at t=8T.

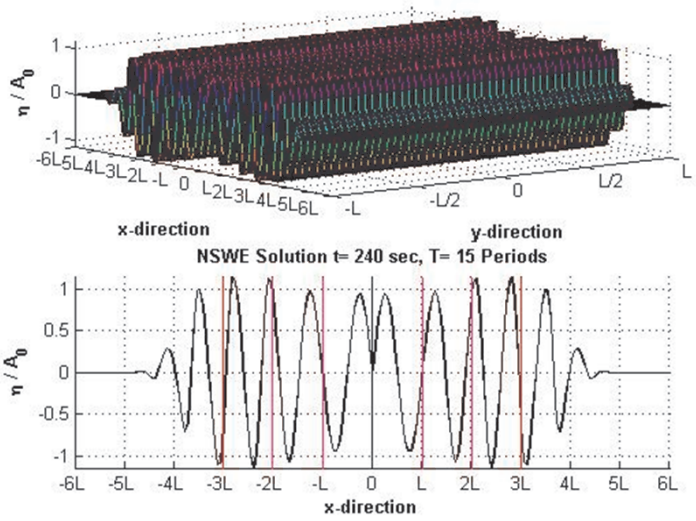

Figure C.20. Variation of the Normalized Free Surface in Shallow Water by Using NSWE at t=15T.

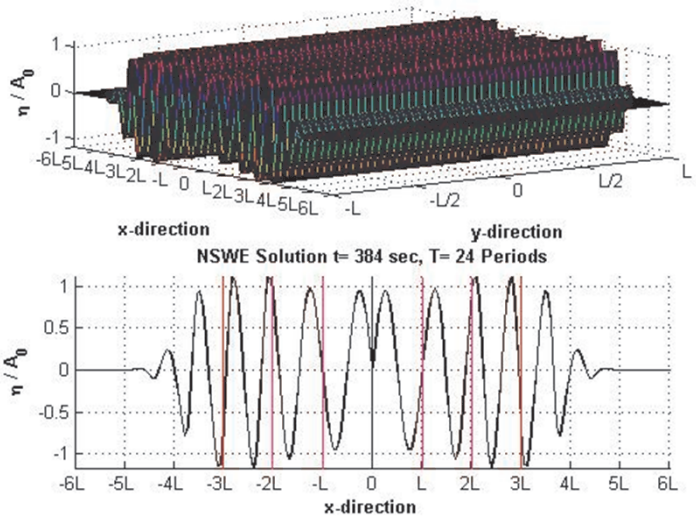

Figure C.21. Variation of the Normalized Free Surface in Shallow Water by Using NSWE at t=24T.

REFERENCES

Airy, G.B., 1845 "Tides and Waves", *Encyclopedia Metropolitana*, Section VI.

Alcrudo F., P. Garcia-Navarro, 1993, "A High-Resolution Godunov-Type Scheme in Finite Volume for the 2-D Shallow-Water Equations International", *International Journal for Numerical Methods in Fluids*, Vol. 16, pp. 489-505.

Ball, F.K., E. Silvester, R., Macmillan, 1964, "An Exact Theory of Simple Finite Water Oscillations on a Rotating Earth", *Hydraulics and Fluid Mechanics*, Vol. 1, pp. 293-305.

Balzano, A., 1998, "Evaluation of Methods for Numerical Simulation of Wetting and Drying in Shallow Water Flow Models", *Coastal Engineering*, Vol. 34, pp. 83-107.

Bellos V., J.G. Sakkas 1987, "1D Dam-Break Flood Propagation on Dry Bed", J*ournal of Hydraulic Engineering, American Society of Civil Engineering*, Vol. 113, No. 12 pp. 1510-1524.

Belytschko, T., Y.Y. Lu, L. Gu, 1994, "Element-Free Galerkin Methods", *International Journal for Numerical Methods in Engineering*, Vol. 37, pp. 229-256.

Berkhoff, J.C.W., N. Booy, A.C. Radder, 1982, "Verification of Numerical Wave Propagation Models for Simple Harmonic Linear Water Waves", *Coastal Engineering*, Vol. 6, pp. 255-279.

Bodony, D.J., 2006, "Analysis of Sponge Zones for Computational", *Fluid Mechanics*, Vol. 212, pp. 681-702.

Bokhove, O., 2005, "Flooding and Drying in Discontinuous Galerkin Finite Element Disretizations of Shallow-Water Equations", *One Dimension, Journal of Scientific Computing*, Vol. 22, pp. 47-82.

Börekçi, O., 2005, "The Radial Basis Function Collocation Method: A Meshless Method for the Solution of Boundary Value Problems", *Department of Civil Engineering, Lecture notes, Boğaziçi University.*

Boussinesq, J.V., 1872 "Theorie Des Ondes et Des Remous Qui Se Propaent Le Long D'un Canal Rectangulaire Horizontal, En Communiquant Au Liquide Contenu Dans Ce Canal Des Vitesses Sensiblement Pareilles De La Surface Au Dond", *Journal de Mathématiques Pures et Appliquées*, Vol. 17, pp. 55-108.

Boztosun, I., A. Charafi, M. Zerroukat and K. Djidjeli, 2002, "Thin-Plate Spline Radial Basis Function Scheme for Advection-Diffusion Problems", *Electronic Journals of Boundary Elements*, Vol. 1 , No.2, pp. 267-282.

Brocchim, M., D.H. Peregrine, 1996, "Integral Flow Properties of Swash Zone and Averaging", *Journal of Fluid Mechanics*, Vol. 317, pp. 241-273.

Buhmann, M.D. 2003, "Radial Basis Functions: Theory and Implementations", *Cambridge Monographs on Applied and Computational Mathematics*, Cambridge University Press, Cambridge.

Buhmann, M.D., 2003, "Radial Basis Functions-Theory and Implementations", *Cambridge University Press*, Cambridge, UK.

Carlson, R.E., T.A. Foley, 1991, "The Parameter R2 in Multiquadric Interpolation", *Computers and Mathematics with Applications*, Vol. 21, pp. 29-42.

Carrier, G.F., 1966, "Gravity Waves on Water of Variable Depth", *Journal of Fluid Mechanics*, Vol. 24, pp. 641-659.

Carrier, G.F., C.F. Noiseux, 1983, "The Reflection of Obliquely Incident Tsunamis", *Journal of Fluid Mechanics*, Vol. 133, pp. 147-160.

Carrier, G.F., H.P. Greenspan, 1958, "Water Waves of Finite Amplitude on a Sloping Beach", *Journal of Fluid Mechanics*, Vol. 4, pp. 97-109.

Carrier, G.F., T.T. Wu, and H. Yeh, 2003, "Tsunami Run-Up and Draw-Down on a Plane Beach", *Journal of Fluid Mechanics*, Vol. 475, pp. 79-99.

Cheng, R.T., V. Casulli, J.W. Gartner, 1993, "Tidal, Residual, Intertidal, Mudflat Model and its Applications to San Francisco Bay", *California Estuarine Coastal and Shelf Science*, Vol. 36, pp. 235-280.

Chantasiriwan, S., 2007, "Multiquadric Collocation Method for Time-Dependent Heat Conduction Problems with Temperature-Dependent Thermal Properties", *Journal of Heat Transfer*, Vol. 129, No. 2, pp. 109-113.

Chapra, C., P. Canale, 1988, "Numerical Methods for Engineers" : *McGraw-Hill*, New York.

Charney, J.G., R. Fjörtoft, J. Von Numann, 1950, "Numerical Integration of the Baratropic Vorticity Equation", *Tellus*, Vol. 2, pp. 237-254.

Chawla, A., Kirby, J.T., 2000, "A Source Function Method for Generation of Waves on Currents in Boussinesq Models", *Applied Ocean Research*, Vol. 22, pp. 75-83.

Cheng, A.H.D., M.A. Golberg, E.J. Kansa, G. Zammito, 2003, "Exponential Convergence and H-C Multiquadric Collocation Method for Partial Differential Equations", *Numerical Methods for Partial Differential Equations*, Vol. 19, No. 5, pp. 571-594.

Colonius, T., 2004, "Modeling Artificial Boundary Conditions for Compressible", *Flow Annual Review of Fluid Mechanics*, Vol. 36, pp. 315-345.

Colonius, T., H. Ran, 2002, "A Super-Grid-Scale Model for Simulating Compressible Flow on Unbounded Domains", *Journal of Computational Physics*, Vol. 182, pp. 191-212.

Colonius, T., S.K. Lele, P. Moin, 1993, "Boundary Conditions for Direct Computation of Aerodynamic Sound Generation", *American Institute of Aeronautics and*

Astronautics Journal, Vol. 31, pp. 1574-1582

Courant, R., K. Friedrichs, H. Lewy, 1967, "On the Partial Difference Equations of Mathematical Physics", *Journal of Research and Development*, Vol. 11, No. 2, pp. 215-234.

Dao, M.H., P. Tkalich, 2007, "Tsunami Propagation Modeling- A Sensitivity Study", Natural Hazards and Earth System Sciences, Vol. 7, pp. 741-754.

DiLorenzo, J.L., 1988, "The Overtide and Filtering Response of Small Inlet/bay Systems", *Hydrodynamics and Sediment Dynamics of Tidal Inlets, Coastal and Estuarine Studies*, Vol. 29, pp. 24-53.

Dietrich, J.C., R.L. Kolar, R.A. Luettich, C.T., Miller, M.W., Farthing, W.G. Gray, and G.F., Pinder, 2004, "Assessment of ADCIRC's Wetting and Drying Algorithm", *Computational Methods in Water Resources, Proceedings of the 15th International Conference on Computational Methods in Water Resources (CMWR XV)*, Vol. 55, pp. 2.

Dowling T.E., A.P. Ingersoll, 1989, "Jupiters Great Red Spot as a Shallow Water System", *Journal of the Atmospheric Sciences*, Vol. 46, pp. 3256-3278.

Dronkers, J.J., 1964, "Tidal Computations in Rivers and Coastal Waters", *North-Holland*, Amsterdam.

Dube, S.K., P.C. Shinha, G.D. Roy, 1985, "The Numerical Simulation of Storm Surges Along the Bangla Desh coast", *Dynamics of Atmospheres and Oceans*, Vol. 9, pp. 121-133.

Engquist, Bjorn and Majda, 1977, "Andrew Absorbing Boundary Conditions for the Numerical Simulation of Waves" *Mathematics of Computation*, Vol. 31, No. 139, pp. 629-651.

Fasshauer, G., 2007, "Meshfree Approximation Methods with MATLAB", *World Sci-*

entific Publishers, Singapore.

Fasshauer, G.E., 1996, "Solving Partial Differential Equations by Collocation with Radial Basis Functions", *Northwestern University*, Evanston.

Franchello, G., E. Krausmann, 2008, "HyFlux 2: A Numerical Model for the Impact Assessment of Severe Inundation Scenario to Chemical Facilities and Downstream Environment", *Scientific and Technical Research Series, European Commission.*

Franke, C., R. Schaback, 1998, "Convergence Order Estimates of Meshless Collocation Methods Using Radial Basis Functions", *Advances in Computational Mathematics*, Vol. 8, No. 4, pp. 381-399.

Franke, R., 1982 "Scattered Data Interpolation: Tests of Some Methods", *Mathematics of Computation*, Vol. 38, No. 157, pp. 181-200.

Freund, J.B., 1997, "Proposed Inflow/Outflow Boundary Condition for Direct Computation of Aerodynamic Sound", *American Institute of Aeronautics and Astronautics Journal*, Vol. 35, pp. 740-742.

Friedrichs, C.T., O.S. Madsen, 1992, "Nonlinear Diffusion of the Tidal Signal in Frictionally Dominated Embayments", *Journal of Geophysical Research*, Vol. 97, pp. 5637-5650.

Galperin, E.A, E.J. Kansa, 2002, "Application of Global Optimization and Radial Basis Functions to Numerical Solutions of Weakly Singular Volterra Integral Equations", *Computers & Mathematics with Applications*, Vol. 43, No. 3-5, pp. 491-499.

Gallagher, B.S., W.H. Munk, 1971, "Tides in Shallow Water: Spectroscopy", *Tellus*, Vol. 23, pp. 346-363.

Garvine, R.W, 1987, "Estuary Plume and Fronts in Shelf Waters: A Layer Model", *Journal of Physical Oceanography*, Vol. 17, pp. 1877-1896.

Giles, M.B., 1990, "Nonreflecting Boundary Conditions for Euler Equation Calculations", *The American Institute of Aeronautics and Astronautics Journal*, Vol. 28, pp. 2050-2058.

Givoli, D., 1991, "Non-Reflecting Boundary Conditions", *Journal of Computational Physics*, Vol. 94, No. 1, pp, 1-29.

Goldberg, M.A., C.S. Chen, 1997, "Discrete Projection Methods for Integral Equation", *Computational Mechanics Publications*, Southampton.

Goto C., Y. Ogawa, N. Shuto, F. Imamura, 1997, "IUGG/IOC TIME Project: Numerical Method of Tsunami Simulation with the Leap-Frog Scheme", *Intergovernmental Oceanographic Commission of United Nations Educational, Scientific and Cultural Organization.*

Grilli, S., R. Subramanya, L.A. Svendsen and J. Veeramony, 1994, "Shoaling of Solitary Waves on Plane Beaches. Wtrwy, Fort Coast. Ocean Engrg. Vol. 120, No.6, pp. 609-628.

Grilli, S.T., I.A. Svendsen and R. Subramanya, 1997, "Breaking Criterion and Characteristics for Solitary Waves on Slope", *Journal of Waterway, Port, Coastal, and Ocean Engineering*, Vol. 123, No. 3, pp. 102-112.

Grilli. S., H. Yeh, P. Liu, and C. Synolakis, 1997, "Fully Nonlinear Potential Fmodels Used for Long Wave runup Prediction," *In Long-Wave Runup Models*, Vol. 3, pp. 116-180.

Hall, J.V., J.W. Watts, 1953, "Laboratory Investigation of the Vertical Rise of Solitary Waves on Impermeable Slopes", *Tech. Memo. 33. Beach Erosion Board, US Army Corps of Engineers.*

Hamming, R.W., 1959, "Stable Predictor-Corrector Methods for Ordinary Differential Equaitons", *Journal of the Association for Computing Machinery*, Vol. 6, pp. 37.

Hardy, L. R., 1971, "Multiquadric Equations of Topography and Other Irregular Surfaces", *Journal of Geophysical Research*, Vol. 76, pp. 1905-1915.

Hendershott, M.C., B.A. Warren and C. Wunsch, 1981, "Long Waves and Ocean Tides", *Evolution of Physical Oceanography, Massachusetts Institute of Technology*, Vol. 2, pp. 292-341.

Heryudono, A. and T. Driscoll, 2007, "Adaptive Radial Basis Function Methods with Residual Subsampling Technique for Interpolation and Collocation Problems", C*omputers and Mathematics with Applications*, Vol. 53, No. 6, pp. 927-939.

Hibberd, S., D.H. Peregrine, 1978, "Surf and Run-Up on a Beach: a Uniform Bore", *Journal of Fluid Mechanics*, Vol. 95, pp. 323-345.

Holdahl, R., H. Holden, K.A. Lie, 1998, "Unconditionally Stable Splitting Methods for the Shallow Water Equations", *BIT Numerical Mathematics*, Vol. 39, pp. 451-472.

Hon Y.C., Lu M.W., Xue W.M., and Zhu Y.M., 1997, "Multiquadric Method for the Numerical Solution of a Biphasic Mixture Model", *Applied Mathematics and Computation*, Vol. 88, pp. 153-175.

Hon, Y.C., X.Z. Mao, 1997, "A Multiquadric Interpolation Method for Solving Initial Value Problems", *Journal of Scientific Computing*, Vol. 12, pp. 51-55.

Hu, F.Q., 2008, "Development of PML Absorbing Boundary Conditions for Computational Aeroacoustics: A Progress Review", *Computers and Fluids*, Vol. 37, pp. 336-348.

Hu, F.Q., X.D. Li, D.K. Lin, 2008, "Absorbing Boundary Conditions for Nonlinear Euler and Navier-Stokes Equations Based on the Perfectly Matched Layer Technique", *Journal of Computational Physics*, Vol. 227, pp. 4398-4424.

Imamura, F., 1989, "Tsunami Numerical Simulation with the Staggered Leap-Frog Scheme (Numerical Code of TUNAMI-N1)", *School of Civil Engineering, Asian*

Institute of Technology and Disaster Control Research Center.

Imamura, F., 1995, "Numerical Method of Tsunami Simulation with the Leap-Frog Scheme", *Part 2: Propagation in the Ocean in the Spherical Coordinates, TUNAMI-F1 and its Program List.*

Imamura, F., H. Yeh, P. Liu and C, Synolakis, 1996, "Review of Tsunami Simulation with a Finite Difference Method", *Long Wave Runup Models, Proceedings of the International Workshop, Friday Harbour, World Scientific Publishing*, Vol. 1, pp. 25-42.

Ippen, A. T., 1966, "Tidal Dynamics in Estuaries, Part 1; Estuaries of Rectangular Section in Estuary and Coastline Hydrodynamics", *Estuary and Coastline Dynamics*, Vol. 1, pp. 493-545.

Iske, A., 2003, "Radial Basis Functions:Basics, Advanced Topics and Meshfree Methods for Transport Problems", *University Torino*, Vol. 63, pp. 300-320.

Israeli, M., S.A. Orszag, 1981, "Approximation of Radiation Boundary Conditions", *Journal of Computational Physics*, Vol. 41, pp. 115-135.

Johns, B., 2982, "Numerical Integration of the Shallow Water Equations Over a Sloping Shelf", *International Journal for Numerical Methods in Fluids*, Vol. 2, pp. 253-261.

Johnson, R.S., 1980, "A Modern Introduction to the Mathematical Theory of Water Waves", *Cambridge University Press.*

Kabbaj, A., C. Le Provost, 1980, "Nonlinear Tidal Waves in Channels; a Serturbation Method Adapted to the Importance of Quadratic Bottom Friction", *Tellus*, Vol. 32, pp. 143-163.

Kanoğlu, U. 2004, "Nonlinear Evolution and Runup-Rundown of Long Waves over a Sloping Beach", *Journal of Fluid Mechanics*, Vol. 513, pp. 363-372.

Kanoğlu, U., and C.E. Synolakis, 1998, "Long Wave Runup on Piecewise Linear Topographies", *Journal of Fluid Mechanics*, Vol. 374, pp. 1-28.

Kansa E.J., Y.C. Hon, 2000, "Circumventing the Ill-Conditioning Problem with Multiquadric Radial Basis Functions: Applications to Elliptic Partial Differential Equations", *Computers and Mathematics with Applications*, Vol. 39, pp. 123-137.

Kansa, E. J., 1990, "Multiquadrics-A Scattered Data Approximation Scheme with Applications to Computational Fluid Dynamics I: Surface Approximations and Partial Derivative Estimates", *Computers and Mathematics with Applications*, Vol. 19, pp. 127-146.

Kansa, E. J., 1990, "Multiquadrics-A Scattered Data Approximation Scheme With Applications to Computational Fluid Dynamics II: Solutions of Parabolic, Hyperbolic and Elliptic Partial Differential Equations", *Computers and Mathematics with Applications*, Vol. 19, pp.147-161.

Karni, S., 1996, "Far-Field Filtering Operators for Suppression of Reflections from Artificial Boundaries", *Journal of Numerical Analysis*, Vol. 33, pp. 1014-1047.

Keller, J.B., H.B. Keller, 1964, "Water wave Run-Up on a Beach, ONR Research Report" *Contract NONR-3828(00)*, Department Navy, Washington.

Kim, S.K, P.L.F. Liu and J.A. Ligget, 1983, "Boundary Integral Equation Solutions for Solitary Wave Generation", *Propagation and Run-Up Coastal Engineering*, Vol. 7, pp. 299-317.

Kinnmark, LP.E., 1986, "The Shallow Water Wave Equations: Formulation, Analysis and Application", *Lecture Notes in Engineering*, Vol. 15, pp. 187.

Kirby, J.T. 1996, "Nonlinear, Dispersive Long Waves in Water of Variable Depth", Research Report No. CACR-96-02, *Center for Applied Coastal Research*, University of Delaware, Vol. 1, pp. 71.

Knight, D.W., 1973, "Long wave Propagation in an Idealized Estuary", *Journal of the Hydraulics Division*, American Society of Civil Engineers, Vol. 99, pp. 993-1007.

Kowalik, Z., T.S. Murty, 1993, "Numerical Modeling of Ocean Dynamics, *World Scientific Publication*, Vol. 481 pp 10-15.

Kowalik, Z. T.S. Murty, 1995, "Numerical Modeling of Ocean Dynamics", *World Scientic*, Singapore.

Kreiss, H., 1957, "Some Remarks About Nonlinear Oscillations in Tidal Channels", *Tellus*, Vol. 9, pp. 53-68.

Kurkin A.A., A.C. Kozelkov, A.I. Zaitsev, N. Zahibo and A.C. Yalçıner, 2003, "Tsunami Risk for the Caribbean Sea Coast, Izvestiya", *Russian Academy of Engineering Sciences*, Vol. 4, pp. 126-149.

Lamb, H., 1932, "Hydrodynamics (6th ed.)", *University Press*, Cambridge.

Larsson, E. B. Fornberg, 2003, "A Numerical Study of Some Radial Basis Function based Solution Methods for Elliptic PDEs", *Uppsala University*, Sweeden.

Lewis, C.H. W.M. Adams, 1983, "Development of a Tsunami Flooding Model Having Versatile Formulation of Moving Boundary Conditions", *The Tsunami Society Monograph Series*, Vol. 1, pp. 128.

Lewis, C.H. W.M. Adams, 1983, "Development of a Tsunami-Fooding Model Having Versatile Formation of Moving Boundary Conditions", *The Tsunami Society Monograph Series*, Vol. 1, pp. 128.

Li, Y., F. Raichlen, 2001, "Solitary Wave Runup on Plane Slopes", *Journal of Waterway*, Ocean Engineering, American Society of Civil Engineers, Vol. 127, pp. 33-44.

Li, Y., F. Raichlen, 1999, "Solitary Wave Run-Up on Plane Slopes" *Research Report,*

W. M. Keck Laboratory of Hydraulics, and Water Resources, California Institute of Technology.

Liu, P.L.-F., S.-B. Woo, Y.-S. Cho, 1998, "Computer Programs for Tsunami Propagation and Inundation", *Technical report, Cornell University.*

Liu, P.L.-F., Y.-S. Cho, M.J. Briggs, U. Kanoğlu and C.E. Synolakis, 1995, "Run-Up of Solitary Waves on a Circular Island", *Journal of Fluid Mechanics*, Vol. 320, pp. 259-285.

Liu, P.L.-F., Y.-S. Cho, S.B. Yoon, S.N., Seo, 1994, "Numerical Simulations of the 1960 Chilean Tsunami Propagation and Inundation at Hilo", *Recent Development in Tsunami Research*, pages Vol. 1, pp. 99-115.

Lui, Y., Z. Xin, M. Lu, 2005, "A Meshless Method Based on Least-Squares Approach for Steady and Unsteady-State Heat Conduction Problems", *An International Journal of Computation and Methodology Numerical Heat Transfer, Part B, Fundamentals*, Vol. 47, pp. 257-275.

Lynch, D.R., W.G. Gray, 1978, "Analytic Solutions for Computer Flow Model Testing", *Journal of the Hydraulics Division*, American Society of Civil Engineers, Vol. 104, pp. 1409-1428.

Madych, W.R., 1992, "Miscellaneous Error Bounds for Multiquadric and Related Interpolants", *Computers Mathematical with Applications*, Vol. 24, pp. 121-138.

Madsen, R A., R. Murray, O.R. Sorensen, 1991, "A New Form of Boussinesq Equations with Improved Linear Dispersion Characteristics", *Coastal Engineering*, Vol. 15, pp. 371-388.

Milne, W.E., 1953, "Numerical Solution of Differential Equations", *Viley*, New York.

Moody, J., C. Darken, 1989, "Fast Learning in Networks of Locally-Tuned Processing Units.", *Neural Computation*, Vol. 1, pp. 281-294.

Nayroles, B., G. Touzot, 1992, "Pierre Villon, Generalizing the Finite Element Method: Diffuse Approximation and Diffuse Elements", *Computational Mechanics*, Vol. 10, pp. 307-318.

Nguyen, V.P., T. Rabczukb, S. Bordasc, M. Duflotd, "Meshless Methods: A Review and Computer Implementation Aspects", *Mathematics and Computers in Simulation*, Vol. 79, No. 3, pp. 763-813.

Nihoul, J.C.J., F.C. Ronday, 1975, "The Influence of Tidal Stress", *Residual Calculation*, Vol.29, pp. 484-490.

Nwogu, O., J. Waterway, 1993, "An Alternative form of the Boussinesq Equations for Nearshore wave Propagation", *Port Coast and Ocean Engineering*, Vol. 119, No. 6, pp. 618-638.

Ogink H.J.M., J.G. Grijsen and A.J.H. Wijbenga, 1986, "Aspects of Flood Level Computations", *International Symposium Flood Frequency and Risk Analysis.*

Ohyama, T. and K. Nadaoka, 1991, "Development of a Numerical wave Tank for Analysis of Nonlinear and Irregular wave Fields", *Fluid Dynamics Research*, Vol. 8, pp. 231-251.

Okada, Y., 1985, "Surface Deformation Due to Shear and Tensile Faults in a Half-Space", *Bulletin of the Seismological Society of America*, Vol. 75, No.4, pp. 1135-1154.

Orlanski, I., 1976, "A Simple Boundary Condition for Unbounded Hyperbolic Flows", *Journal of Computational Physics*, Vol. 21, pp. 251-269.

Özer, C., A.C. Yalçıner, 2011, "Sensitivity Study of Hydrodynamic Parameters During Numerical Simulations of Tsunami Inundation", *Pure and Applied Geophysics.*

Özer, C., H. Karakuş, A.C. Yalçıner, 2008 "Investigation of Hydrodynamic Demands of Tsunamis in Inundation Zone", *Proceedings of 7th International Conference on*

Coastal and Port Engineering in Developing Countries.

Özkan-Haller, H., J.T. Kirby, 1997, "A Fourier-Chebyshev Collocation Method for the Shallow Water Equations Including Shoreline Runup", *Applied Ocean Research*, Vol. 19, pp. 21-34.

Pearson, C.A., 1980, "Numerical Method for Shallow-Water Motion Onto a Beach", *Computational Methods in Nonlinear Mechanics, North Holland Publishing Company*, Vol. 1, pp. 379-391.

Pedersen, G., B. Gjevik, 1983, "Run-Up of Solitary Waves", Journal of Fluid Mechanics, Vol. 135, pp. 283-299.

Peregrine, D.H., 1967, "Long Waves on a Beach", J. Fluid Mech., Vol. 27, pp. 815-82.

Peterson, P., J. Hauser, W.C. Thacker, D. Eppel, C. Taylor, E. Hinton, D. R. J. Owen and E. Onat, 1984, "An Error-Minimizing Algorithm for the Non-Linear Shallow-Water Wave Equations with Moving Boundaries", *Numerical Methods for Non-Linear Problems*, Pineridge Press, Vol, pp. 826-836.

Poinsot, T.J., S.K. Lele, 1992, "Boundary Conditions for Direct Simulations of Compressible Viscous Flows", *Journal of Computational Physics*, Vol. 101, pp. 104-129.

Prandle, D., M. Rahman, 1980, "Responses in Estuaries", *Journal of Physical Oceanography*, Vol. 10, pp. 1552-1573.

Prasad, R.S., I.A. Svensen, 2003, "Moving Shoreline Boundary Conditions for Nearshore Models", *Coastal Engineering*, Vol. 49, pp. 239-261.

Proudman, J., 1953, "Dynamical Oceanography", *London: Methuen*; New York.

Proudman, J., 1957, "Oscillations of Tide and Surge in an Estuary of Finite Length", *Journal of Fluid Mechanics*, Vol. 2, pp. 371-382.

Rahman, M., 1995, "Water Waves", *Clarendon Press*, Oxford, United Kingdon.

Runchal, A.K., 1975, "Numerical Model for Storm Surge and Tidal Run-Up Studies", *Symposium on Modeling Techniques Volume II, 2nd Annual Symposium of The Waterways, Harbors and Coastal Engineering Division, American Society of Civil Engineers*, Vol. 1, pp. 1516-1534.

Ridderinkhof, H. 1990, *Residual Currents and Mixing in the Wadden Sea*, Ph.D. Thesis, University of Utrecht.

Sachdev, P.L., D. Paliannapan, R. Sarathy, 1996, "Regular and Chaotic Flows in Paraboloidal Basins and Eddies", *Chaos, Solitons and Fractals*, Vol. 7, pp. 383-408.

Sampine L.F., M.K. Gordon, 1975, "Computer Solution of Ordinary Differential Equations: the Initial Value Problem", *Freeman*.

Sarra, S.A., 2004, "Adaptive Radial Basis Function Methods for Time Dependent Partial Differential Equations", *Applied Numerical Mathematics*, Vol. 54, No.1, pp. 79-94.

Satake, K. 2002, "Tsunamis, in International Handbook of Earthquake and Engineering Seismology", *International Association of Seismology and Seismology and Physics of the Earths Interior, Committee on Education, and International Association for Earthquake Engineering*, Vol. 2, pp. 436-451.

Sato, S., 1996, "Numerical Simulation of 1993 Southwest Hokkaido Earthquake Tsunami Around Okushiri Island", *Journal of Waterway, Port, Coastal, and Ocean Engineering*, Vol. 1, pp. 209-215.

Schaback R., 1995, "Error Estimates and Condition Numbers for Radial Basis Function Interpolation" *Advances in Computational Mathematics*, Vol. 3, No. 3, pp. 251-264.

Shapiro R., 1975, "Linear Filtering Mathematics of Computation", *Atmospheric Sciences*, Vol. 29, No. 1, pp. 1094-1097.

Shapiro R., 1971, "The use of Linear Filtering as a Parameterization of Atmospheric Diffusion", *Atmospheric Sciences*, Vol. 28, pp. 523-531.

Shuto, N., 1967, "Run-Up of Long Waves on a Sloping Beach", *Coastal Engineering*, Vol, 10, pp. 23-38.

Siden, G.L.D., D.R. Lynch, 1988, "Wave Equation Hydrodynamics on Deforming Elements", *International Journal for Numerical Methods in Fluids*, Vol. 8, pp. 1071-1093.

Shapiro, R., 1970, "Smoothing, Filtering and Boundary Effects Rev.", *Geophys Space Physics*, Vol. 8, pp. 359-387.

Shi, F., J.T. Kirby, J.C. Harris, J.D. Geiman, S.T. Grilli, 2012, "A High-Order Adaptive Time-Stepping TVD Solver for Boussinesq Modeling of Breaking Waves and Coastal Inundation", *Ocean Modelling*, Vol. 43-44, pp. 36-51.

Shokin, Y.I., L.B. Chubarow, U. Müller, 1980, "Finite Difference Simulation of Tsunami" *Propogation in Theoretical and Experimental Fluid Mechanics*, Vol. 1, pp. 599-606.

Shu, C., H. Ding, K.S. Yeo, 2004, "Solution of Partial Differential Equations by a Global Radial Basis Function-Based Differential Quadrature Method", *Engineering Analysis with Boundary Elements*, Vol. 28, No. 10, pp. 1217-26.

Shuto, N., 1991, "Numerical Simulation of Tsunamis- Its Present and Near Future", *Natural Hazards*, Vol. 4, pp. 171-191.

Shuto, N., C. Goto F. Imamura, 1990, "Numerical Simulation as a Means of Warning for Near-Field Tsunamis", *Coastal Engineering in Japan*, Vol. 33, No. 2, pp. 173-193.

Simons, T.J. 1980, "Circulation Models of Lake and Inland Seas", *Canadian Dept. of Fisheries and Oceans.*

Sielecki, A., M.G. Wurtele, 1970, "The Numerical Integration of the Nonlinear Shallow-Water Equations with Sloping Boundaries", *Journal of Computational Physics*, Vol. 6, pp. 219-236.

Sommerfeld, R., 1949, "Partial Differential Equations in Physics", *Academic Press*, New York.

Soroushian, A., J. Farjoodi, 2006, "A Unified Starting Procedure for the Houbolt Method", *Communications in Numerical Methods in Engineering*, Vol.23, pp. 1-13.

Spielvogel, L.Q., 1975, "Single Wave Run-Up on Sloping Beaches". Journal of Fluid Mechanics, Vol. 74, pp. 685-694.

Stelling, G.S., 1983, *On the Construction of Computational Methods, for Shallow-Water Flow Problems*, Ph.D. Thesis Delft University of Technology.

Sumer, B.M., A. Ansal, K.O. Cetin, J. Damgaard, A.R. Gunbak, N-E. Ottesen Hansen, A. Sawicki, C.E. Synolakis, A.C. Yalçıner, Y. Yuksel, K. Zen, 2007, "Earthquake-Induced Liquefaction around Marine Structures", *Coastal and Ocean Engineering*, Vol. 133, No.1, pp. 55-59.

Synolakis, C., E. Bernard, 2006, "Tsunami Science Before and Beyond Boxing Day 2004", *Philosophical Transactions of the Royal Society*, Vol. 364, pp. 2231-2265.

Synolakis, C., E.N. Bernard, V.V. Titov, U. Kanoğlu, F.I. Gonzalez, 2008, "Validation and Verification of Tsunami Numerical Models", *Pure and Applied Geophysics*, Vol. 165, pp. 2197-2228.

Synolakis, C.E., 1987, "The Runup of Solitary Waves", *Journal of Fluid Mechanics*, Vol. 185, pp. 523-545.

Tadepalli, S. C.E. Synolakis, 1994, "The Run-Up of N-Waves on Sloping Beaches", Proceedings of the Royal Society of Londan, Vol. 445, pp. 99-112.

Tam, C.K.W., Z. Dong, 1996, "Radiation and Uutflow Boundary Conditions for Direct Computation of Acoustic and Flow Disturbances in a Nonuniform Mean Flow", *Journal of Computational Acoustics*, Vol. 4, pp. 175-201.

Tarwater, A.E., 1985, "Parameter Study of Hardy's Multiquadric Method for Scattered Data Interpolation", *Technical report UCRL-54670*, Lawrence Livermore Nationaln Laboratory.

Thacker, W.C. 1981, "Some Exact Solutions to the Nonlinear Shallow-Water Wave Equations", *Journal of Fluid Mechanics*, Vol. 107, pp. 499-508.

Titov, V.V., C.E. Synolakis, 1995, "Modeling of Breaking and Non-Breaking Long-Wave Evolution and Run-Up Using VTCS-2", *Journal of Waterway, Port, Coastal, and Ocean Engineering, Coastal, Ocean Engng*, Vol. 121, pp. 308-461.

Titov, V.V., C.E. Synolakis, 1998, "Numerical Modeling of Tidal Wave Run-Up, Journal of Waterway", *Port, Coastal and Ocean Engineering*, Vol. 124 No.4, pp. 157-171.

Tsynkov, S.V. 1998, "Numerical Solution of Problems on Unbounded Domains", *Applied Numerical Mathematics*, Vol. 27, pp. 465.532.

Tuck, E.O., L.S. Hwang, 1972, "Long Wave Generation on a Sloping Beach", *Journal of Fluid Mechanics*, Vol. 51, pp. 449-461.

Ursell, F., 1953, "The Long Wave Paradox in the Theory of Gravity Waves", *Mathematical Proceedings of the Cambridge Philosophical Society*, Vol. 49, pp. 685-694.

Viana S.A, D. Rodger, H.C. Lai, 2007, "Overview of Meshless Methods", *International Compumag Society Newsletter*, Vol. 14, pp. 3-6.

Vincent, S., J.P. Caltagirone, P. Bonneton, 2001, "Numerical Modelling of Bore Propagation and Run-Up on Sloping Beaches using a Mac Cormack TVD scheme", *Journal of Hydraulic Research*, Vol. 39, pp. 41-49.

Wang, J.G., G.R. Liu, 1980, "A Point Interpolation Meshless Method on Radial Basis Function", *International Journal of Numerical Methods In Engineering*, Vol.54, pp.1623-1648, Singapore, 2001

Wei, G., J.T. Kirby, 1995, "A Time-Dependent Numerical Code for the Extended Boussinesq Equations", *Journal of Waterway, Port, Coastal, and Ocean Engineering*, Vol. 121, No. 5, pp. 251-261.

Wei, G., J.T. Kirby, 1999, "Generation of waves in Boussinesq Models Using a Source Function Method", *Coastal Engineering*, Vol. 36, pp. 271-299.

Wendland, H., 2004, "Scattered Data Approximation", *Cambridge University Press*, Newyork.

Williams, H.A., E. Jensen, 2000, "Two-Dimensional Nonlinear Advection-Diffusion in a Model of Surfactant Spreading on a Thin Liquid Film", *Journal of Applied Mathematics*, Vol. 66, pp. 55-82.

Wind, H.G., C.B. Vreugdenhil, 1986, "Rip Current Generation Near Structures", *Journal of Fluid Mechanics*, Vol. 171, pp. 459-476.

Wong, A.S.M., Y.C. Hon, T.S. Li, S.L. Chung, E.J. Kansa, 1999, "Mutlizone Decomposition for Simulation of Time-Dependent Problems Using the Multiquadric Scheme", *Computers & Mathematics with Applications*, Vol. 37, No. 8, pp. 23-43.

Wu Z., Y.C. Hon 2003, "Convergence Error Estimate in Solving Free Boundary Diffusion Problem by Radial Basis Functions Method", *Engineering Analysis with Boundary Elements*, Vol. 27, pp. 73-79.

Yalçıner, A.C., A. Suppasri, E. Mas, N. Kalligeris, O. Necmioğlu, F. Imamura, C. Özer,

A. Zaitsev, N.M. Ozel, C. Synolakis, 2012, "Field Survey on the Coastal Impacts of March 11, 2011 Great East Japan Tsunami", *Pure and Applied Geophysics.*

Yalçıner, A., E. Pelinovsky, T. Talipova, A. Kurkin, A. Kozelkov, A. Zaitsev, 2004, "Tsunamis in the Black Sea: Comparison of the Historical", *Instrumental, and Numerical Data, Journal of Geophysical Research*, Vol. 109, pp. 12023.

Yalçıner, A.C., B. Alpar, Y. Altinok, I. Ozbay, F. Imamura, 2002, "Tsunamis in the Sea of Marmara: Historical Documents for the Past", *Models for Future, Marine Geology*, Vol. 190, pp. 445-463.

Yalçıner, A.C., C. Özer, H. Karakuş, A. Zaytsev, I. Güler, 2010, "Evaluation of Coastal Risk at Selected Sites Against Eastern Mediterranean Tsunamis", *Proceedings of 32nd International Conference on Coastal Engineering.*

Yalçıner, A.C., C.E. Synolakis, B. Alpar, J. Borrero, Y. Altinok, F. Imamura, S. Tinti, Ş. Ersoy, U. Kuran, S. Pamukcu, U. Kanoğlu, 2001, "Field Surveys and Modeling 1999 Izmit Tsunami", *International Tsunami Sympo-Sium ITS 2001*, Vol. 4-6, pp. 557-563.

Yalçıner, A.C., E. Pelinovsky, C. Synolakis E. Okal, 2003, "NATO Science Series, Submarine Landslides and Tsunamis", *Kluwer Academic Publishers.*

Yeh, H., A. Ghazali, I. Marton, 1989, "Experimental Study of Bore Run-Up.", *Journal of Fluid Mechanics*, Vol. 206, pp. 563- 578.

Yoon, S.B., J.H. Cho, 2001, "Numerical Simulation of Coastal Inundation over Discontinuous Topography", *Water Engineering Research*, Vol. 2, pp. 75-87.

Zahibo, N., E. Pelinovsky, A.C. Yalçıner, A. Kurkin, A. Kozelkov, A. Zaitsev, 2003, "Modeling the 1867 Virgin Island Tsunami", *Journal of Natural Hazards and Earth System Sciences, European Geosciences Union*, Vol. 3, pp. 367-376.

Zaitsev, A., A.C. Yalçıner, E. Pelinovsky, A. Kurkin, C. Özer, I. Insel, H. Karakuş,

G. Özyurt, 2008, "Tsunamis in Eastern Mediterranean, Histories, Possibilities and Realities", *Proceedings of 7th International Conference on Coastal and Port Engineering in Developing Countries*.

Zaitsev, A.I., A.C. Kozelkov, A.A. Kurkin, E.N. Pelinovsky, T.G. Talipova, A.C. Yalçıner, 2002, "Tsunami Modeling in Black Sea", Published in Izvestiya of Russian Academy of Engineering Sciences", *Applied Mathematics and Mechanics*, Vol. 3, pp. 27-45.

Zelt, J.A., 1986, *Tsunamis: The Response of Harbours with Sloping Boundaries to Long Wave Excitation*, Ph.D. Thesis, California Institute of Technology, Pasadena.

Zelt, J.A., 1991, "The Run-Up of Nonbreaking and Breaking Solitary Waves", *Coastal Engineering*, Vol. 15 No. 3, pp. 205-246.

Zelt, J.A., F. Raichlen, 1990, "A Lagrangian Model for Wave-Induced Harbor Oscillations", *Journal of Fluid Mechanics*, Vol. 213, pp. 203-225.

Zelt, J.A. F. Raichlen, 1991, "Overland Own from Solitary Waves, Journal of Waterway, Port, Coastal and Ocean Engineering", *American Society of Civil Engineers*, Vol. 117, pp. 247-263.

Zerroukat, M., K. Djidjeli, A. Charafi, 2000, "Explicit and Implicit Meshless Methods for Linear Advection-Diffusion Type Partial Differential Equations", *International Journal For Numerical Methods in Engineering*, Vol. 48, pp. 19-35.

Zhang, J.E., 1996, *L Run-Up of Ocean Waves on Beaches II. Nonlinear Waves in a Fluid-Filled Elastic Tube*, Ph.D. Thesis, California Institute of Technology, Pasadena.

Zhou X., Y.C. Hon, K.F. Cheung 2004, "A Grid-Free, Nonlinear Shallow-Water Model with Moving Boundary", *Engineering Analysis with Boundary Elements*, Vol. 28, No. 8, pp. 967-973.